

REPUBLIC OF TURKEY
MUĞLA SITKI KOÇMAN UNIVERSITY
GRADUATE SCHOOL OF
NATURAL AND APPLIED SCIENCES

DEPARTMENT OF MINING ENGINEERING

INVESTIGATION OF THE DRY GRINDING BEHAVIOUR
OF A CHROMITE ORE FROM MUĞLA-KARACAÖREN
REGION IN A STANDARD BOND BALL MILL

MASTER OF SCIENCE

ZEHRA GÖKALP

DECEMBER 2018

MUĞLA

MUĞLA SITKI KOÇMAN UNIVERSITY
Graduate School of Natural and Applied Sciences

APPROVAL OF THE THESIS

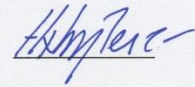
The thesis submitted by **ZEHRA GÖKALP** with the title of "**INVESTIGATION OF THE DRY GRINDING BEHAVIOUR OF A CHROMITE ORE FROM MUĞLA-KARACAÖREN REGION IN A STANDARD BOND BALL MILL**" has been unanimously accepted by the jury members on the 5th of December, 2018 to fulfill the requirements for the degree of Master of Science in the Department of Mining Engineering.

THESIS JURY MEMBERS

Prof. Dr. A. Hakan BENZER (Head of Jury)

Department of Mining Engineering
Hacettepe University, Ankara

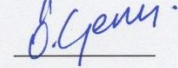
Signature:



Assoc. Prof. Dr. Ömürden GENÇ (Supervisor)

Department of Mining Engineering
Muğla Sıtkı Koçman University, Muğla

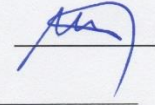
Signature:



Prof. Dr. Taki GÜLER (Member)

Department of Mining Engineering
Muğla Sıtkı Koçman University, Muğla

Signature:

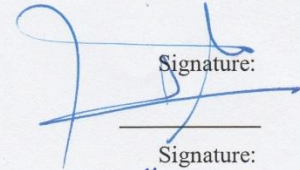


APPROVAL OF HEAD OF THE DEPARTMENT

Assoc. Prof. Dr. Avni GÜNEY

Head of Department, Mining Engineering

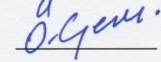
Signature:



Assoc. Prof. Dr. Ömürden GENÇ

Supervisor, Department of Mining Engineering

Signature:



Date of Defense: 05/12/2018

I hereby declare that all information in this document has been obtained and presented in accordance with academic rules and ethical conduct. I also declare that, as required by these rules and conduct, I have fully cited and referenced all material and results that are not original to this work.

Zehra Gökalp

05/12/2018

ACKNOWLEDGEMENT

With great honor, I would like to express my utmost and sincere gratitude to my supervisor Assoc. Prof. Dr. Ömürden Genç from the Mining Engineering Department of Muğla Sıtkı Koçman University for her selfless guidance, suggestions, encouragement and support to complete this thesis. I deem myself very lucky to have the chance of working with her. I do also appreciate very much her understanding and helpfulness with my academic development, for her valuable comments, insights and fast feedback. She always made wise suggestions and devoted here time whenever I needed.

I would like to thank to Prof. Dr. A. Hakan Benzer from the Mining Engineering Department of Hacettepe University, Prof. Dr. W.J Whiten (Emeritus Professor, The University of Queensland, JKMRC), Prof. Dr. Taki Güler from the Mining Engineering Department of Muğla Sıtkı Koçman University, Prof. Dr. Murat Gül and Dr. Instructor Ceren Küçükuyşal from the Geological Engineering Department of Muğla Sıtkı Koçman University for their valuable advices.

The success of this thesis was made possible through the cooperation and assistance of a number of dedicated people. I would like to thank to the research assistants Ercan Polat, undergraduate students Abdalla Napari Abdulai, Dilay Turan, Gülay Terzi, Cemil Uysal, from the Mining Engineering Department of Muğla Sıtkı Koçman University for their valuable help during sampling, sample preparation stages and experimental analysis.

M. Fatih Şirinoğulları, Batuhan Türkoğlu, Mehmet Çadır, Yakup Özkan, Abdul Samed İbrahim, Anıl Gül, Enis Ozan, Tanzer Doğan, Mehmet Büyükçoban, Nazmi Göktürk Öztürk for their help during the experimental analysis.

I would also like to thank to Krom-El İnşaat, Madencilik Ticaret A.Ş. (ETİ Krom A.Ş.) for the permission to perform sampling studies at the mine-site.

This thesis has been granted (Project Grant Number:17/291) by the Muğla Sıtkı Koçman University Research Projects Coordination Office.

Last but not least, I would like to pay my appreciation to my beloved family and friends for their love and care, and also the encouragement all the time. I would like to express my special thanks to my father, Aziz Gökalp, who always supported me during all steps I took throughout all my life, my mother, Menice Gökalp, who accompanied me whenever I needed. I would like to express my eternal thanks to my dear brothers İslam Gökalp who is a young scientist and İdris Gökalp who is a bachelor student of Material and Metallurgical Engineering for their patience, invaluable support, love and care throughout this study.

ÖZET

MUĞLA-KARACAÖREN BÖLGESİ KROM CEVHERİNİN KURU ÖĞÜTME DAVRANIMININ STANDART BOND BİLYALI DEĞİRMENİNDE İNCELENMESİ

Zehra GÖKALP

Yüksek Lisans Tezi

Fen Bilimleri Enstitüsü

Maden Mühendisliği Ana Bilim Dalı

Danışman: Doç. Dr. Ömürden GENÇ

Aralık 2018, 135 sayfa

Bu tezin amacı, krom cevherinin bilyalı değirmende öğütme performansının, öğütücü ortam boyu ve dağılımının değirmen ürünü inceliği ve özgül kırılma hızı fonksiyonları üzerine etkilerinin kuru öğütme koşullarında incelenmesiyle değerlendirilmesidir. Ayrıca, değirmen ürünü inceliğine bağlı olarak öğütme enerjisi gereksiniminin tahmin edilmesidir. Bu amaçla, Muğla-Karacaören bölgesinden temin edilen ocak çıkışı cevher, çeneli kırıcı, çubuklu ve standard Bond bilyalı değirmenleri kullanılarak bir dizi kırma ve kuru öğütme işlemlerinden geçirilmiştir. Çubuklu değirmen öğütme aşamasından, 3.35mm'den ince malzeme elde edilmiş ve Bond bilyalı değirmeninde yürütülen kesikli öğütme testlerinde kullanılmıştır. Böylece, kesikli öğütme testlerinde tam bir tane boyu dağılımı kullanılmıştır. Testler, farklı bilya şarjı dağılımları kullanılarak 25sn, 1dk, 3dk, 5dk, 10dk ve 15dk'lık kesikli öğütme zaman aralıklarında yürütülmüştür. Test sonuçlarının birbirleri ile karşılaştırılabilirliğini belirlemek amacıyla, tekrarlanabilirlik testleri yürütülmüştür. Değirmen beslemesi ve çıkışı malzemenin tane boyu dağılımları en iri boydan (3.35mm) 0.038mm'ye kadar Ro-tap kullanılarak kuru elemeye belirlenmiştir. Kesikli öğütme işleminin özgül enerji tüketimleri Bond'un enerji eşitliğinden tahmin edilmiştir. Değirmen beslemesi, çıkışı tane boyu dağılımları ve teorik Broadbent-Callcott kırılma fonksiyonu, özgül kırılma hızı fonksiyonlarının mükemmel karışım matematiksel boyut küçültme modelinden geri hesaplanmasında kullanılmıştır. Özgül kırılma hızlarının geri hesaplanmasında JKSİM Met cevher hazırlama yazılımının model uydurma modülü kullanılmıştır.

Test sonuçlarının tekrarlanabilir olduğu belirlenmiştir. Bilya boyu ve şarj dağılımlarının özgül kırılma hızı fonksiyonları üzerine etkilerinin önerilen yöntem ile başarılı bir şekilde yansıtılabildiği belirlenmiştir. Önerilen yöntem ile, her bir bilya şarjı uygulamasında sistematik boyut küçültme elde edilebilmiştir. Değirmende durma zamanı arttıkça, daha ince boyut dağılımı elde edilmiştir. Fakat, 15dk'lık öğütme zamanı aralığında değirmen astarında ve bilya yüzeylerinde malzeme sıvanması gözlemlenmiştir. Durma zamanının artmasıyla, -0.038mm'nin altındaki malzeme

miktarında önemli düzeyde bir artış sağlanamamıştır. 25mm ve 20mm tek boyutlu bilya şarjı uygulamalarının öğütme performansı, $-3.35+0.850\text{mm}$ tane boyu fraksiyonunun öğütülmesinde düşmüştür. Fakat, 20mm tek boyutlu şarj uygulaması, 0.212mm'den ince tane fraksiyonlarının öğütülmesinde yüksek öğütme performansı göstermiştir. 40mm, 30mm ve 25mm tek boyutlu şarj kompozisyonları, 10dk'dan daha kısa durma zamanı aralıklarında, Standard Bond bilya şarjına göre daha yüksek öğütme performansı göstermiştir. Şarj dağılımı inceldikçe, değirmen ürününün irileştiği gözlemlenmiştir. Farklı incelik değerlerine sahip bilya dağılımları uygulaması, 0.212mm' den ince boyut fraksiyonlarındaki ince malzeme miktarı üretimini önemli düzeyde değiştirmemiştir. Sonuçlar, kromun öğütülmesinde yüksek öğütme performansı elde edebilmek için 20mm'den iri, farklı boyutlarda bilya kullanılması gerektiğini göstermiştir. Farklı şarj uygulamalarında, durma zamanı ve değirmen ürünü'nün P80 boyu arasında anlamlı korelasyonlar çıkartılabilmektedir. Öğütme enerjisi gereksinimi ve değirmen ürünü inceliği (P80) arasında logaritmik bir korelasyon olduğu gözlemlenmiştir. Malzeme durma zamanı ve özgül enerji tüketimleri arasında test koşulları için ilişkiler kurulabilmektedir. Özgül kırılma hızlarının durma zamanı ile değiştiği bulunmuştur. Tek boyutlu bilya şarjı uygulamaları arasında, en yüksek kırılma hızları, malzemenin 25mm'lik bilya şarjı ile 1dk, ve 3dk'lık zaman aralıkları için öğütülmesinde elde edilmiştir. 20mm'lik bilya şarjı uygulamasının 10dk'lık durma zamanından sonra, özgül kırılma hızlarını artırdığını göstermiştir. Tek boyutlu bilya şarjı uygulamaları için, 15dk'dan daha kısa durma zamanı aralıklarında, değirmendeki maksimum bilya boyu (b_{max}) tarafından kırılacak maksimum tane boyu (X_m) arasında anlamlı korelasyonlar çıkartılabilmektedir. X_m ve maksimum kırılma hızı (r_{max}) değerleri arasında korelasyonlar kurulabilmektedir. b_{max} ve r_{max} değerleri arasında da oldukça iyi korelasyonlar kurulabilmektedir.

Tam bir boyut dağılımının bilyalı değirmene beslenmiş olması nedeniyle, test sonuçlarının endüstriyel ölçekli uygulamaları temsil edebileceği düşünülmüştür. Bilya boyunun özgül kırılma hızları üzerine etkileri yansıtılabilmektedir. Sonuçlar, işlem optimizasyonu için, kuru öğütme koşullarında bilya şarjı dağılımlarının özgül kırılma hızı fonksiyonları üzerine etkileri konusunun derinlemesine anlaşılmasını sağlayan kullanışlı bilgiler sağlamıştır. Boyut küçültme performansı üzerine yapılan değerlendirmeler, krom cevherinin bilyalı değirmende kuru öğütülmesi konusunda literatüre orjinal bilgiler sağlamıştır.

Anahtar Kelimeler: Öğütme, Matematiksel Modelleme, Bilyalı Değirmen, Enerji,

Krom

ABSTRACT

INVESTIGATION OF THE DRY GRINDING BEHAVIOUR OF A CHROMITE ORE FROM MUĞLA-KARACAÖREN REGION IN A STANDARD BOND BALL MILL

Zehra GÖKALP

Master of Science (M.Sc.)

Graduate School of Natural and Applied Sciences

Department of Mining Engineering

Supervisor: Assoc. Prof. Dr. Ömürden GENÇ

December 2018, 135 pages

The purpose of this thesis is to evaluate the ball mill grinding performance of a chromite ore by investigating the grinding media size and charge distribution effects on mill product fineness and specific breakage rate functions in dry grinding conditions. Additionally, to estimate grinding energy requirement on the basis of mill product fineness. For this purpose, run-of-mine ore was provided from Muğla-Karacaören region and subjected to a series crushing and dry grinding processes by using a jaw crusher, rod mill and standard Bond ball mill. Material finer than 3.35mm was obtained from rod mill grinding stage and used in the batch grinding tests in a Bond ball mill. Thus, a full particle size distribution (-3.35mm) was used in all the batch test conditions. Tests were conducted at batch grinding time intervals of 25sec, 1min, 3min, 5min, 10min and 15min by using different ball charge distributions. Reproducibility tests were performed to determine if test results were comparable over each other. Particle size distributions of mill feed and discharge materials were determined by dry screening in a Ro-tap from the top size (3.35mm) down to 0.038mm. Specific energy consumptions of batch grinding process were estimated from Bond's energy equation. Mill feed, discharge particle size distributions and Broadbent-Callcott theoretical breakage function were used to back-calculate specific breakage rate functions from perfect mixing mathematical size reduction model. Model fitting module of the JKSimMet mineral processing software was used in the back-calculation of specific breakage rates.

Test results were determined to be repeatable. Ball size and charge distribution effects were found to be successfully reflected on specific breakage rate functions with the proposed methodology. Systematic size reduction was achieved in each ball charge application case with the proposed methodology. Finer particle size distribution was obtained as the retention in the mill was increased. However, coating on the mill liner and on the surface of the balls were observed for 15min grinding time interval.

A significant increase in the amount of -0.038mm material could not have been achieved with the increase in residence time. Grinding performance of 25mm and 20mm monosize ball charge applications were observed to decrease in grinding the size fraction of $-3.35+0.850\text{mm}$. However, 20mm monosize charge application indicated higher grinding performance in grinding the size fractions finer than 0.212mm. 40mm, 30mm and 25mm monosize charge compositions indicated higher grinding performance as compared to Standard Bond ball charge at residence time intervals shorter than 10min. As the charge distribution got finer, coarser mill product was observed. Production of fine material amount did not change significantly in the size fractions finer than 0.212mm with the application of ball distributions with different fineness values. Results indicated that, different ball sizes which are coarser than 20mm should be used in the charge in grinding of chromite ore for higher grinding performance. Meaningful correlations could have been drawn between residence time and P80 size of the mill product in different charge applications. A logarithmic correlation between grinding energy requirement and mill product fineness (P80) was observed. Relationships between material residence time and specific energy consumptions could have been established for the test conditions. Specific breakage rates were found to change with residence time. Among the monosize ball charge applications, highest breakage rates were obtained by grinding the material with 25mm ball charge for 1min and 3min time intervals. 20mm ball charge application indicated to increase the specific breakage rates after 10min residence time. Meaningful correlations could have been derived between maximum particle size (X_m) that can be broken by the maximum ball size in the mill and maximum ball size (b_{max}) for monosize charge applications at residence time intervals shorter than 15min. Correlations could have been established between X_m and maximum breakage rate (r_{max}) values. Relatively good correlations could have been established between b_{max} and r_{max} values as well.

Test results were thought to be representative of the industrial scale applications as a full size distribution was fed to ball mills. Ball size effects could have been reflected on the specific breakage rates. Results, provided useful information for insights about ball charge distribution effects on specific breakage rate functions in dry grinding conditions for process optimization. Evaluations on size reduction performance provided original information to the literature on dry grinding of chromite ore in a ball mill.

Keywords: Grinding, Mathematical Modelling, Ball Mill, Energy, Chromite



To my family...

TABLE OF CONTENTS

ACKNOWLEDGEMENT	iii
ÖZET	iv
ABSTRACT	vii
LIST OF TABLE	xii
LIST OF FIGURE	xiv
LIST OF ABBREVIATIONS	xxi
1. INTRODUCTION	1
2. GENERAL INFORMATION ON CHROMITE ORE	4
2.1. Chromite Deposits.....	5
2.2. Physical and Chemical Properties of Chromite.....	7
2.3. Mineralogy of Chromite Ore.....	8
2.4. Chromite Reserves In The World.....	9
2.5. Genesis of Chromite Deposits In Turkey.....	10
2.6. Chromite Ore Deposits and Reserves In Turkey.....	12
2.7. Chromite Ore Concentration Processes.....	13
3. COMMINATION	16
3.1. Comminution Fundamentals	16
3.1.1. Comminution Theories.....	17
3.2. Mathematical Models of Comminution	18
3.2.1. Matrix model	19
3.2.2. Kinetic model.....	23
3.2.3. Size-Mass balance batch model.....	24
3.2.4. Population balance model.....	25
3.2.5. Estimation of ball mill model parameters.....	26
3.2.6. Estimation of specific breakage rate from batch grinding tests.....	26
3.2.7. Breakage distribution function	28
3.2.8. Discharge rate and residence time distribution functions.....	29
3.2.9. Perfect mixing model.....	30
3.3.10. Discrete element modelling (DEM).....	34
4. EXPERIMENTAL	35
4.1. Field Sampling	35

4.2. Description of The Karacaören Chromite Ore Deposit.....	36
4.3. Material Characterization	36
4.3.1. Standard Bond work index test	37
4.4. Sample Preparation Stages.....	40
4.5. Batch Grinding Tests.....	41
4.6. Particle Size Distribution Analysis	42
5. RESULTS AND DISCUSSIONS	43
5.1. Repeatability Tests.....	43
5.2. Calculation of Bond Ball Filling Ratio	48
5.3. Calculation of Number Of Balls	49
5.4. Batch Grinding Test Conditions.....	49
5.4.1. Selected grinding media size distributions.....	49
5.4.2. Batch grinding test mill feed particle size distributions.....	53
5.5. Batch Grinding Test Results	54
5.6. Comparison of Batch Grinding Test Results	61
5.6.1. Evaluation of mill product fineness as a function of residence time	73
5.7. Specific Energy Consumption Evaluation	81
5.7.1. Relationship between specific energy consumption and P80	82
5.7.2. Relationship between residence time and specific energy consumption	83
6. SPECIFIC BREAKAGE RATE FUNCTION ESTIMATION.....	91
6.1. Variation of Specific Breakage Rate Functions with Particle Size at Different Ball Charge Compositions	94
6.1.1. Evaluation of monosize ball distribution effect on specific breakage rate functions	102
6.1.2. Evaluation of ball distribution fineness effect on specific breakage rate functions	109
6.1.3. Evaluation of ball size distribution effect on specific breakage rate functions	118
7. GENERAL DISCUSSIONS	122
8. CONCLUSIONS AND RECOMMENDATIONS.....	124
REFERENCES.....	126
APPENDIX.....	133
CURRICULUM VITAE.....	134

LIST OF TABLES

Table 2.1. Main properties of chromite ore.....	7
Table 2.2. Atomic properties of chromite ore.....	7
Table 2.3. Physical and other properties of chromite ore	7
Table 2.4. Chromium (Cr) minerals and their properties.....	8
Table 2.5. Chromite ore, gangue and guided minerals	9
Table 2.6. World's chromite mine production and reserves	9
Table 2.7. Chromite ore deposits in Turkey.....	10
Table 2.8. Physical properties of chromite, olivine and serpentine (Dahlin and Rule, 1993)	15
Table 3.1. Feed and product size distributions from a size-reduction process (Lynch,1977).....	19
Table 3.2. Mass balance for a size-reduction process (Lynch,1977).....	20
Table 3.3. The product from a size-reduction process expressed in terms of the feed (Lynch,1977).....	20
Table 3.4. General matrix equation of breakage (Lynch,1977)	21
Table 3.5. Selection in a size-reduction process (Lynch,1977)	22
Table 4.1. XRF results	37
Table 4.2. Standard Bond ball charge distribution (Turkish Standards 7700).....	38
Table 4.3. Rod mill charge composition distribution.....	40
Table 5.1. RMS of the test results	48
Table 5.2. Grinding media (charge) distributions	50
Table 5.3. Standard Bond ball size distribution (Test-1)	51
Table 5.4. Monosize ball distribution applications	51
Table 5.5. Ball size distribution coarser than Standard Bond ball size distribution (Test-6)	51
Table 5.6. Ball size distribution finer than Standard Bond ball size distribution (Test-7)	51
Table 5.7. Ball size distribution finer than Standard Bond ball size distribution (Test-8)	51
Table 5.8. Ball size distribution of charge-1 (Test-9).....	52
Table 5.9. Ball size distribution of charge-2 (Test-10).....	52
Table 5.10. Ball size distribution of charge-3 (Test-11).....	52

Table 6.1. Broadbent and Callcott breakage (appearance) function used in the JKSimMet software92

Table 6.2. Standard deviation (SD) variations obtained in the back-calculation of breakage rates from perfect mixing model using JKSimMet Software95



LIST OF FIGURES

Figure 2.1. Distribution of chromite ore deposits in Turkey.....	11
Figure 4.1. Sampling of the run-of-mine chromite ore from the stockpile.....	35
Figure 4.2. Standard Bond ball mill.....	38
Figure 4.3. Standard Bond Work Index test mill feed and product size distributions.....	39
Figure 4.4. Hand crushing of run-of-mine ore samples.....	40
Figure 5.1. Comparison of the mill feed particle size distributions for the tests.....	44
Figure 5.2. Particle size distributions of the repeatability test-1.....	44
Figure 5.3. Particle size distributions of the repeatability test-2.....	45
Figure 5.4. Comparison of the particle size distributions for batch grinding time at 25 sec.....	45
Figure 5.5. Comparison of the particle size distributions for batch grinding time at 1 min.....	46
Figure 5.6. Comparison of the particle size distributions for batch grinding time at 3 min.....	46
Figure 5.7. Comparison of the particle size distributions for batch grinding time at 5 min.....	47
Figure 5.8. Comparison of the particle size distributions for batch grinding time at 10 min.....	47
Figure 5.9. Comparison of the particle size distributions for batch grinding time at 15 min.....	48
Figure 5.10. Comparison among the standard bond and the selected coarser and finer charge distributions.....	52
Figure 5.11. Selected charge distributions with the same weighed average ball size.....	53
Figure 5.12. Variation of mill feed particle size distributions.....	54
Figure 5.13. Particle size distributions obtained by batch grinding with Standard Bond ball size distribution.....	55
Figure 5.14. Particle size distributions obtained by batch grinding with monosize ball distribution of 40mm.....	56
Figure 5.15. Particle size distributions obtained by batch grinding with monosize ball distribution of 30mm.....	56
Figure 5.16. Particle size distributions obtained by batch grinding with mono-size ball distribution of 25mm.....	57
Figure 5.17. Particle size distributions obtained by batch grinding with mono-size ball distribution of 20mm.....	57

Figure 5.18. Particle size distributions obtained by batch grinding with ball size distribution coarser than Standard Bond charge distribution (D average=36.79mm).....	58
Figure 5.19. Particle size distributions obtained by batch grinding with ball size distribution finer than Standard Bond charge distribution (D average=25.51mm).....	58
Figure 5.20. Particle size distributions obtained by batch grinding with ball size distribution finer than Standard Bond charge distribution (D average=21.18mm).....	59
Figure 5.21. Particle size distributions obtained by batch grinding with ball size distribution of charge-1 (D average=30.59mm).....	59
Figure 5.22. Particle size distributions obtained by batch grinding with ball size distribution of charge-2 (D average=30.42mm).....	60
Figure 5.23. Particle size distributions obtained by batch grinding with ball size distribution of charge-3 (D average=30.64mm).....	60
Figure 5.24. Particle size distributions at 25sec obtained by batch grinding with Standard Bond charge and monosize distributions	62
Figure 5.25. Particle size distributions at 1min obtained by batch grinding with Standard Bond charge and monosize distributions	62
Figure 5.26. Particle size distributions at 3min obtained by batch grinding with Standard Bond charge and monosize distributions	63
Figure 5.27. Particle size distributions at 5min obtained by batch grinding with Standard Bond charge and monosize distributions	63
Figure 5.28. Particle size distributions at 10min obtained by batch grinding with Standard Bond charge and monosize distributions	64
Figure 5.29. Particle size distributions at 15min obtained by batch grinding with Standard Bond charge and monosize distributions	64
Figure 5.30. Particle size distributions at 25sec obtained by batch grinding with Standard Bond, coarser and finer charge compositions	66
Figure 5.31. Particle size distributions at 1min obtained by batch grinding with Standard Bond, coarser and finer charge compositions	67
Figure 5.32. Particle size distributions at 3min obtained by batch grinding with Standard Bond, coarser and finer charge compositions	67
Figure 5.33. Particle size distributions at 5min obtained by batch grinding with Standard Bond, coarser and finer charge compositions	68
Figure 5.34. Particle size distributions at 10min obtained by batch grinding with Standard Bond, coarser and finer charge compositions	68
Figure 5.35. Particle size distributions obtained by batch grinding with Standard Bond, charge-1, charge-2 and charge-3 compositions for 25sec	70

Figure 5.36. Particle size distributions obtained by batch grinding with Standard Bond, charge-1, charge-2 and charge-3 compositions for 1min	70
Figure 5.37. Particle size distributions obtained by batch grinding with Standard Bond, charge-1, charge-2 and charge-3 compositions for 3min	71
Figure 5.38. Particle size distributions obtained by batch grinding with Standard Bond, charge-1, charge-2 and charge-3 compositions for 5min	71
Figure 5.39. Particle size distributions obtained by batch grinding with Standard Bond, charge-1, charge-2 and charge-3 compositions for 10min	72
Figure 5.40. Comparisons of relationships between residence time and P80 for the Bond and monosize charge distribution applications	74
Figure 5.41. Relationship between residence time and P80 for the Bond charge distribution application.....	74
Figure 5.42. Relationship between residence time and P80 for 40mm monosize charge distribution application.....	75
Figure 5.43. Relationship between residence time and P80 for 30mm monosize charge distribution application.....	75
Figure 5.44. Relationship between residence time and P80 for 25mm monosize charge distribution application.....	76
Figure 5.45. Relationship between residence time and P80 for 20mm monosize charge distribution application.....	76
Figure 5.46. Comparison of the relationship between residence time and P80 for Standard Bond, coarser and finer charge distributions.....	77
Figure 5.47. Relationship between residence time and P80 for coarser charge distribution (Test-6).....	77
Figure 5.48. Relationship between residence time and P80 for finer charge distribution (Test-7).....	78
Figure 5.49. Relationship between residence time and P80 for finer charge distribution (Test-8).....	78
Figure 5.50. Comparison of the relationship between residence time and P80 for different charge distributions.....	79
Figure 5.51. Relationship between residence time and P80 for charge-1 distribution (Test-9).....	80
Figure 5.52. Relationship between residence time and P80 for charge-2 distribution (Test-10).....	80
Figure 5.53. Relationship between residence time and P80 for charge-3 distribution (Test-11).....	81
Figure 5.54. Overall relationship between specific energy consumption and P80	82

Figure 5.55. Relationship between residence time and energy consumption for Bond and monosize charge distribution applications	83
Figure 5.56. Relationship between residence time and energy consumption for Bond charge distribution application	84
Figure 5.57. Relationship between residence time and energy consumption for 40mm monosize charge distribution application.....	84
Figure 5.58. Relationship between residence time and energy consumption for 30mm monosize charge distribution application.....	85
Figure 5.59. Relationship between residence time and energy consumption for 25mm monosize charge distribution application.....	85
Figure 5.60. Relationship between residence time and energy consumption for 20mm monosize charge distribution application.....	86
Figure 5.61. Comparison of the relationship between residence time and energy consumption for Bond, coarser, and finer charge distribution applications	86
Figure 5.62. Relationship between residence time and energy consumption for coarser charge distribution application (test-6)	87
Figure 5.63. Relationship between residence time and energy consumption for finer charge distribution application (test-7)	87
Figure 5.64. Relationship between residence time and energy consumption for finer charge distribution application (test-8)	88
Figure 5.65. Comparison of the relationship between residence time and energy consumption for Bond, charge-1 (test-9), charge-2 (test-10) and charge-3 (test-11) distribution applications.....	88
Figure 5.66. Relationship between residence time and energy consumption for charge-1 (test-9) distribution application	89
Figure 5.67. Relationship between residence time and energy consumption for charge-2 (test-10) distribution application	89
Figure 5.68. Relationship between residence time and energy consumption for charge-3 (test-11) distribution application	90
Figure 6.1. Specific breakage rates obtained by grinding with Standard Bond charge distribution	95
Figure 6.2. Specific breakage rates obtained by grinding with 40mm monosize ball charge distribution.....	96
Figure 6.3. Specific breakage rates obtained by grinding with 40mm monosize ball charge distribution (Enlarged y-scale)	96
Figure 6.4. Specific breakage rates obtained by grinding with 30mm monosize ball charge distribution.....	96

Figure 6.5. Specific breakage rates obtained by grinding with 30mm monosize ball charge distribution (Enlarged y-scale)	97
Figure 6.6. Specific breakage rates obtained by grinding with 25mm monosize ball charge distribution.....	97
Figure 6.7. Specific breakage rates obtained by grinding with 25mm monosize ball charge distribution (Enlarged y-scale)	97
Figure 6.8. Specific breakage rates obtained by grinding with 20mm monosize ball charge distribution.....	98
Figure 6.9. Specific breakage rates obtained by grinding with 20mm monosize ball charge distribution (Enlarged y-scale)	98
Figure 6.10. Specific breakage rates obtained by grinding with charge-1 distribution (test-9)	100
Figure 6.11. Specific breakage rates obtained by grinding with charge-2 distribution (test-10)	100
Figure 6.12. Specific breakage rates obtained by grinding with charge-3 distribution (test-11)	101
Figure 6.13. Specific breakage rates obtained by grinding with Bond and monosize distributions for 25 sec	102
Figure 6.14. Specific breakage rates obtained by grinding with Bond and monosize distributions for 1min	102
Figure 6.15. Specific breakage rates obtained by grinding with Bond and monosize distributions for 3min	103
Figure 6.16. Specific breakage rates obtained by grinding with Bond and monosize distributions for 5min	103
Figure 6.17. Specific breakage rates obtained by grinding with Bond and monosize distributions for 10min	103
Figure 6.18. Relationship between X_m and b_{max} for 25sec	104
Figure 6.19. Relationship between X_m and b_{max} for 1min	105
Figure 6.20. Relationship between X_m and b_{max} for 3min	105
Figure 6.21. Relationship between X_m and b_{max} for 5min	105
Figure 6.22. Relationship between X_m and b_{max} for 10 min	106
Figure 6.23. Relationship between X_m and b_{max} for 15 min	106
Figure 6.24. Relationship between b_{max} (mm) and r_{max} (min-1) for 25 sec	107
Figure 6.25. Relationship between b_{max} (mm) and r_{max} (min-1) for 1min.....	107
Figure 6.26. Relationship between b_{max} (mm) and r_{max} (min-1) for 3min.....	108
Figure 6.27. Relationship between b_{max} (mm) and r_{max} (min-1) for 5min.....	108
Figure 6.28. Relationship between b_{max} (mm) and r_{max} (min-1) for 10 min.....	108

Figure 6.29. Relationship between b_{max} (mm) and r_{max} (min-1) for 15 min.....	109
Figure 6.30. Specific breakage rates for 25 sec obtained by grinding with ball distributions of different fineness values.....	109
Figure 6.31. Specific breakage rates for 1min obtained by grinding with ball distributions of different fineness values.....	110
Figure 6.32. Specific breakage rates for 3min obtained by grinding with ball distributions of different fineness values.....	110
Figure 6.33. Specific breakage rates for 5min obtained by grinding with ball distributions of different fineness values.....	110
Figure 6.34. Specific breakage rates for 10min obtained by grinding with ball distributions of different fineness values.....	111
Figure 6.35. Relationship between X_m and b_{max} for 25sec	112
Figure 6.36. Relationship between X_m and b_{max} for 1min	112
Figure 6.37. Relationship between X_m and b_{max} for 3min	113
Figure 6.38. Relationship between X_m and b_{max} for 5min	113
Figure 6.39. Relationship between X_m and b_{max} for 10 min	113
Figure 6.40. Relationship between X_m (mm) and r_{max} (min-1) for 25sec.....	114
Figure 6.41. Relationship between X_m (mm) and r_{max} (min-1) for 1min.....	114
Figure 6.42. Relationship between X_m (mm) and r_{max} (min-1) for 3min.....	115
Figure 6.43. Relationship between X_m (mm) and r_{max} (min-1) for 5min.....	115
Figure 6.44. Relationship between X_m (mm) and r_{max} (min-1) for 10 min.....	115
Figure 6.45. Relationship between X_m (mm) and r_{max} (min-1) for 25sec.....	116
Figure 6.46. Relationship between X_m (mm) and r_{max} (min-1) for 1min.....	117
Figure 6.47. Relationship between X_m (mm) and r_{max} (min-1) for 3min.....	117
Figure 6.48. Relationship between X_m (mm) and r_{max} (min-1) for 5min.....	117
Figure 6.49. Relationship between X_m (mm) and r_{max} (min-1) for 10 min.....	118
Figure 6.50. Specific breakage rates for 25sec obtained by grinding with different ball distributions.....	118
Figure 6.51. Specific breakage rates for 1min obtained by grinding with different ball distributions.....	118
Figure 6.52. Specific breakage rates for 3min obtained by grinding with different ball distributions.....	119
Figure 6.53. Specific breakage rates for 5min obtained by grinding with different ball distributions.....	119
Figure 6.54. Specific breakage rates for 10min obtained by grinding with different ball distributions.....	119

Figure 6.55. Relationship between b_{max} (mm) and r_{max} (min-1) for different charge compositions.....121

Figure 6.56. Relationship between X_m size and r_{max} (min-1) for 3min121



LIST OF ABBREVIATIONS

EAF	Electric Arc Furnace
MGS	Multi Gravity Separator
ROM	Run of Mine
AG	Autogenous Grinding
SAG	Semi Autogenous Grinding
RTD	Residence Time Distribution
DEM	Discrete Element Modelling
XRF	X-Ray Fluorescence
RMS	Root Mean Square

1. INTRODUCTION

Chromite reserves of Turkey are estimated to be about 26 million tons as stated in the report of USGS (2018) and thus, chromite ore processing has a vital importance in Turkey.

Comminution, which includes crushing and grinding unit operations, is the first in the mineral processing plants after mining operations. The ore should be ground in mills to obtain the required particle size distribution for concentration stages so that, the ore can be sold in the market. Comminution is an energy intensive process and consumes about 3-4% of the electricity generated worldwide and typically, 70% of the total energy requirement in a typical mineral processing plant is consumed in comminution operations as stated in Genç (2008). In this context, it is the most important processing stage in mineral processing plants. Rod and ball mills are widely applied technologies for grinding of the ore in chromite processing plants. Especially, ball mill operation is very energy intensive due to a series of operational conditions such that, the energy can be consumed in overgrinding the material and poor breakage actions can exist in the mill as stated in Austin (1984). For example; under filling of the mill by material that will result in steel to steel contact without particle breakage between the balls whereas overfilling of the mill with excess material which will result to the existence of ball-powder-ball action which is known as cushioning effect as stated in Austin (1984). Both conditions will reduce the grinding performance and increase the energy consumption and hence, understanding of the ball mill grinding performance is crucial in order to be able to determine the optimum operational conditions for the milling process as given in Genç (2008). Specific energy consumption of the process can be reduced which will accordingly reduce the annual total electrical energy consumption of the grinding stage when mills are operated at optimum conditions as stated in Genç (2008).

Best way for optimization of the energy consumption per ton of material produced is to build up reliable comprehensive mathematical models of the size reduction equipment as stated in Genç (2008). If reliable models of grinding equipment can be established, mills can be simulated for the estimation of the optimum conditions and thus, size reduction or grinding models are required for the design and simulation of comminution equipment and circuits as given in Genç (2008).

Components of size reduction models are specific breakage rate, discharge rate and breakage distribution functions of particles in the mill as mentioned in Genç (2008). Reliable laboratory and industrial scale grinding data which gives information on grinding performance of the mills under different operational conditions, are required to establish reliable predictive grinding models as stated in Genç (2008). Thus, it is important to investigate the effect of different operational parameters such as ball size, ball load, feed size distribution etc. on grinding performance and thus, resulting data can be used to estimate specific breakage rate functions to establish models of grinding mills as stated in Genç (2008). Relationship among the operational and design parameters of the size reduction equipment, breakage and discharge rates should be defined for simulation work as stated in Genç (2008).

Ball charge distribution is one of the important parameter of ball mill grinding which effects size reduction performance and consequently energy consumption of the mills as given in Genç (2008). Ball size effects on specific breakage rates of particles should be investigated and defined so that, realistic estimations on mill products can be done. Various size reduction models are defined in the literature to estimate breakage rates of particles most of which are complex that require a series of laboratory batch tests to estimate model parameters as mentioned in Genç (2008). Modelling approach, which is well known and widely applied was used in many research studies that requires batch grinding tests on monosize particles and determination of empirical coefficients for the estimation of specific breakage rates of monosize particles, was proposed by Austin (1984). More than one solution can be obtained in the estimation of empirical coefficients and thus, it is not an easily applicable modelling study by the engineers and researchers due to its complexity as mentioned in Genç (2008). Perfect mixing modelling approach which was developed by Whiten (1976) does not require complex

calculations for the estimation of specific breakage rates of particles and is more practical and thus, widely used to model grinding mills in industrial scale applications as mentioned in Genç (2008).

In this thesis, an average specific breakage rate function was estimated from the perfect mixing model by using a full mill feed size distribution instead of estimating the specific breakage rates of monosize particles as in the work of Austin et.al. (1984). Batch grinding tests were performed using different ball charge distributions in which material was ground in the mill for different residence time intervals and the changes in specific breakage rates of particles were investigated as stated in Genç (2008). Effects of ball size and its distribution on mill product fineness and breakage rate functions could have been investigated as different ball charge distributions were used in the batch tests for chromite ore grinding. Specific energy consumptions of the grinding processes were estimated according to the Bond's theory (1952) and results were evaluated as a function of mill product fineness and residence time.

2. GENERAL INFORMATION ON CHROMITE ORE

Chromium is a chemical element and its symbol is “Cr” with a atomic number of 24 and atomic weight of 52g/mole and the name of the element is coming from the Greek word “Chroma” which means color as many chromium compounds are colored as given in Brandes (1956). Chromium metal can be economically produced from a chromite ore. It is a steely-grey, lustrous, hard and brittle transition metal as given by Brandes et.al. (1956) and as stated in Acar and Anagül (2018). Chromium has remarkable magnetic properties and is the only elemental solid which shows anti-ferromagnetic at room temperatures and below and it changes to paramagnetic above 38°C as mentioned in Fawcett (1988). Chromite is an oxide mineral composed of iron, chromium, and oxygen with a chemical formula of FeCr_2O_4 as mentioned in Acar and Anagül (2018).

Sellable chromite ore products are chromite concentrate, ferrochrome and chromium metal and the main use of chromite concentrate is the production of stainless steel in the metallurgical industry as given in Papp (1994). Approximately 90% of chromium is used in stainless steel production and special steel production by electroplating with chromium in the industry mostly to produce ferrochromium and chromium metal as mentioned in Callaghan (2013). 6% is recorded to be used in chemical industries such as pigment, catalyst and wood preservative and the rest which is 4% is used in foundry and refractory industries as it shows high resistance to temperatures around 2000°C as given in Callaghan (2013). Ferrochromium alloy (FeCr) is commercially produced from chromite by carbothermic, silicothermic or aluminothermic reactions and chromium metal is produced from chromite by roasting and leaching processes followed by reduction with aluminum as stated in Acar and Anagül (2018). Chromium metal has a high corrosion resistance and hardness value thus, stainless steel can be made highly resistant to corrosion and discoloration by adding metallic chromium as mentioned in Acar and Anagül (2018).

2.1. Chromite Deposits

The ore mineral in all chromite ore deposits is chromite as stated in Anonymous (2017). Chromite ore deposits in the world are magmatic and found in various levels within basic and ultrabasic rocks but found mostly in ultrabasic rocks as stated in Anonymous (2017). Chromite crystals are primarily fractionally crystallized from magma and accumulate at certain levels due to their density to form chromite ore deposits and chromite is mostly crystallized after olivine and before orthopyroxenes as given in Anonymous (2017).

Chromite is generally found as orthocumulate lenses in ultrabasic rocks such as peridotites and also occurs in layered ultramafic intrusive rocks and found in metamorphic rocks such as serpentinites as stated in Gu and Wills (1988). Chromite is associated with olivine, magnetite and serpentine and clayish gangue embedded in chromite crystals formed by ultrabasic rocks such as dunite and serpentinite as given in the report of DPT (2001). Chromite ore is characterized as massive, disseminated, nodular, orbicular, banded, massive banded and disseminated banded according to the abundance, texture and embedding type of the chromite crystals in the ultrabasic hosting rock as given in the report of DPT (2001). Chromite deposits generally exist as stratiform and podiform type since they are feasible to process them as stated in Murthy et.al. (2011) and Papp and Lipin (2001). The origin of the ultrabasic-basic rock assemblages in the chromite deposits, geological location, mineralogy, texture, etc. are the characteristics used to classify chromite deposits into three main types by Gültekin (2006), and Önal et.al. (1986) which are given as below:

1. Chromite deposits associated with stratiform intrusions found in straddle continental regions (cratons) such as Bushveld (South Africa) and Stillwater (United States) and they are large, layered beddings of continuity for kilometers and structurally complex as stated by Gültekin (2006), and Önal et.al. (1986). The small grains are tall, uniformly crystalline with low Cr/Fe ratio and high amount of iron ore and stratified type deposits constitute 90% of the world's chromium reserve whose ages are mainly Paleozoic as given in Gültekin (2006), and Önal et.al. (1986).

2. Chromite deposits known as podiform type are associated with ultrabasic-basic rock assemblages which are known as ophiolite deposits and often referred as Alpine types due to their appearance during the Alpine belt formation as given in Gültekin (2006), and Önal et.al. (1986). Alpine types are lenticular or irregular shaped, generally small sized, complex structures and coarse grains have irregular crystal shape, high Cr/Fe ratio and high chromium content and their ages are inverted type of which are usually observed at places where tectonism is abundant, and the changes that they undergo are tectonic movements and magmatic events as given in Gültekin (2006), and Önal et.al. (1986).
3. Chromite deposits which are connected to concentric ultrabasic rock assemblages with concentric interior planes are not economically feasible today as there is no production from these types of beds, which are usually found in Alaska as stated by Gültekin (2006), and Önal et.al. (1986). However, it is known that, studies on the enrichment tests of chromite ore from these type of deposits showed that, such beds usually contain high amount of iron chromium ore and their economics have been carried out in the United States as stated by Gültekin (2006), and Önal et.al. (1986).

The result of magmatic differentiation, during cooling from magmatism result in the formation of rich chromite deposits as given in the report of DPT (2001). All of the chromite deposits were formed in the auto-magmatic phase and the degree of crystallization of the chromite minerals is very high and they sometimes crystallize before the olivine and sometimes with the silicates, according to the degree of saturation of Magma as stated in Önal et.al. (1986). Its typical specific gravity is between 4.1-4.5g/cm³ and hardness is 5.5 and Cr₂O₃ content in the chromite composition ranges from 17 to 68% which determines the quality of the ore as expected that, this ratio is 48% and that of Fe/Cr ratio is 1/3 in the market as stated in Hacıoğlu (2010).

2.2. Physical and Chemical Properties of Chromite

Main characteristics of chromite ore is presented in Table 2.1 whereas atomic, physical and other properties are presented in Table 2.2 and Table 2.3 respectively as given in Hacıoğlu (2010).

Table 2.1. Main characteristics of chromite ore (Hacıoğlu, 2010)

Chromite ore characteristics	
Atom Number	24
Element Series	Transition Metals
Group, Periods, Blocks	6,4,d
Appearance	Metallic Silver
Atom Weight	51.9961 g·mol ⁻¹
Electron Array	[Ar] 3d ⁵ 4s ¹
Energy Level, Electron Press	2, 8, 13, 1 (Image)

Table 2.2. Atomic properties of chromite ore (Hacıoğlu, 2010)

Chromite's	Properties
Crystal Structure	Cubic
Electronegativity	1.66 (Pauling scale)
Ionization Energy	1 st : 652.90 kJ·mol
Atom Radius	128 ppm
Covalent Radius	139±5 ppm

Table 2.3. Physical and other properties of chromite ore (Hacıoğlu, 2010)

Physical Properties		Other Properties	
Substance State	Solid	Thermal Conductivity	(300K) 93.90 W·m ⁻¹ ·K ⁻¹
Density	7.19 g·cm ⁻³	Electrical Resistance	(20 °C) 125 nΩ·m
Liquid state	6.30 g·cm ⁻³	Young's modulus	279 GPa
Melting point	2180 K, 1907°C	Shear Modulus	115 GPa
Boiling Point	2944 K, 2671°C	Thermal Expansion	(25°C) 4.90 μm·m ⁻¹ ·K ⁻¹
Melting Heat	21.00 kJ·mol ⁻¹	Sound Speed	(20°C) 5940 m/s
Evaporation Heat	339.50 kJ·mol ⁻¹	Mohs Hardness	8.5
Heat Capacity (at 25 °C)	23.35 J·mol ⁻¹ ·K ⁻¹	Vickers Hardness	1060 MPa
		Brinell Hardness	1120 MPa
		Poisson's ratio	0.21

2.3. Mineralogy of Chromite Ore

There are variety of chromium bearing minerals such as fuchsite $[K(Al, Cr)_2(AlSi_3O_{10})(OH)_2]$ and uverovite $[Ca_3Cr_2(SiO_4)_3]$ in nature as stated by Knorring et.al. (1986). However, chromite is the only mineral that can be economically mined to produce chromium and chromite is an iron chromium oxide mineral with a chemical formula of $FeCr_2O_4$ as given in the report of DPT (2001). Chromite mineral belonging to the spinel group is crystalized in the cubic system and the theoretical formula is given by $FeCr_2O_4(Mg, Fe)(Cr, Al, Fe)_2O_4$ as recorded in the report of DPT (2001).

Due to the spinel structure, “Fe” and “Cr” may be substituted by “Mg” and “Al” and some other elements to form $(Mg, Fe)(Cr, Al, Fe)_2O_4$ which represents the common occurrence of chromite in nature as stated by Acar and Anagül (2018). The grade of “Cr” varies in the ore depending on the degree of replacement of the elements in the spinel crystal structure of the chromite ore as stated by Acar and Anagül (2018).

The typical accompanying secondary minerals found in chromite deposits are mainly harsburgite, olivine, serpentine, and talc while magnesite and hematite vary in the minor amounts as stated by Günay and Çolakoğlu (2015). Chromium (Cr) minerals and their properties are given in Table 2.4 as given in the report of DPT (2001). Typical chromite ore, gangue and guided minerals in addition to chromium minerals and their properties are given in

Table 2.5 as given by Hacıoğlu (2010).

Table 2.4. Chromium (Cr) minerals and their properties (Hacıoğlu, 2010)

Chromium minerals	Cr ₂ O ₃ %	Crystal system	Color	Stripe Color	Hardness	Specific weight (g/cm ³)
Chromite	68.00	Cubic	Black	Dark Brown	5.5	4.5
Uvarovite	30.60	Cubic	Green	Green	7	3.1
Krokoit	30.10	Monoclinal	Yellow-Red	Orange	2.5	
Dietzeit	15.30	Monoclinal	Golden Yellow	-	3.4	3.7
Phoneix	17.50	Orthorombic	Yellow-Red	Brick-Red	3	5.7
Bellit	17.30	Hexagonal	Yellow-Orange	-	2.5	5.5

Table 2.5. Chromite ore, gangue and guided minerals (Hacıoğlu,2010)

Chromite ore minerals	Gangue Minerals	Guided minerals
Magnetite	Olivine (Forsterite to Fayalite)	Kammererite
Titanomagnetite	Pyroxene (Enstatite, Hypersten, Bronzite)	Uvarovite
Pyrotine	Serpentine Group (Antigorite, Lizardite, Chrysotile)	-
Chalcopyrite	Magnesia	-
Pyrite, Ilmenite, Rutile	Talc	-
Platinum Group Metals	Chlorite	-

2.4. Chromite Reserves in the World

World's total chromite reserve is recorded to be 510 million tons with a 45% Cr₂O₃ content and Turkey is ranked fourth in the world with a share of around 9% with 2.8 million tons of chromite production as recorded in the report of USGS (2018). World's chromite production and reserves are given in Table 2.6 as recorded in the report of USGS (2018).

Table 2.6. World's chromite mine production and reserves (USGS, 2018)

Country	Mine Production ¹ (thousand tons)		Reserves ² (Shipping grade) ³
	2016	2017 ⁴	
Kazakhstan	5,380	5,400	230,000
South Africa	14,700	15,000	200,000
India	3,200	3,200	54,000
Turkey	2,800	2,800	26,000
Others	4,160	4,200	NA
World total (rounded)	30,200	31,000	510,000

¹gross weight of marketable chromite ore

²based on specific definition and may change according to market conditions

³equivalents of 45% Cr₂O₃ grade

⁴estimated

Turkey was in the first row in the world rankings in chromite ore production for some years and in the world it is placed in the row between 3rd and 6th in the recent years as mentioned in the report of DPT (2001).

2.5. Genesis of Chromite Deposits in Turkey

Ultrabasic rocks with generic name of peridotites which host chromite minerals are ophiolitic rocks cover wide areas in Turkey and are located along the Alpine orogeny belt as given in Acar and Anagül (2018). The chromite deposits in these peridotites are named as alpine type (podiform type) and their complex structural associations, textural properties and relatively small scale of deposition are characteristics of alpine type chromite deposits as given in Acar and Anagül (2018). They are spreaded alongside the tethyan belt across Turkey within ultrabasic rocks with disorganized distribution. There are more than 800 chromite occurrences within individual or a group deposition identified in Turkey and can be grouped into six regions geographically according to their importance which are given in Table 2.7 and Figure 2.1 respectively as stated in Acar and Anagül (2018).

Table 2.7. Chromite ore deposits in Turkey (Acar and Anagül, 2018)

Rank	Region
1	Guleman (Elazığ)
2	Fethiye-Köyceğiz-Denizli
3	Bursa-Kütahya-Eskişehir
4	Mersin-Karsanti-Pınarbaşı
5	Erzincan-Kopdağ
6	İskenderun-Kahramanmaraş

CHROMITE ORE DEPOSITS IN TURKEY

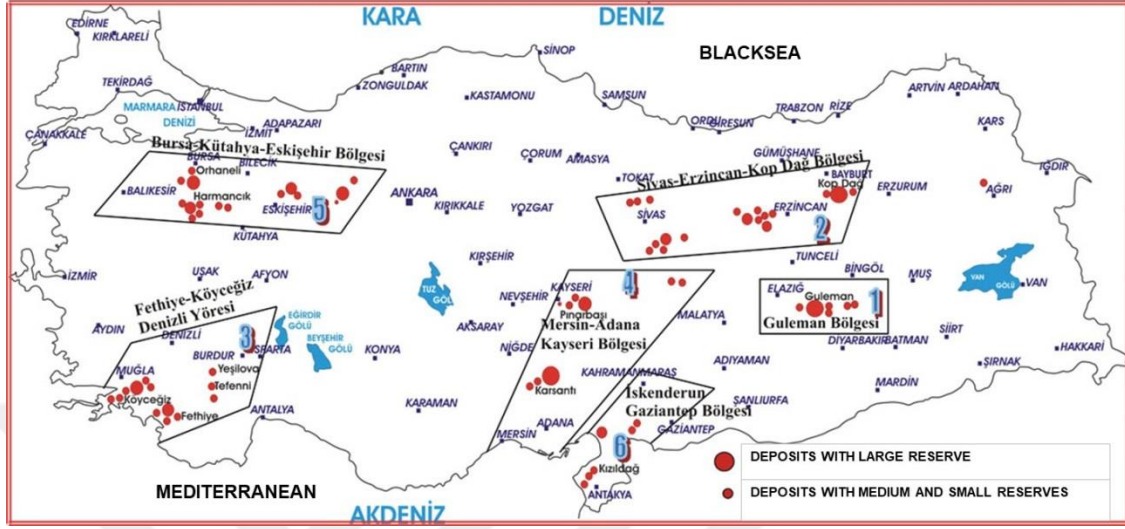


Figure 2.1. Distribution of chromite ore deposits in Turkey

There are important chromite deposits in the Guleman region which is a district 65-70km south east of Elazığ and these deposits are called “Sark chromite” deposits and are classified into three types according to geology as mentioned by Özkan (1982) and Çakmak (2006). The Kef mountain type chromite beds are one of these and they are in the form of two similar beds lined up 800meters long in east-west direction as stated in Çakmak (2006). These are called the Kef and western Kef mountain chromite deposits and the length of the western Kef mountain deposit is about 1km and the thickness of this deposit varies between a few meters to 50m as given in Acar and Anagül (2018).

The chromite deposit in Guleman region shows different physical, structural and elemental characteristics in different locations such that, the massive chromite ore body has Cr_2O_3 grade usually between 20% and 46% while the Al content of the high-grade ores varies depending on the location between 8% and 16% as given in Acar and Anagül (2018). The Cr_2O_3 grade of the pure chromite ore is limited to approximately 48-50% especially in the Kef region due to the substitution of Fe and Cr elements by Al and Mg in spinel crystal structure which is relatively high as compared to the other regions as stated in Acar and Anagül (2018). Chromite crystals with less than 1mm size are embedded in a matrix composed of olivine and serpentine in lower grade ore bodies and

the grade of that type of chromite ores changes between a few per cent to 30% Cr_2O_3 as stated in Acar and Anagül (2018). It is required to concentrate that type of ores to higher grades before feeding them to electric arc furnace (EAF) and the reasons for such concentration process are given as follows: the reduction process is conducted at high temperatures in EAF so the mass to be smelted should be reduced by removing the siliceous gangue in order to reduce the energy consumption; the Fe content of the gangue minerals decreases the Cr/Fe ratio of the feed which reports to the metal during reduction process and leads to the production of lower quality FeCr alloy with lower Cr%, Mg and Al contents of the feed should be kept in certain level as they affect the smelting temperature and viscosity of the furnace feed and also gangue minerals which are olivine and serpentine are rich in Mg and Al and they need to be removed from the feed down to certain levels before the reduction process and Si content of the gangue material effects the quality of the finished FeCr alloy as some portion of Si may report to the metal as stated in Acar and Anagül (2018).

2.6. Chromite Ore Deposits and Reserves in Turkey

Peridotites which are ultrabasic rocks cover large areas in Turkey and a significant distribution pattern showing the chromite deposits in Turkey are spread across the country over the peridotites as given in the report of DPT (2001). Totally, one thousand single or groups of chromite ore bed occurrences are available in Turkey and their distribution in the geographical direction can be classified into regions which are known as major occurrences and given below with $\text{Cr}_2\text{O}_3\%$ content values as mentioned in the report of DPT (2001).

1. Guleman-Elazığ region in which the deposits are; West Kef (6.8 million tons, 33%), Eastern Kef (500,000tons, 40-45%), Sori Quarries (2.5 million tons, 42-48% and 43-47%) as given in the report of DPT (2001),
2. Fethiye-Köyceğiz-Denizli region in which the deposits are; Kazandere-Karaismailler (800,000tons, 30-38%), Üzümlü-Sazlı (100,000tons, 36%), Biticealan (102,000tons, 44-

48%), Kazandere (236,000tons, 37.5%), Kandak (100,000tons, 40-46%) as given in the report of DPT (2001),

3. Bursa-Kütahya-Eskişehir region in which the deposits are; Harmancık-Başalan (163,000tons, 20%), Ömeraltı-Kınalıbatak (100,000tons, 23%), Miran-Hudut-Koca Ocaklar (120,000tons, 43%), Orhaneli-Karıncalı (40,000tons, 5-30%),

4. Bursa region in which the deposit is Büyükorhan-Kırocak (277,000tons, 10-18%), as given in the report of DPT (2001),

5. Eskişehir region in which the deposits are; Eskişehir-Karaburhan (1,800,000tons, 22-26%), Eskişehir-Karacaören (35,000tons, 15-45%), Kavak Chromites (1 million tons, 30-45%) as given in the report of DPT (2001),

6. Mersin-Adana-Kayseri region in which the deposits are; Adana-Aladağ (198 million tons, 5.60%), Kayseri-Pınarbaşı-Dedeman (490,000 tons, 20-30%) as given in the report of DPT (2001),

7. Sivas-Erzincan-Kopdağ region in which the deposits are; Sivas-Kangal-Karanlıkdere (2.3 million tons, 5-15%),

8. Erzurum-Erzincan-Bayburt region in which the deposit is Erzincan-Kopdağ (3.6 million tons, 38-54%) as given in the report of DPT (2001),

9. Sivas region in which the deposit is Karadere (55,000 tons, 43-44%) as given in the report of DPT (2001),

10. İskenderun-Kahramanmaraş region in which the deposit is Hatay-Kızıldağ (117,000 tons, 34-44%) as given in the report of DPT (2001).

2.7. Chromite ore concentration processes

Chromite concentrates that contain different chromite grades, varying from lumpy chromite to fine size concentrates, are produced in Turkey and gravity methods which are based on the density differences between chromite and gangue minerals are often used in concentration plants as mentioned in Burt (1987) and Güney et.al. (2009). Heavy

medium separation and jigs in coarse sizes whereas spiral, shaking table, magnetic separators, multi gravity separators and flotation in fine sizes (approximately below 0.5mm) are well known methods as mentioned in Burt (1987) and Güney et.al. (2009).

Jigging and shaking table processes are combined in some plants such as in Eti Krom Inc. AGK Plant in Elazığ in Turkey as mentioned by Acar and Anagül (2018). Spirals are preferred in South Africa due to their high capacities and lower construction layout although their efficiency is low as mentioned by Acar and Anagül (2018). Shaking tables are mostly applied in Turkey due to the precise control of operational parameters as stated by Güney et.al. (1993), Güney (1992;1994), Özdağ et.al. (1993;1994), Uçbaş and Özdağ (1994). However, performance of shaking tables is inefficient below 100µm and thus, their recoveries are low and rejected waste material from shaking tables have considerable economic value as mentioned in Güney et.al. (1993), Güney (1992;1994), Özdağ et.al. (1993;1994), Uçbaş and Özdağ (1994).

The most encountered problems in the plants are disregarded mineral properties and over-grinding of materials and both cases consume significant amount of energy and valuable mineral losses in slime fractions as given in Yüce et.al. (2017). In this context, it is very important to investigate the mineralogical structure of the ores, liberation degree of valuable and gangue minerals, grindability which can be characterized by the Bond work index value.

Heavy medium separation is another method used to concentrate chromite ore which can be applied as in Kazakhstan below 100mm to clean massive high-grade chromite ore from the internal and external dilution of hosting rock as mentioned by Acar and Anagül (2018). Optical and X-ray sorters have been recently applied for coarsely liberated minerals as mentioned by Acar and Anagül (2018). However, there is not any recorded application in industrial scale plants as stated in Acar and Anagül (2018). Optical sorters may become popular for the concentration of coarse sizes of light colored gangue such as serpentine and olivine as similar to hand picking as stated in Acar and Anagül (2018). High intensity wet magnetic separators were used but they were inefficient in terms of recovery and product grade as given in Acar and Anagül (2018). Wet magnetic separators can be applied to separate free hematite (Fe_2O_3) from the final concentrate to

increase the Cr/Fe ratio and it was shown that, Cr/Fe ratio of a chromite ore from Kayseri region can be increased from 2.19 to 2.30 with 95.39% recovery by applying 2200 Gauss in permanent wet magnetic separator as given in Acar and Anagül (2018).

Flotation, hydrometallurgy, Multi Gravity (MGS) and magnetic separation processes have become popular in the concentration of low grade chromite ores and plant tailings in the recent years as stated in Acar and Anagül (2018). As the difference between magnetic susceptibility between chromite and gangue minerals is limited, low separation efficiencies and concentrate qualities are obtained as also stated in Acar and Anagül (2018).

Table 2.8. Physical properties of chromite, olivine and serpentine (Dahlin and Rule, 1993)

Mineral	Chemical Formula	Magnetic Susceptibility χ ($10^{-9} \text{ m}^3/\text{kg}$)	Density (g/cm^3)	Color
Chromite	$(\text{Mg, Fe})(\text{Cr, Al, Fe})_2\text{O}_4$	586-1088	4.1-4.9	Black
Olivine	$(\text{Mg}^{2+}, \text{Fe}^{2+})_2\text{SiO}_4$	204-2088	3.3-3.4	White-Gray
Serpentine	$(\text{Mg, Fe, Ni, Al, Zn, Mn})_{2-3}(\text{Si, Al, Fe})_2\text{O}_5(\text{OH})_4$	1100-6300	2.5-3.2	Dark Green

3. COMMINATION

3.1. Comminution Fundamentals

Comminution can be defined as the reduction of solid materials from a coarser particle size to a smaller particle size by crushing and grinding mechanisms as stated in Lynch (2015). Objective of comminution processes for ores is to reduce the size of coarse rocks to a size at which particles of valuable minerals can be liberated and concentrated as given in Lynch (2015). Crushing reduces the particle size of run-of-mine ore to a level that, the grinding mill can produce valuable and gangue minerals as liberated particles as stated in Lynch (2015). Crushing mechanisms are impact, compression, abrasion, and attrition as mentioned in Lynch (2015). Compression is performed by compression of ore against rigid or particle surfaces, impact is performed by rapid loading where force is applied almost normally to the particle or rigid surface in both mechanisms as stated in Wills and Finch (2016) and also as given in Lynch (2015). Crushing is a dry process and it is performed in several stages and reduction ratio which is defined as the ratio of maximum particle size entering the crusher to the maximum particle size leaving the crusher, can be within the range of three to six as given in Lynch (2015). Crushers in use are gyratory, jaw, cone, roll and impact crushers as stated in Lynch (2015).

Grinding mechanisms are impact (tumbling mills), compression (roller mills), abrasion (tumbling mills) as given in Lynch (2015). Grinding of ores are performed usually wet as most concentration processes are carried out as slurries whereas dry grinding has limited applications as given in Lynch (2015). Tumbling mills use steel rods, steel balls, or sized ore which are applied in AG and SAG mills as grinding media whereas stirred or agitated mills use a stirrer to provide motion to the steel, ceramic or rock media as given in Lynch (2015). Both vertical and horizontal configurations exist and can be operated with smaller media sizes and thus they are more suitable for fine grinding than tumbling mills as stated in Lynch (2015). Stirred mills are thought to be more energy efficient up to 50 per cent as compared to conventional ball mills as stated by Stief et.al. (1987) and they are now widely used for fine comminution as given in Lynch (2015).

3.1.1. Comminution Theories

Comminution theories concerned with the relationship between energy input and the particle size produced from a given feed size and the general form of the energy-size reduction relationship is given by Equation (3.1) in Kelly and Spottiswood (1982) as also given in Genç (2008). This empirical equation is the generalized form of the theoretical and empirical energy-size reduction equations of Rittinger, Kick, Bond, Holmes, Charles, Svensson and Murkes and others as stated in Kelly and Spottiswood (1982) and also given in Genç (2008).

$$\frac{dE_o}{dx} = \frac{-K}{x^n} \quad (3.1)$$

“ E_o ” is the specific energy necessary to supply the surface energy of the new surface, “ x ” is the particle size, “ n ” and “ K ” are constants as stated in Kelly and Spottiswood (1982). Breakage energy is proportional to the new surface area produced according to the Rittinger theory, and the relationship is given by Equation (3.2) as stated in Kelly and Spottiswood (1982) and also given in Genç (2008).

$$E_o = K_2 \left(\frac{1}{x_o} - \frac{1}{x_t} \right) \quad (3.2)$$

“ x_t ” is the initial particle size, “ x_o ” is the particle size after the breakage event, “ K_2 ” is a constant as given in Kelly and Spottiswood (1982).

Equivalent geometrical changes in the sizes of particles require equal energy according to Kick’s law and the relationship is given by Equation (3.3) where “ K_3 ” is a constant as stated in Kelly and Spottiswood (1982) and also given in Genç (2008).

$$E_o = K_3 \ln \left(\frac{x_t}{x_o} \right) \quad (3.3)$$

Bond's comminution theory is given by Equation (3.4) as given in Kelly and Spottiswood (1982).

$$E_o = K_4 \left(\frac{1}{\sqrt{x_{80,o}}} - \frac{1}{\sqrt{x_{80,l}}} \right) \quad (3.4)$$

“ $x_{80,o}$ ” is “80%” passing size before the breakage event, “ $x_{80,l}$ ” is the 80 per cent passing size after the breakage event and “ K_4 ” is a constant as given in Kelly and Spottiswood (1982).

Holmes, Charles, Murkes and Svensson have used a size distribution in the energy-size reduction relationship which is given by Equation (3.5) as given in Kelly and Spottiswood (1982).

$$E_o = K_5 (x^*)^{-n_1} \quad (3.5)$$

“ x^* ” is the size modulus as described in the Gates-Gaudin-Schuhmann equation, “ n_1 ” and “ K_5 ” are constants as given in Kelly and Spottiswood (1982).

3.2. Mathematical Models of Comminution

Size reduction models are required for the design and simulation of comminution equipment and if reliable models of comminution machines could be established, mills could be simulated for the estimation of the optimum conditions for the grinding process as mentioned in Genç (2008). Specific breakage rates of particles at different operational conditions should be investigated to establish reliable grinding models to be able to make reliable predictions on mill product fineness and thus size reduction performance at different operational conditions as mentioned in Genç (2008). Additionally, relationships between breakage rate and design and operational parameters should be established to perform simulations using the established grinding models. In this context, grinding models were introduced as mentioned in Genç (2008).

There are two basic models to represent size reduction process which are matrix and kinetic models as given in Lynch (1977). Comminution is considered as a succession of breakage events in the matrix model and feed to each breakage event is the product from the previous event as stated in Lynch (1977). Comminution is considered as a continuous process in the kinetic model and the longer the period of grinding and greater is the size reduction attained as stated in Lynch (1977) and also given in Genç (2008). Both models are based on the concepts of selection or breakage rate function which can be defined as the probability of breakage and breakage distribution or appearance function which can be defined as the characteristic size distribution after breakage event and classification or discharge rate function or size dependent diffusion coefficient which can be defined as the differential movement of particles through or out of a continuous mill that is generally size-dependent as stated in Lynch (1977) and also given in Genç (2008).

3.2.1. Matrix model

Probability of breakage of each size fraction and size distribution of each broken product was given in a matrix model by Broadbent and Callcott (1956) as given in Lynch (1977).

Table 3.1. Feed and product size distributions from a size-reduction process (Lynch, 1977)

Size range	Feed	Product
1	f1	p1
2	f2	p2
3	f3	p3
.	.	.
.	.	.
n	fn	Pn
n+1	fn+1	pn+1

Size fraction (range) one is the maximum size and “(n+1)th” size fraction refers to the subsieve sample in Table 3.1 as given in Lynch (1977). Particles in all size fractions have some probability of being broken and the products of breakage may fall in that size interval and in any smaller size interval during the grinding process as stated in Lynch (1977) and also given in Genç (2008).

Table 3.2. Mass balance for a size-reduction process (Lynch,1977)

Size range	Feed	Product						
1	f_1	$P_{1,1}$	0	0	.	.	0	0
2	f_2	$P_{2,1}$	$P_{2,2}$	0	.	.	0	0
3	f_3	$P_{3,1}$	$P_{3,2}$	$P_{3,3}$.	.	0	0
.
.
N	f_n	$P_{n,1}$	$P_{n,2}$	$P_{n,3}$.	.	$P_{n,n}$	0
n+1	f_{n+1}	$P_{n+1,1}$	$P_{n+1,2}$	$P_{n+1,3}$.	.	$P_{n+1,n}$	$P_{n+1,n+1}$

“ $\sum_1^{n+1} f_i$ ” represents the total feed mass F as given in Lynch (1977). The particles falling in the subsieve fraction which is “n+1” can be calculated for both feed and product by subtracting the cumulative weight retained on size “n” from “F” and the element “ $p_{i,j}$ ” in the array representing the products of breakage may be written as “ $p_{i,j}=X_{i,j} \cdot F_j$ ” where “ $X_{i,j}$ ” represents the mass fraction of the particles in the “jth” size fraction in the feed which fall in the “ith” size fraction in the product as stated in Lynch (1977) and the product array may be re-written as shown in Table 3.3 as also given in Genç (2008).

Table 3.3. The product from a size-reduction process expressed in terms of the feed (Lynch, 1977)

$X_{1,1} \cdot f_1$	0	0	.	.	0
$X_{2,1} \cdot f_1$	$X_{2,2} \cdot f_2$	0	.	.	0
$X_{3,1} \cdot f_1$	$X_{3,2} \cdot f_2$	$X_{3,3} \cdot f_3$.	.	0
.
.
$X_{n,1} \cdot f_1$	$X_{n,2} \cdot f_2$	$X_{n,3} \cdot f_3$.	.	$X_{n,n} \cdot f_n$

Size reduction process can be represented by the matrix equation given in Equation (3.6) as stated in Lynch (1977) and also given in Genç (2008).

$$p = X \cdot f \tag{3.6}$$

Table 3.4. General matrix equation of breakage (Lynch, 1977)

$$\begin{bmatrix} x_{1,1} & 0 & 0 & \cdot & \cdot & 0 \\ x_{2,1} & x_{2,2} & 0 & \cdot & \cdot & 0 \\ x_{3,1} & x_{3,2} & x_{3,3} & \cdot & \cdot & 0 \\ x_{4,1} & x_{4,2} & x_{4,3} & \cdot & \cdot & 0 \\ x_{5,1} & x_{5,2} & x_{5,3} & \cdot & \cdot & 0 \\ \cdot & \cdot & \cdot & \cdot & \cdot & 0 \\ \cdot & \cdot & \cdot & \cdot & \cdot & 0 \\ x_{n,1} & x_{n,2} & x_{n,3} & \cdot & \cdot & x_{n,n} \end{bmatrix} * \begin{bmatrix} f_1 \\ f_2 \\ f_3 \\ f_4 \\ f_5 \\ \cdot \\ \cdot \\ f_n \end{bmatrix} = \begin{bmatrix} x_{1,1} \cdot f_1 + 0 + \dots + 0 \\ x_{2,1} \cdot f_1 + x_{2,2} \cdot f_2 + 0 + \dots + 0 \\ x_{3,1} \cdot f_1 + x_{3,2} \cdot f_2 + x_{3,3} \cdot f_3 + \dots + 0 \\ x_{4,1} \cdot f_1 + x_{4,2} \cdot f_2 + x_{4,3} \cdot f_3 + \dots + 0 \\ x_{5,1} \cdot f_1 + x_{5,2} \cdot f_2 + x_{5,3} \cdot f_3 + \dots + 0 \\ \dots \\ \dots \\ x_{n,1} \cdot f_1 + x_{n,2} \cdot f_2 + x_{n,3} \cdot f_3 + \dots + 0 \end{bmatrix} = \begin{bmatrix} p_1 \\ p_2 \\ p_3 \\ p_4 \\ p_5 \\ \cdot \\ \cdot \\ p_n \end{bmatrix}$$

3.3.3.1. The selection function

Particles of all sizes which enter a grinding process have some probability of being broken and this probability may change as the size of the particle changes and a certain proportion of the particles in each size fraction is selected for breakage and the remainder pass through the process unbroken during the size reduction process as stated in Lynch (1977). If “S₁” is the proportion of particles in the largest size range which is selected for breakage, then the mass of particles in that size range which is broken will be “S₁.f₁” and the mass of particles that are broken in the “nth” size range will be “S_n.f_n” as given in Lynch (1977). Matrix equation can be written as in Table 3.5 as given in Lynch (1977).

Table 3.5. Selection in a size-reduction process (Lynch, 1977)

$$\begin{bmatrix} S_1 & 0 & 0 & 0 & \cdot & \cdot & 0 \\ 0 & S_2 & 0 & 0 & \cdot & \cdot & 0 \\ 0 & 0 & S_3 & 0 & \cdot & \cdot & 0 \\ \cdot & \cdot & \cdot & \cdot & \cdot & \cdot & \cdot \\ \cdot & \cdot & \cdot & \cdot & \cdot & \cdot & \cdot \\ 0 & 0 & 0 & 0 & \cdot & \cdot & S_n \end{bmatrix} * \begin{bmatrix} f_1 \\ f_2 \\ f_3 \\ \cdot \\ \cdot \\ f_n \end{bmatrix} = \begin{bmatrix} S_1 & f_1 \\ S_2 & f_2 \\ S_3 & f_3 \\ \cdot & \cdot \\ \cdot & \cdot \\ S_n & f_n \end{bmatrix}$$

Selection function is denoted by S and the particles which are broken are represented by “S.f” as stated in Lynch (1977). The remainder of particles will pass through the process unbroken and the unbroken fraction will be “(1-S_n).f_n” for the “nth” size range and the total mass of particles which pass through the process unbroken may be represented by the product “(I-S).f” as given in Lynch (1977). Breakage process can be represented by Equation (3.7) and (3.8) as stated in Lynch (1977) and also given in Genç (2008).

$$p = B.S.f + (I - S).f \quad (3.7)$$

$$p = (B.S + I - S).f \quad (3.8)$$

3.3.2.2. The classification function

Many breakage events occur during a comminution process where selection and breakage occur in each breakage event as stated in Lynch (1977). However, product from each event may be subjected to some size classification process before some fraction of it is subjected to the next breakage event and the mathematical model of this event is given as in Equation (3.9) if the classification is insignificant and C approaches 0 as given in Lynch (1977).

$$p = (I - C).(B.S + I - S).[I - C.(B.S + I - S)]^{-1}.f \quad (3.9)$$

3.2.2. Kinetic model

Kinetic models are known as size-mass balance models or population balance models and these models consider comminution as a first order rate process as given in Genç (2008). The kinetic models were expressed in terms of continuous functions and as discretized distributions and resemble to matrix models as given in Genç (2008). Kinetic models consider the comminution as a continuous process with the amount of breakage dependent on the mass of material in a particular particle size fraction and the residence time of the particles of that size interval as given in Genç (2008). The first-order kinetic equation which defines the rate of breakage of particles was stated by Loveday (1967) as given in Equation (3.10) and also as given in Genç (2008).

$$\frac{dW(D)}{dt} = -k(D) * W(D) \quad (3.10)$$

“W(D)” is the weight of particles with a size of “D” and “K(D)” is the rate constant for size “D” which characterizes the rate of disappearance of each size fraction in Equation (3.10) as stated in Genç (2008). First order rate or kinetic model assumes that, the production of ground material per unit time within the mill depends only on the mass of that size fraction which is present in the mill contents as explained in Napier Munn et.al. (2005) and given in Genç (2008). First order breakage (normal breakage) prevail when particles are small as compared to the ball diameter. Breakage distributions have a constant slope and specific breakage rates of particles decrease as particles become smaller as stated by Austin (1984) and also as given in Genç (2008). Non-first order breakage (abnormal breakage) prevail when particles are too large for the ball diameter and if the mill is considered as a black box of volume “V” by containing a mass of powder “W” and the rate of breakage of size “i” will be given by Equation (3.11) as stated by Austin (1984) and also given in Genç (2008).

$$i = S_i \cdot w_i W \quad (3.11)$$

“i” is the size interval, “w_i W” is the mass of size “i”, “S_i” is the specific breakage rate as stated by Austin (1984) and also given in Genç (2008).

3.2.3. Size-Mass balance batch model

Breakage rate of particles of size “i” in a batch grinding is defined by Gardner and Austin (1962) by Equation (3.12) as given in Genç (2008).

$$\frac{dw_i(t)}{dt} = -r_i w_i(t) + \sum_{j=1}^{i-1} b_{ij} r_j w_j(t) \quad n \geq i \geq j \geq 1 \quad (3.12)$$

“ $W_i(t)$ ” is the mass fraction of particle size “i” at time “t”, “ r_i ” is the specific breakage rate of size “i”, “ b_{ij} ” is the breakage distribution function representing the mass fraction size “j” that appears at size “i” fraction after breakage and the net rate of production of size “i” material equals the sum rate of appearance from breakage of all coarser sizes minus the rate of its disappearance by breakage according to Equation (3.12) as given in Genç (2008).

The specific breakage rate (selection function) which is denoted by “ r_i ” and the breakage distribution (appearance function) which is denoted by “ b_{ij} ” are independent of time due to the first order hypothesis in the batch grinding model given in Equation (3.12) as given in Genç (2008). Breakage rate and breakage function can be determined from either laboratory batch grinding tests or back-calculation using functions given by Austin et al. (1984) as stated in Genç (2008). The solution of the batch grinding model for all particle size fractions was described by Reid (1965), Herbst and Fuerstenau (1968), Luckie and Austin (1972) as stated in Genç (2008). Validity of the first order hypothesis and ability of the batch grinding parameters to describe continuous grinding systems have been questioned in the literature by Harris (1969), Fruhwein (1976), Lynch (1977), Jowett and Weller (1979), Berube et al. (1979), Gupta (1986), Austin et al. (1982), Hopple (1983), Fuerstenau and Aboouzeid (1991) and it was reported that, specific breakage rate did not follow the first order hypothesis for different materials under certain experimental conditions as given in Genç (2008).

3.2.4. Population balance model

Population balance modelling approach was widely applied for the analysis of the comminution process among the size reduction models as stated in Lynch (1977) and the model was introduced by Epstein (1948) as stated in Genç (2008). Comminution process was described by two basic mechanisms as stated in Lynch (1977). These are, probability of breakage of a particle of size “y” in the “nth” step of the breakage process as denoted by “P_n(y)” and the distribution by weight of the particles of size “x” less than or equal to “y” arising from the breakage of a unit mass of size y as denoted by “F(x,y)” as stated in Lynch (1977) and also given in Genç (2008).

Any information about the material transport mechanism was not included in the Epstein’s model given by Epstein (1948) as stated in Lynch (1977). A matrix model was developed by Broadbent and Callcott (1956) and was applied to the grinding of coal which defines a size dependent material transport mechanism that was described as a classification function as stated in Lynch (1977) and also given in Genç (2008). Performance of a steady-state, fully mixed, continuous mill was described by Austin and Gardner (1962) based on the size-mass balance on the mill and the model is given by Equation (3.13) as stated in Lynch (1977) and also given in Genç (2008).

$$f_i - r_i w_i \tau + \tau \sum_{j=1}^{i-1} b_{ij} r_j w_j = p_i \quad n \geq i \geq j \geq 1 \quad (3.13)$$

“f_i” is the weight fraction of size “i” in the mill feed, “r_i” is the specific breakage rate of size fraction “i”, “w_i” is the weight fraction of size “i” in the mill contents, “b_{ij}” is the mass fraction of the size “j” that appears at size “i” fraction after breakage, “p_i” is the weight fraction of size “i” in mill discharge or product, “τ” is the mean residence time defined by the ratio of powder mass in the mill which is denoted by “W” to the mass of feed rate which is denoted by “F” and the value of “τ” is determined from experimental measurement of the residence time distribution (RTD) as stated in Lynch (1977) and also as given in Genç (2008). Many other researchers developed the model after Epstein (1948) such that, Kelsall et.al. (1969), Whiten (1974), Herbst and Fuerstenau (1968),

Herbst et.al. (1972), Austin and Brame (1983) and the model concepts are widely used in modern process simulation as stated in Genç (2008).

3.2.5. Estimation of ball mill model parameters

Three fundamental mathematical functions are defined in the ball model structure according to population balance approach which are specific breakage rate or selection function denoted by “ r ” which represents the probability of particles selected to be broken and breakage distribution or appearance function denoted by “ B ” which defines the breakage pattern of a particle after single breakage as stated in Lynch (1977). Transport or residence time distribution function (RTD) defines the transportation of particles through and out of the mill as stated in Austin (1984) and also given in Genç (2008).

Specific breakage rate function is a size reduction model parameter and gives information on the size reduction performance of the equipments. Breakage rate function denoted by “ r_i ” can be determined by two techniques which are laboratory batch grinding tests and back-calculation techniques as stated in Genç (2008).

3.2.6. Estimation of specific breakage rate from batch grinding tests

Size-discrete form of the population balance equation for batch comminution is linear and assumes first-order breakage kinetics as stated in Austin (1971). If the starting mill feed is all within the top size interval, the first size interval which is numbered as one will have material “ $W_1(0)=1$ ” in a batch mill as given in Austin (1984). The feed is ground for a time interval of “ t_1 ”, and the sample is removed from the mill as stated in Austin (1984). The fraction remaining still within the original size interval is determined by sieving and weighing and the sample is returned to the mill for further grinding for a time interval of “ t_2 ” and reanalyzed and so on as stated in Austin (1984) and also given in Genç (2008). This is a typical batch grinding procedure and the rate of disappearance of size one might fit to a first-order law as stated in Austin (1984) and also given in

Genç (2008). Breakage rate of material that is in the top size interval is given by Equation (3.14) as stated in Austin (1984).

$$\frac{d[w_1(t)W]}{dt} \propto w_1(t)W \quad (3.14)$$

Total mass “W” is constant in Equation (3.14) and thus the equation can be rewritten as in Equation (3.15) as stated in Austin (1984):

$$\frac{dw_1(t)}{dt} = -S_1 w_1(t) \quad (3.15)$$

Where; “S₁” is the proportionality constant and called specific rate of breakage with units of hour to the minus one as stated in Austin (1984) and also given in Genç (2008).

If “S₁” does not change with time, it can be concluded that, it is a first-order breakage process and in that case, Equation (3.15) can be rewritten as given in Equation (3.16) as stated in Austin (1984).

$$\log[w_1(t)] = \log[w_1(0)] - S_1 t / 2.3 \quad (3.16)$$

“w₁(t)” is the weight fraction of the mill hold-up of size one at time “t” and “S₁” is the specific breakage rate in Equation (3.16) as stated in Austin (1984) and also given in Genç (2008). Variation of the specific breakage rate denoted by “S_i” with particle size is given in Equation (3.17) as stated in Austin et.al. (1984) and also given in Genç (2008).

$$S_i = a_T X_i^\alpha \quad (3.17)$$

“X_i” is the upper limits of the size interval indexed by “i” in mm and “a_T” and “α” are model parameters that depend on the properties of the material and the grinding conditions as stated in Austin et.al. (1984) and also given in Genç (2008).

Operational variables in batch ball mills are ball diameter and ball size distribution, mill speed, grindability of material, material feed size distribution, fractional ball loading,

fractional material filling as stated in Austin et.al. (1984). Correlations between breakage rate parameters and the process variables such as mill diameter, ball diameter, ball load, percent critical speed were developed by Austin et al. (1984) as stated in Genç (2008). Breakage rate parameters were estimated from experimental size distributions for different grinding time intervals as given by Koka and Trass (1987), Yekeler et al. (2000), Kotake et al. (2000), Austin and Bagga (1981) as stated in Genç (2008). The kinetics of dry grinding of cement clinker and coals were investigated in a laboratory tumbling mill by Austin and Bagga (1981) as stated in Genç (2008). Effect of powder filling, fraction of mill critical speed on breakage rates were investigated by batch kinetic tests according to Austin's approach (1984) by Deniz (2002; 2003) as stated in Genç (2008). Effects of ball diameter and feed size on breakage rates using dry batch grinding conditions on limestone, trass and clinker samples based on a kinetic model were investigated by Deniz (2002) and the dry and wet grinding kinetics of a chromite ore from Konya-Beyşehir region and the effect of pulp density in a ceramic mill according to Austin's approach (1984) was investigated by Özkan et.al. (2006) as stated in Genç (2008).

3.2.7. Breakage distribution function

Breakage distribution function is a material specific parameter of comminution models and assumed to be invariant with process conditions that is usually expressed in a form which is independent of particle size as given in Genç (2008). Breakage function changes with comminution energy level but it may or may not change with particle size depending on the material tested as given in Narayanan (1986) and also stated in Genç (2008). Non-normalizable breakage distribution functions were reported by Austin and Luckie (1971;1972), Laplante and Redstone (1983), Spring et al. (1984), Gao and Forssberg (1990).

The breakage function is assumed to be normalized which means that, the cumulative breakage distribution function expressed on a relative basis which is given by " x_i/x_j " is independent of initial particle size as reported in Epstein (1948), Broadbent and Callcott (1956), Gardner and Austin (1962), Kelsall and Reid (1965), Austin et al. (1966), Herbst

and Fuerstenau (1968), Stewart and Restarick (1971), Schönert (1972), Fruhwein (1976), Whiten (1976), Lynch (1977), Krogh (1978), Kavetsky and Whiten (1982), Austin et al. (1982). Broadbent and Callcott (1956) modified Rosin-Rammler equation and defined a standard distribution of particles after breakage by Equation (3.18) as given in Napier Munn et.al. (2005):

$$B_{x,y} = \frac{\left(1 - e^{-x/y}\right)}{\left(1 - e^{-1}\right)} \quad (3.18)$$

“B(x,y)” represents the proportion of particles after breakage and this function represents the proportion of particles initially of size “y” which appear in size fractions smaller than “x” after breakage as stated in Napier Munn et.al. (2005) and also given in Genç (2008). The important point in this concept is the distribution obtained after the breakage of a particle relative to the initial size as stated in Genç (2008). Usage of a standard breakage distribution such as Broadbent and Callcott function was criticized by Bull et al. (1975), Austin and Weller (1982), Austin and Klimpel (1984), Narayanan (1986) as given in Genç (2008).

3.2.8. Discharge rate and residence time distribution functions

Material discharge mechanism was described in a different way in each type of ball mill model as stated in Napier Munn et.al. (2005) and also given in Genç (2008). Material transport was described by using a diagonal classification matrix to represent the size dependent material flow through the mill in the matrix models as stated by Lynch (1977). Retention time distribution (RTD) can be defined as the total time which the material remains in the mill as stated in Austin et al. (1984) and also given in Genç (2008). RTD depends on ball load and mill geometry and formulated in Equation (3.19) as given in Austin et al. (1984).

$$T = \frac{W}{F} \quad (3.19)$$

Where; “W” is the mass of the powder material in the mill or hold-up in the mill in “kg” and “F” is the feed rate in “kg/min” as stated in Napier Munn et.al. (2005) and also given in Genç (2008).

Particle size dependent residence time distribution was used to describe the probability of particles remaining inside the mill for a certain period of time in population balance models as stated by Austin et al. (1984). The RTD function was modelled by experimental measurement using tracer technique by Austin et al. (1984) or empirical equations by Mori et al. (1964) or perfect mixers in series by Kelsall et al. (1968), Horst and Freeh (1970), Gardner and Sukanjuajtee (1972) or a convective-diffusion model by Austin et al. (1971) as given in Genç (2008). RTD function depends on mill operating conditions such as circulating load, mill feed size distribution etc. as these variables affect the mass in the mill as stated in Austin et al. (1984) and given in Genç (2008).

A non-uniform material flow behaviour and a particle size dependent discharge rate function was used to describe the transport mechanism in perfect mixing models by Austin et al. (1984) as given in Genç (2008). Discharge rate function was normalized and related to the mill volumetric feed rate and mill dimensions in perfect mixing models as stated in Napier Munn et.al. (2005) and also given in Genç (2008).

3.2.9. Perfect mixing model

Perfect mixing modelling approach was developed by Whiten (1974) and it is similar to the general population balance model as stated in Napier Munn et.al. (2005) and as given in Genç (2008). According to the perfect mixing modelling approach, the discharge of “ith” size fraction from the mill is given by Equation (3.20) as stated in Napier Munn et.al. (2005) and also given in Genç (2008).

$$d_i = \frac{P_i}{S_i} \quad (3.20)$$

Where; “s_i” is the mass of size fraction “i” in tons in the mill hold-up which is denoted by “S” as in tons and “p_i” is the mass flow rate of particle fraction which is denoted by

“i” out of the mill as product as stated in Napier Munn et.al. (2005) and also given in Genç (2008).

Breakage rate as denoted by “r” can be back-calculated independent of discharge rate function based on mill hold-up from Equation (3.21) as stated in Napier Munn et.al. (2005) and also given in Genç (2008).

$$f_i - p_i + \sum_{j=1}^i a_{ij} r_j s_j - r_i s_i = 0 \quad (3.21)$$

Where; “ f_i ” is the mass flow rate of size fraction “i” in the mill feed, “ p_i ” is the mass flow rate of size fraction “i” in mill discharge, “ r_i ” is the specific breakage rate of size fraction “i”, “ a_{ij} ” is the mass fraction of size “j” that appear in size “i” after breakage, “ d_i ” is the specific discharge rate of size fraction “i”, “ s_i ” is the mass of size fraction “i” in the mill hold-up as given by Napier Munn et al. (2005) and also stated in Genç (2008). In the model “ f_i ”, “ p_i ” and “ s_i ” are vector, “ d_i ” and “ r_i ” are diagonal matrices and “ a_{ij} ” is a lower triangular matrix as stated in Napier Munn et.al. (2005) and also given in Genç (2008).

Wet and dry grinding ball mills were modelled by back-calculating the ratio of breakage rate to discharge rate represented by “r/d” in the literature by Napier Munn et al. (2005), Zhang (1992), Weedon (2001), Man (2001), Benzer (2000), Hashim (2003) as stated in Genç (2008). The ratio of breakage rate to discharge rate represented by “r/d” was defined as the ball mill model parameter was back-calculated from Equation (3.22) as stated in Napier Munn et.al. (2005) and also given in Genç (2008).

$$f_i + \sum_{j=1}^i a_{ij} p_j \left(\frac{r_j}{d_j} \right) - p_i \left(\frac{r_i}{d_i} \right) - p_i = 0 \quad (3.22)$$

Where; “ p_i ” is the mass flow rate of size fraction “i” in mill discharge in tons per hour, “ f_i ” is the mass flow rate of size fraction “i” in the mill feed in tons per hour, “ r_i ” is the breakage rate of size fraction “i” in hour to the minus one, “ d_i ” is the discharge rate of

size fraction “i” in hour to the minus one, “a_{ij}” is the appearance function (mass fraction of the size “j” that appears at size “i” fraction after breakage) as stated in Napier Munn et al. (2005) and also given in Genç (2008).

“a_{ij}” is a step triangular breakage matrix and multiplication of “r_i” and “a_{ij}” is the rate of breakage within that size fraction as stated in Napier Munn et al. (2005) and also given in Genç (2008). “d_i” is scaled in terms of mill volume and volumetric feed rate “Q” to the term “d_i*” for the correction of variations in residence time as stated in Napier Munn et.al. (2005) and also given in Genç (2008). “D” and “L” are the diameter and the length of the mill respectively as stated in Napier Munn et.al. (2005) and also given in Genç (2008). “d_i*” is a function of particle size as stated in Napier Munn et.al. (2005) and also given in Genç (2008).

$$d^* = \frac{d_i}{4Q/D^2L} \quad (3.23)$$

$$\frac{r_i}{d_i^*} = \frac{r_i}{d_i} \left(\frac{4Q}{D^2L} \right) \quad (3.24)$$

Ratio of breakage rate to normalized discharge rate functions were defined by spline functions by Whiten (1972) in modelling of the mills as stated in Napier Munn et.al. (2005) and also given in Genç (2008). For this calculation suitable points for “r” or “r/d” values at particle sizes were picked out and drawn a smooth line through them and fit to the model as stated in Napier Munn et.al. (2005) and also given in Genç (2008). The points called “spline knots” and define the “r/d” curve as stated in Genç (2008).

Briefly, perfect mixing modelling approach removes the complexities in the general population balance model since it was assumed that, the mill is perfectly mixed as stated in Genç (2008). It is more simple and specific breakage rates of particles can be directly calculated once the mill feed, discharge size distributions and material breakage functions are measured as stated in Genç (2008). The approach was widely applied in modelling of the industrial scale mills as given in the literature by Whiten (1972), Kavetsky and Whiten (1982a;1982b), Whiten and Kavetsky (1983), Kavetsky and

McKee (1984), Narayanan (1986;1987), Narayanan et al. (1987), McKee and Napier Munn (1990), Zhang (1992), Lynch et al. (2000), Benzer (2000), Benzer et al. (2001), Weedon (2001), Man (2001), Hasim (2003), Genç (2008), Hosseinzadehgharehgheshlang (2014). Hosseinzadehgharehgheshlang (2014) conducted laboratory scale batch grinding experiments in a Bond mill using different ball size and feed size distributions for copper-molybdenum ore. Breakage rates were estimated using the kinetic and perfect mixing models by Hosseinzadehgharehgheshlang (2014).

3.2.9.1. Ball size scaling in perfect mixing model

Impact and attrition mechanisms occur in a ball mill and thus, the following relationship was derived by Morrell (1992a) as stated in Genç (2008). The following relationships were given in Napier Munn et.al. (2005) and also in Genç (2008).

- Impact breakage $\propto "b^3"$ (ball mass) as given in Napier Munn et.al. (2005)
- Attrition breakage $\propto "1/b"$ (ball surface area) as given in Napier Munn et.al. (2005)

"b" is the ball diameter in "mm" in the above relationships given in Genç (2008). Impact breakage is assumed to be effective above a certain size " X_m " in "mm" while attrition is the main size reduction mechanism at sizes below " X_m " as given in Napier Munn et.al. (2005). " X_m " size is assumed to be equivalent to that at which maximum breakage occurs as stated in Napier Munn et.al. (2005) and given in Genç (2008). " X_m " can be related to maximum ball diameter by Equation (3.25) as given in Napier Munn et.al. (2005) and stated in Genç (2008).

$$X_m = K*b^2 \tag{3.25}$$

"K" is the maximum breakage rate factor and its value is equal to $4.4*10^{-4}$ as given in Napier Munn et.al. (2005) and stated in Genç (2008).

3.2.10. Discrete element modelling (DEM)

The motion of every particle in the flow and each collision between the particles and their environment such as with the mill liner are modelled in discrete element modelling as stated in Genç (2008). Many studies were performed based on this modelling approach as stated in Genç (2008) by Campbell (1990), Barker (1994), Walton (1994), Cleary (1998a, 1998c), Schafer et al. (1996). Discrete Element Modelling method was used to describe the ball mill behaviour in the literature by Mishra and Rajamani (1992,1994), Rajamani et.al. (1999), Cleary (1998a; 1998c; 2000; 2001; 2001a), Cleary and Sawley (1999), Cleary and Hoyer (2000) as stated in Genç (2008). Ball size effect on dry grinding breakage rate was studied by Kano et al. (2001) to show the significant effect of specific impact energy of balls on the grinding rate of particles as given in Genç (2008).

4. EXPERIMENTAL

4.1. Field Sampling

The samples were collected from the run-of-mine ore open stockpile of the Karacaören underground mine by sampling from different spots of the stockpile. The coarse run-of-mine ore particles were collected as samples. A view from the sampling work is given in Figure 4.1. Samples were transported to the Mineral Processing Laboratories at the Mining Engineering Department of Muğla Sıtkı Koçman University.



Figure 4.1. Sampling of the run-of-mine chromite ore from the stockpile

4.2. Description of the Karacaören Chromite Ore Deposit

In the entire area (Karacaören region), only tectonites from the ophiolites can be seen. Tectonites, which are the most important units of ophiolites in terms of chromite deposits, are represented by three members of the peridotites (harzburgite, dunite and pyroxenite veins). The harzburgite constitute more than 65% of the rocks in the study region as given in Muğla Entity Project Report (2017).

In the harzburgites, where lithological differentiation planes are observed very clearly, serpentinized olivine and occasionally folded enstatite and lesser extent cataclastic chromite are seen. Although the harzburgites occupy more space than the dunites in volume, the chromite occurrences around them are developed depend on the dunites. Dunites are usually in the form of bands in thicknesses ranging from 1 cm to 5 m, with obvious boundaries as well as those with interbedded harzburgite and uncertain boundaries. In addition to the pyroxenes in the harzburgite composition, pyroxenite dykes (cut the general structure) were determined with thicknesses ranging from 1 cm to 10 cm and with continuity not exceeding a few meters. The lithological differentiation planes, which can be observed very easily in almost everywhere forming a regular structure in the region. The ore direction is approximately northwest-southeast and the ore is north-easterly inclined.

4.3. Material Characterization

Chemical, mineralogical, and texture analysis and Standard Bond work index grinding test with 75 μ m classifying screen were performed in the context of the material characterization studies.

XRF Spectroscopy (X-ray fluorescence) method was used to identify the elements contained in a sample material. Chemical composition of the ore sample obtained by XRF Analysis is given in Table 4.1. Mineralogical microstructure and texture properties were determined by detailed ore microscopic analysis with Image Analysis System and presented in Appendix 1.

Table 4.1. XRF results

Compound	Cr ₂ O ₃	Fe ₂ O ₃	SiO ₂	Al ₂ O ₃	MgO	CaO	TiO ₂	NiO
%	14.31	9.43	34.83	2.39	43.65	0.18	0.07	0.37

4.3.1. Standard Bond Work Index Test

Standard Bond ball mill grindability test was used to determine the work index value of the material which is a comminution parameter expressing the resistance of the material to crushing and grinding. Work index can be defined as the kilowatt hours per short ton required to reduce the material from a theoretically infinite size to 80% passing size of 100 μ m (Bond, 1960).

The ball mill grindability test was conducted in a standard Bond ball mill with a diameter of 304.8 mm and a length of 304.8 mm (inside dimensions). It is a horizontal axis mill with rounded corners and has a smooth lining. There are no lifters inside of the mill. Access to the mill is through a cover plate on the curved surface. A photograph of the mill is given in Figure 4.2. The mill rotates at 70 rpm. Standard Bond ball series was used in the tests which is tabulated in Table 4.2. Weighted average ball diameter of the distribution was calculated as 31.6mm.



Figure 4.2. Standard Bond ball mill
(Mineral Processing Laboratory, Muğla Sıtkı Koçman University)

Table 4.2. Standard Bond ball charge distribution (Turkish Standards 7700)

Nominal ball diameter (mm)	Average ball diameter (mm)	Number of balls	Weight (g)
38.10	36.83	43	8730
31.75	29.72	67	7197
25.40	25.91	10	705
19.05	19.30	71	2058
12.70	15.49	94	1441
Total		285	20131

Mill product ($-75\mu\text{m}$ material) collected from the last three periods of the test were mixed thoroughly and screened by using a $\sqrt{2}$ sieve series down to $38\mu\text{m}$ to determine P80 size of the Bond test product. Mill product particle size distribution is given in Figure 4.3.

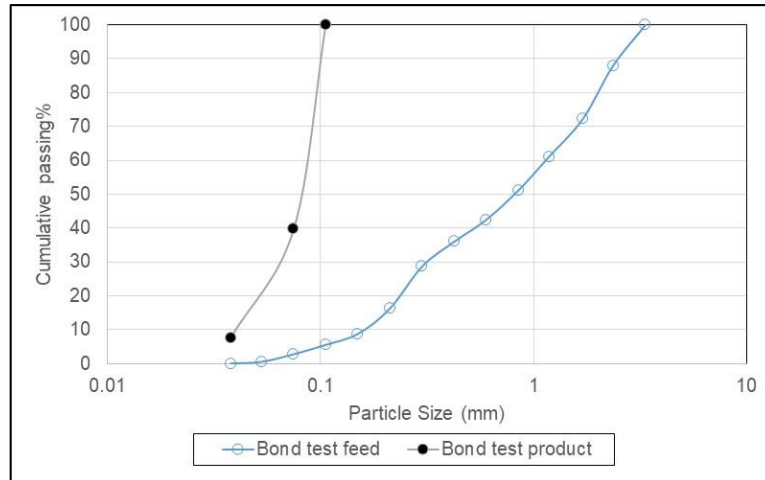


Figure 4.3. Standard Bond Work Index test mill feed and product size distributions

The work index of the ore was calculated as 20.66kWh/t from Equation (4.1) by using a 75µm classifying screen (TS 7700).

$$Wi = \frac{44.5}{P1^{0.23} \times Gbp^{0.82} \times \left(\frac{10}{\sqrt{P}} - \frac{10}{\sqrt{F}} \right)} \times 1.10 \quad (4.1)$$

Where;

Wi: Work index (kWh/t)

P1: Classifying screen (µm)

P: 80% passing size of the mill product (finer than P1 control test screen) (µm)

F: 80% passing size of the mill feed (µm)

The factor 1.10 converts the bond work index in kWh/St to kWh/t.

4.4. Sample Preparation Stages

Run-of-mine samples were initially subjected to hand crushing by using a hammer as the size of the ore particles were too coarse for the jaw crusher feed. 120.70kg sample was used in the sample preparation stage. A view from hand crushing stage is given in Figure 4.4.



Figure 4.4. Hand crushing of run-of-mine ore samples

Following hand crushing, samples were fed to the jaw crusher once. Jaw crusher discharge was sampled by cone and quartering method and ground in the rod mill with an effective diameter of 19.5cm (external diameter: 21.5cm) and an external length of 31.1cm. Rod mill charge composition used in the sample preparation stage is given in Table 4.5.

Table 4.3. Rod mill charge composition distribution

Rod class	1	2	3	4	5
Weight of single rod (kg)	0.40	1.14	2.20	1.62	0.72
Length (cm)	29.30	29.30	29.30	29.30	29.30
Diameter (cm)	1.5	2.5	3.5	3	2
Number of rods	15	1	3	4	6
Total weight (kg)	6.1	1.14	6.60	6.54	4.34

During the sample preparation in the rod milling stage, the sample was kept in the mill for 1min not to produce too much fines. 3.35mm screen was used to screen the rod mill product after each time interval. Material finer than 3.35mm was collected and not returned to the mill again in the second grinding time interval. The grinding was performed until all the material passes 3.35mm screen. -3.35mm material was mixed thoroughly and a sample riffler was used to split the material until obtaining 700cc mill feed samples. Mill feed samples were dried at 70°C for 2 hours before the tests to give off the moisture in the ore. The drying time was kept short not to effect the grindability of the minerals contained in the ore. 700cc sample (reference sample) was passed through $\sqrt{2}$ sieve series from the top size (3.35mm) down to 38 μ m ahead of the batch grinding tests.

4.5. Batch Grinding Tests

Batch grinding tests conducted in the literature according to the Austin's (1984) methodology used monosize particles (single size fraction) as mill feed. In this study, a full particle size distribution which is -3.35mm was obtained by crushing, grinding and screening unit operations and used in the tests. Batch grinding of chromite ore in dry-state in a ball mill using a full mill feed particle size distribution have not been investigated in the literature.

In this context, different ball size distributions were used as a grinding media in the batch tests in addition to the Standard Bond charge distribution to analyze the breakage kinetics. For this purpose, 700cc representative sample was ground in the standard Bond ball mill for a total retention time of 25sec, 1min, 3min, 5min, 10min, 15min for each test condition.

4.6. Particle Size Distribution Analysis

The mill was discharged and ground material was screened by using a $\sqrt{2}$ screen series from the top size which is 3.35mm down to 0.038mm after each grinding stage. Retsch brand test screens that were used in the tests are; 3.35mm, 2.5mm, 1.7mm, 1.18mm, 0.85mm, 0.6mm, 0.425mm, 0.3mm, 0.212mm, 0.15mm, 0.106mm, 0.075mm, 0.053mm, 0.038mm. A ro-tap screen shaker (Retsch brand) was used for dry screening of the samples for 20minutes.



5. RESULTS AND DISCUSSIONS

5.1. Repeatability Tests

700cc ore sample was ground for 25sec, 1min, 3min, 5min, 10min, 15min. The same test was repeated for another 700cc ore sample. The results were statistically analyzed to determine the repeatability. For this purpose, the root mean square (RMS) of the test results were determined from Equation (5.1).

$$RMS = SQRT \left[\frac{\sum_{i=1,n}^n (x_i - y_i)^2}{n} \right] \quad (5.1)$$

Particle size distributions of the feed samples used in the tests are given in Figure 5.1. Batch grinding test results for the analysis of the repeatability are given in Figure 5.21 and Figure 5.3. Results are compared and given in 5.4 to Figure 5.9. Root mean square (RMS) of the results are calculated and tabulated in Table 5.1.

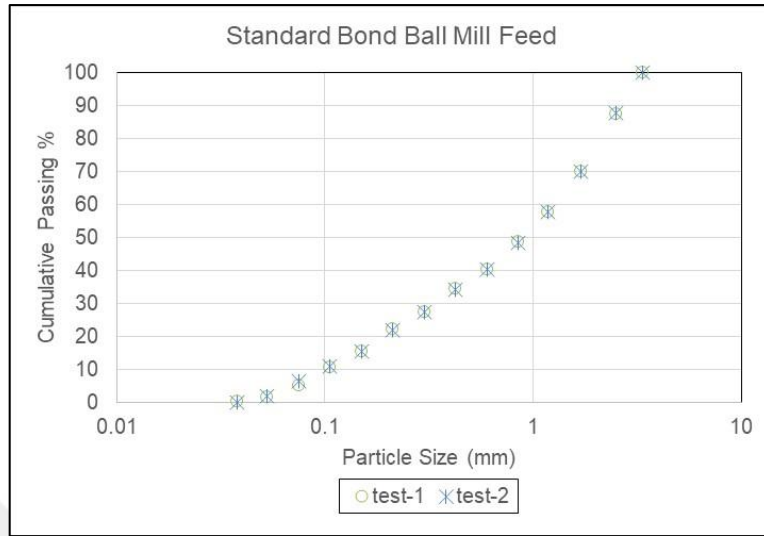


Figure 5.1. Comparison of the mill feed particle size distributions for the tests

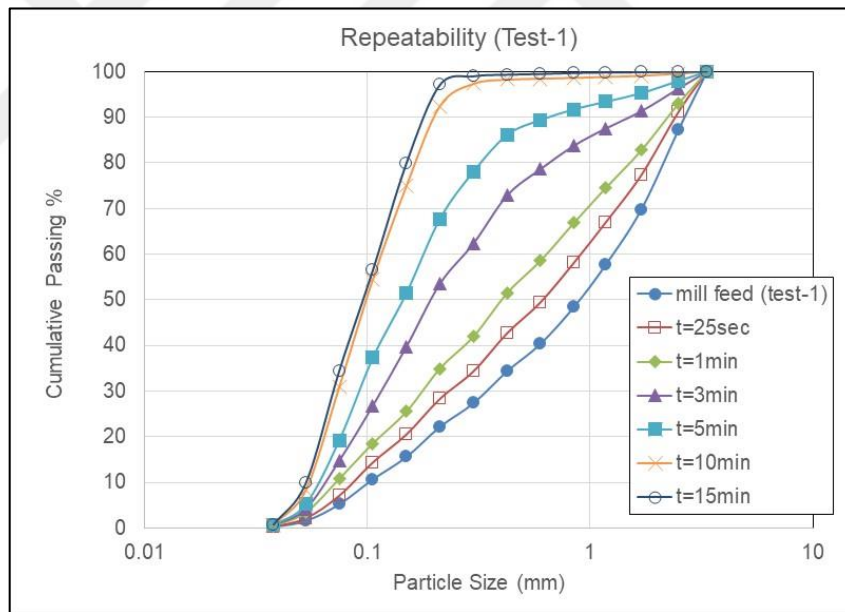


Figure 5.2. Particle size distributions of the repeatability test-1

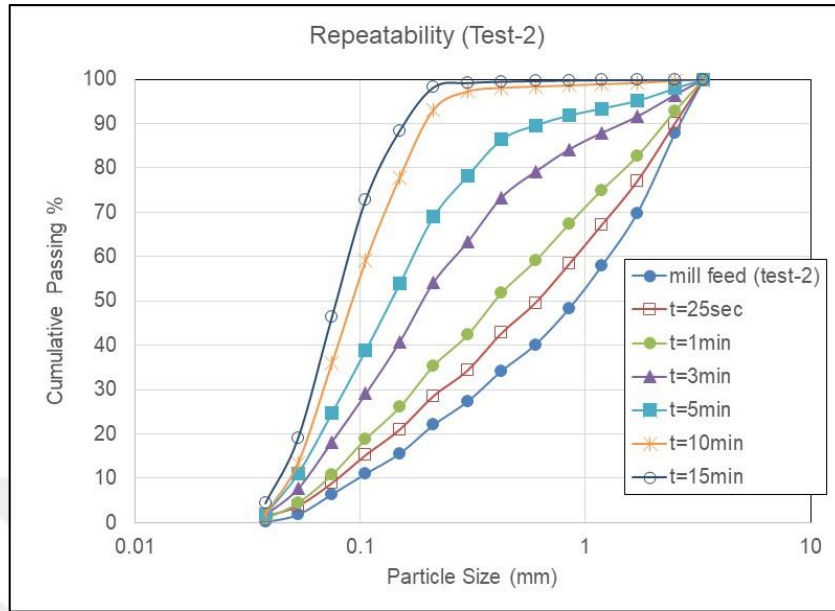


Figure 5.3. Particle size distributions of the repeatability test-2

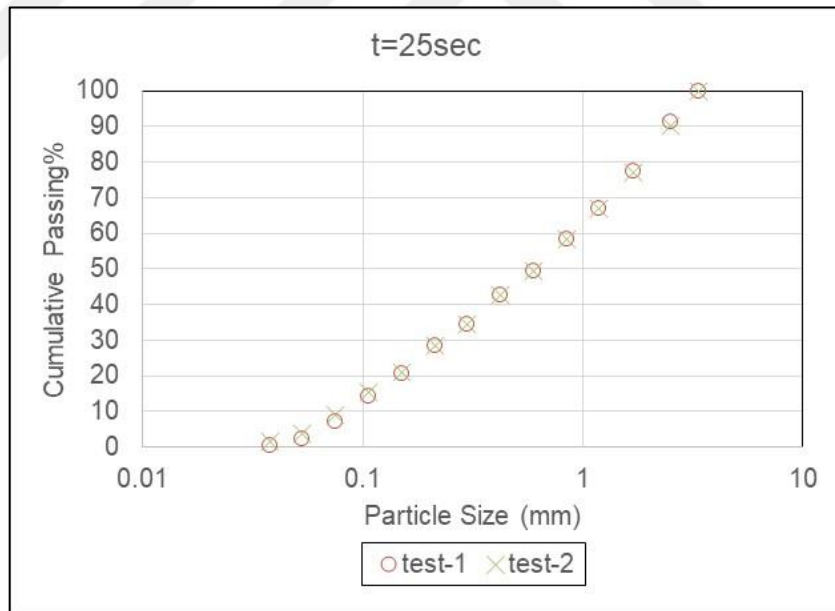


Figure 5.4. Comparison of the particle size distributions for batch grinding time at 25 sec

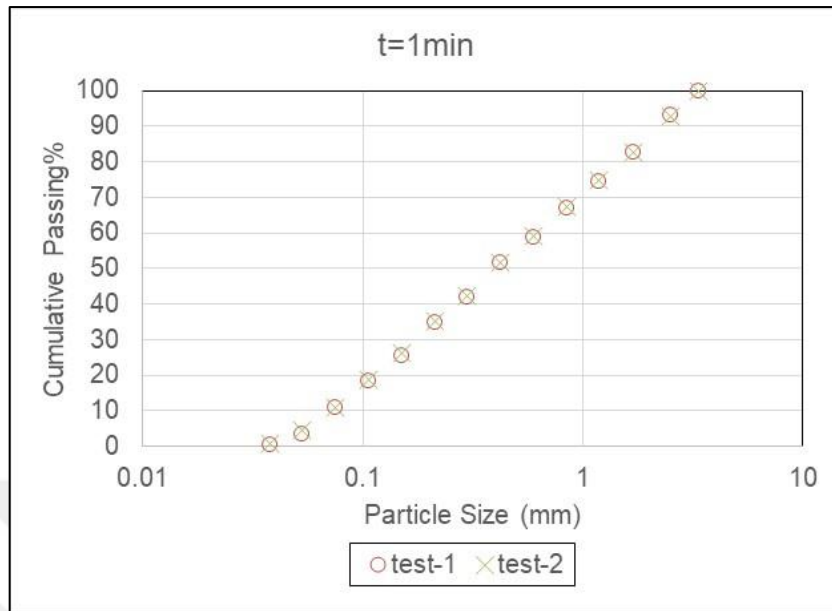


Figure 5.5. Comparison of the particle size distributions for batch grinding time at 1 min

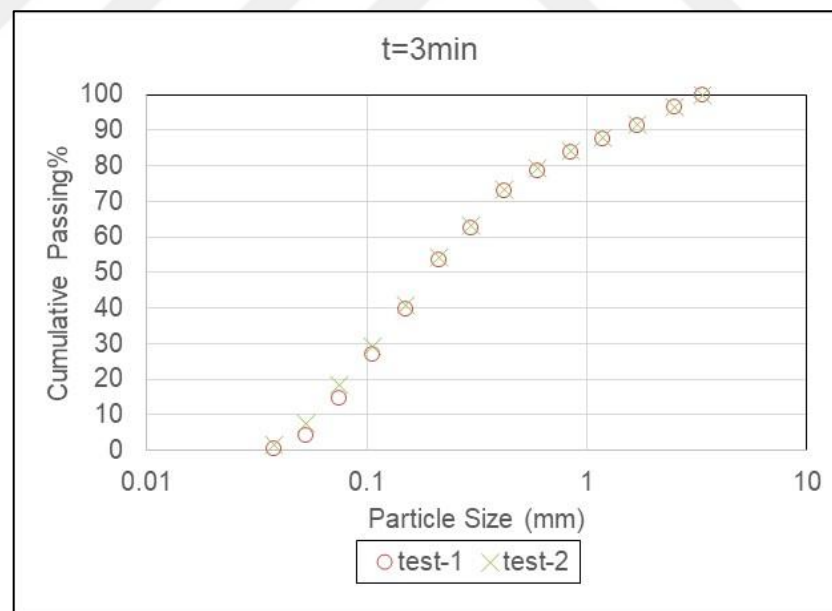


Figure 5.6. Comparison of the particle size distributions for batch grinding time at 3 min

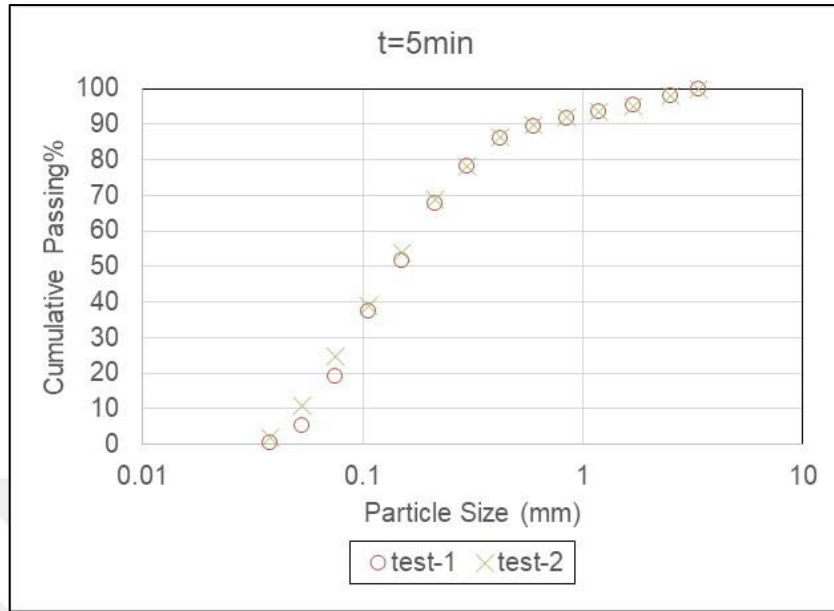


Figure 5.7. Comparison of the particle size distributions for batch grinding time at 5 min

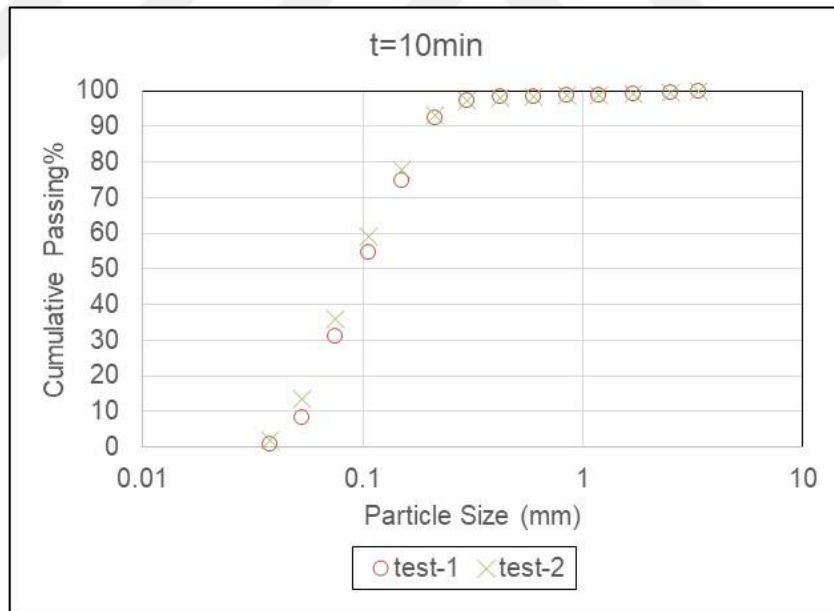


Figure 5.8. Comparison of the particle size distributions for batch grinding time at 10 min

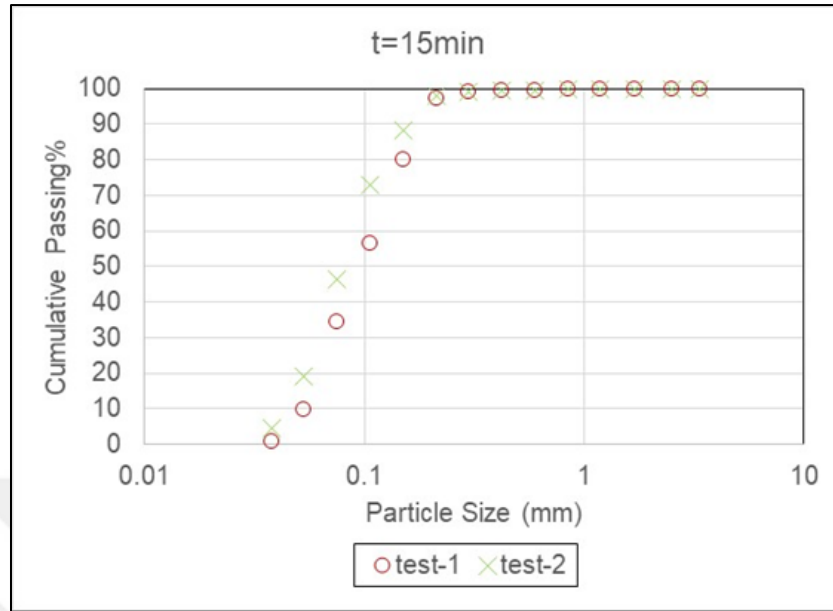


Figure 5.9. Comparison of the particle size distributions for batch grinding time at 15 min

Table 5.1. RMS of the test results

	Mill feed	Cumulative grinding time					
		0.25sec	1min	3min	5min	10min	15min
RMS	0.36	0.84	0.44	1.54	2.30	2.42	6.44

5.2. Calculation of Bond Ball Filling Ratio

Ahead of the selection of the charge distributions, Bond ball mill filling ratio is calculated from Equation (5.2).

$$\text{Ball filling ratio} = \frac{\text{Total ball volume in the mill}}{V_{\text{mill}} \times 0.60} \quad (5.2)$$

Where, V is the volume of the mill. In the calculation, it was assumed that, 60% of the filled mill volume corresponded to the total ball volume. 40% of the filled ball mill volume corresponded to the void volume between the balls. Bond ball filling ratio was calculated as 21.03%. Bond ball filling (ball plus void volumes) was calculated as 21.03%. All the tests were performed by using the Bond ball filling ratio. Volume of the selected ball mass in each ball size class can be calculated by Equation (5.3).

$$v = \frac{m}{d} \quad (5.3)$$

5.3. Calculation of Number of Balls

Balls which were used in the tests, excluded of the balls in the Standard Bond ball size distribution, were casted iron balls with high chromium content. Density of the balls in the Standard Bond ball size distribution were recorded to be 7.2g/cm^3 and casted iron balls 7.6g/cm^3 . Number of balls for each ball size class was calculated by the following equation for the same filling ratio which is 0.21:

$$\text{Number of balls} = \frac{\text{Total ball volume}}{\text{Volume of one ball}} \quad (5.4)$$

Volume of one spherical ball was calculated by Equation 5.5.

$$V_{\text{ball}} = \frac{4}{3} \pi r^3 \quad (5.5)$$

Where; r is the radius of the spherical ball in cm.

5.4. Batch grinding test conditions

5.4.1. Selected grinding media size distributions

Tests were planned to analyze the effect of different ball size and distributions on size reduction performance. For this purpose, monosize and different ball charge distributions were used. Ball charge distributions selected in the study can be grouped in three main classes as follows:

- Monosize ball distribution application (Test group-1)
- Ball size distributions coarser and finer than Standard Bond charge distribution (Test group-2)

- Different ball size distributions which have the same weighed average ball size with that of the Standard Bond ball charge distribution. (Test group-3)

Test group-1 results were used to analyze the effect of ball size on size reduction performance and specific breakage rates in the mill. Ball size distributions arranged in test group-2 were parallel to each other. Thus, the distributions have approximately the same distribution slopes with different weighed average ball size. Test group-2 results were used to analyze the effect of ball size distribution fineness effect on size reduction performance and specific breakage rates. On the other hand, ball size distribution slopes were changed in test group-3. Results were analyzed as compared to the obtained results from the application of Standard Bond charge distribution. However, weighed average ball size was set to the size of the Standard Bond ball size in test group-3. In that case, ball distribution effect on size reduction performance and specific breakage rates in the mill could have been analyzed. Selected grinding media distributions for the batch grinding tests are given in Table 5.2.

Table 5.2. Grinding media (charge) distributions

Test no	Applied ball size distributions
1	Standard Bond ball size distribution ($D_{\text{average}}=30.62\text{mm}$)
2	Mono-size ball distribution of 40mm
3	Mono-size ball distribution of 30mm
4	Mono-size ball distribution of 25mm
5	Mono-size ball distribution of 20mm
6	Ball size distribution coarser than Standard Bond ball size distribution ($D_{\text{average}}=36.70\text{mm}$)
7	Ball size distribution finer than Standard Bond ball size distribution ($D_{\text{average}}=25.45\text{mm}$)
8	Ball size distribution finer than Standard Bond ball size distribution ($D_{\text{average}}=21.18\text{mm}$)
9	Ball size distribution of charge-1 ($D_{\text{average}}=30.59\text{mm}$)
10	Ball size distribution of charge-2 ($D_{\text{average}}=30.42\text{mm}$)
11	Ball size distribution of charge-3 ($D_{\text{average}}=30.64\text{mm}$)

* D_{average} is the weighted average ball size in mm in the selected distribution

Detailed charge distributions used in the batch grinding tests are tabulated in Table 5.3 to Table 5.10 Ball charge distributions as cumulative passing % ball size were calculated and plotted. Comparisons among the Standard Bond ball charge, selected coarser and finer distributions which have the same distribution slopes with that of Bond ball charge distribution are given in Figure 5.10 as cumulative passing % ball size. Other charge distributions which were determined according to the weighted average ball size of the

Standard Bond charge distribution are compared and given in Figure 5.11 as cumulative passing % ball size.

Table 5.3. Standard Bond ball size distribution (Test-1)

Ball Size (mm)	Weight (kg)	Weight%
36.83	8.73	43.37
29.82	7.20	35.75
25.91	0.71	3.50
19.30	2.06	10.22
15.49	1.44	7.16
Total	20.13	100.00

Table 5.4. Monosize ball distribution applications

Tests no	Ball size (mm)	Total weight of balls (kg)	Number of balls
Test-2	40	21.39	84
Test-3	30	21.39	199
Test-4	25	21.32	344
Test-5	20	21.34	670

Table 5.5. Ball size distribution coarser than Standard Bond ball size distribution (Test-6)

Ball Size (mm)	Weight (kg)	Weight%
40	16.88	79.00
30	0.85	4.00
25	2.14	10.00
20	1.50	7.00
Total	21.37	100.00

Table 5.6. Ball size distribution finer than Standard Bond ball size distribution (Test-7)

Ball Size (mm)	Weight (kg)	Weight%
30	9.19	43.00
25	7.69	36.00
20	0.85	4.00
17	2.14	10.00
15	1.50	7.00
Total	21.37	100.00

Table 5.7. Ball size distribution finer than Standard Bond ball size distribution (Test-8)

Ball Size (mm)	Weight (kg)	Weight%
25	9.19	43.00
20	7.69	36.00
17	0.85	4.00
15	3.63	17.00
Total	21.37	100

Table 5.8. Ball size distribution of charge-1 (Test-9)

Ball Size (mm)	Weight (kg)	Weight%
40	5.40	25.27
30	11.46	53.63
25	2.00	9.36
20	0.9	4.21
17	0.91	4.26
15	0.70	3.28
Total	21.37	100.00

Table 5.9. Ball size distribution of charge-2 (Test-10)

Ball Size (mm)	Weight (kg)	Weight%
40	3.7	17.31
30	12.07	56.48
25	5.6	26.20
Total	21.37	100.00

Table 5.10. Ball size distribution of charge-3 (Test-11)

Ball Size (mm)	Weight (kg)	Weight%
40	1.37	6.41
30	20	93.59
Total	21.37	100.00

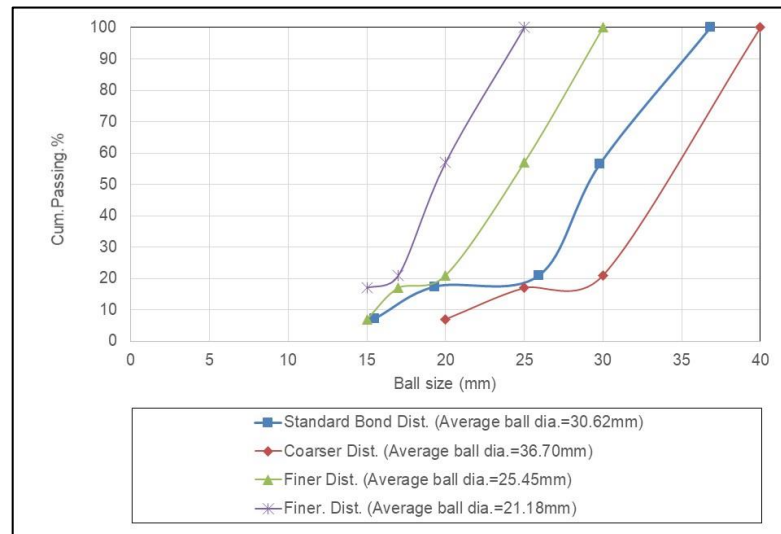


Figure 5.10. Comparison among the standard bond and the selected coarser and finer charge distributions

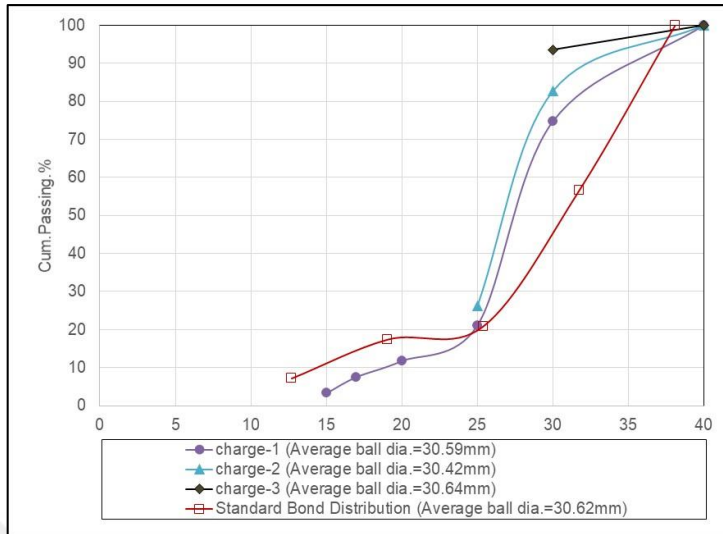


Figure 5.11. Selected charge distributions with the same weighed average ball size

5.4.2. Batch grinding test mill feed particle size distributions

Particle size distributions of the mill feed samples used in the tests are presented in Figure 5.12. Mill feed particle size distributions indicated variations for the batch test grinding conditions.

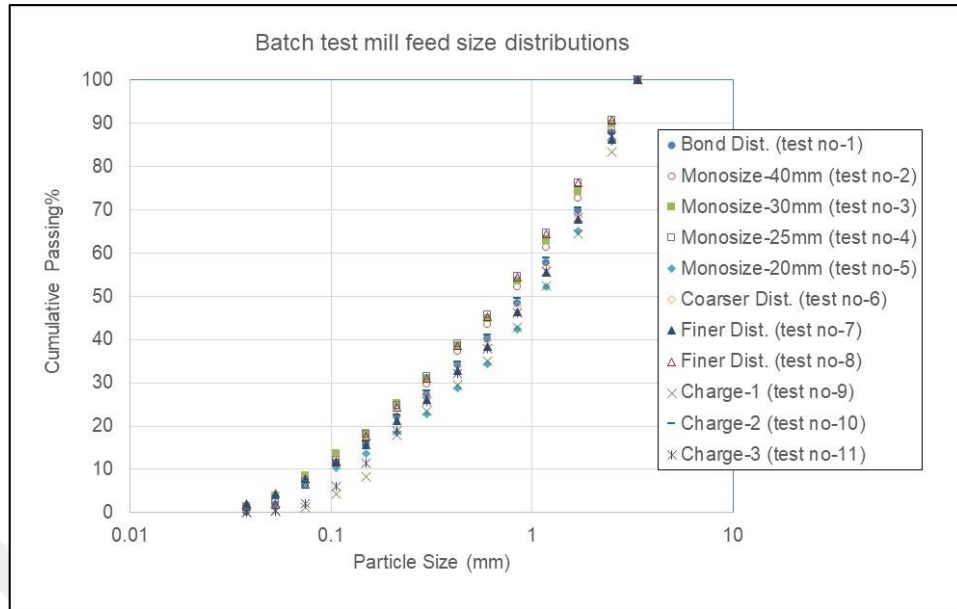


Figure 5.12. Variation of mill feed particle size distributions

5.5. Batch grinding test results

Rod and ball mills are widely used in chromite ore industry. Rod mills are usually used in wet grinding applications. For finer ball mill feeds, wet overflow rod mills are used. For the coarser products, where a minimum amount of extreme fines is desired, center peripheral discharge rod mills are used. It is known that, dry grinding in rod mills is generally not recommended as dry materials flow poorly, which causes swelling of the rod charge leading to rod breakage and tangling. They have applications in grinding of coke breeze in iron ore sintering plants and cement clinker. Energy consumption is lower but the capital cost is high in such applications. Dry grinding rod mills are usually designed for end peripheral discharge but can be center peripheral discharge. Dry rod mills are inefficient in the use of power and have mechanical problems such as rod tangling except in cement clinker grinding as stated in Mular et.al. (2002).

Peripheral discharge steel ball and rod mills produce a uniformly ground product with a minimum amount of fines since they have rapid pass design which provided shorter residence time of material in the mill as stated in the book of Denver Equipment

Company (1962). These mills were used to remove high grade chromite with very little grinding and thus, without overgrinding. This type of process will save significant amount of energy in grinding process as stated in the book of Denver Equipment Company (1962). In this context, it is important to have knowledge about the mill product size distributions thus grind size (P80) at different operational conditions and residence time intervals. Knowledge on the fineness of grind (P80) at shorter and longer residence time intervals have a vital importance in terms of energy saving.

Particle size distributions obtained after batch grinding tests for the selected residence time intervals with the selected ball distributions are presented in Figure 5.13 to Figure 5.23.

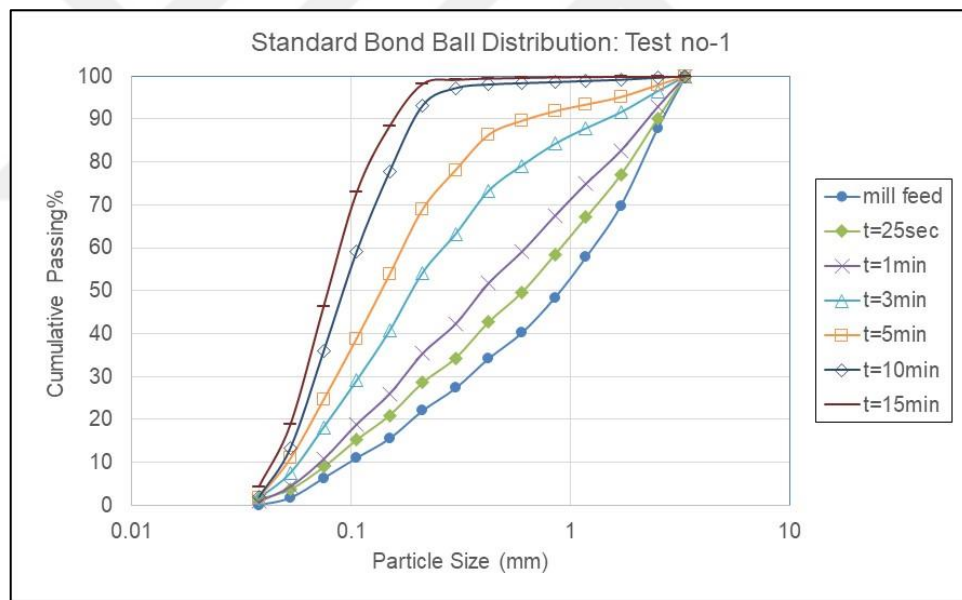


Figure 5.13. Particle size distributions obtained by batch grinding with Standard Bond ball size distribution

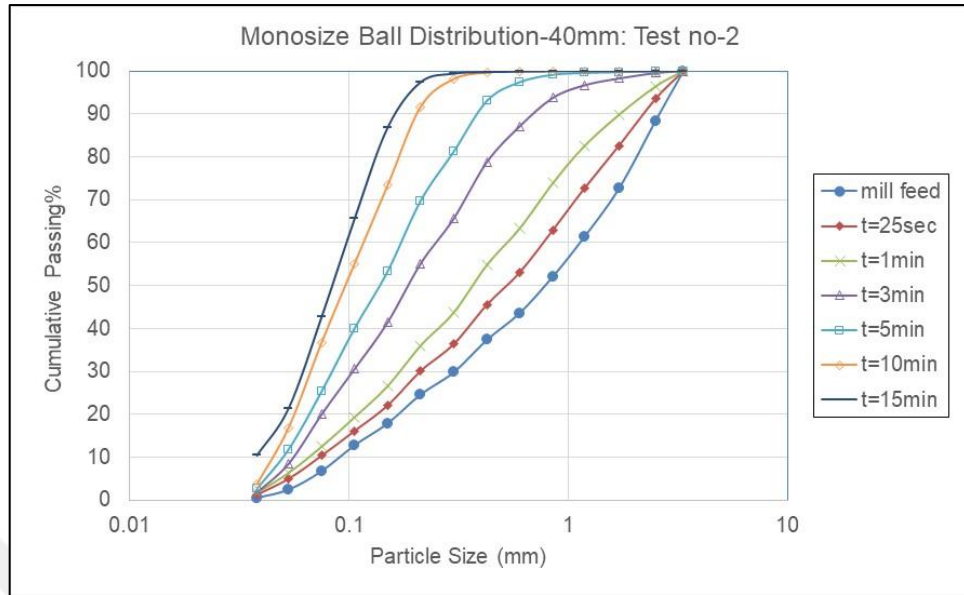


Figure 5.14. Particle size distributions obtained by batch grinding with monosize ball distribution of 40mm

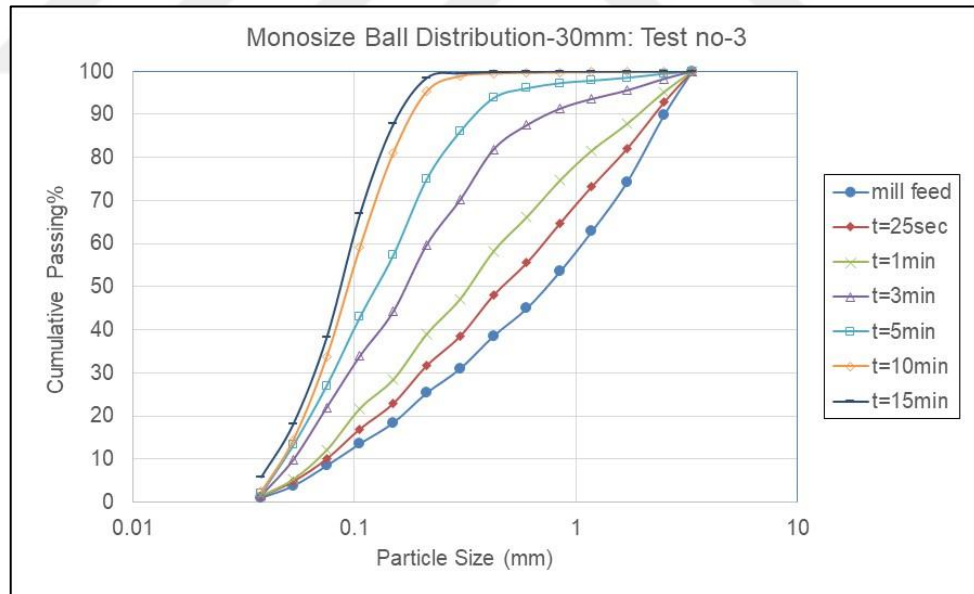


Figure 5.15. Particle size distributions obtained by batch grinding with monosize ball distribution of 30mm

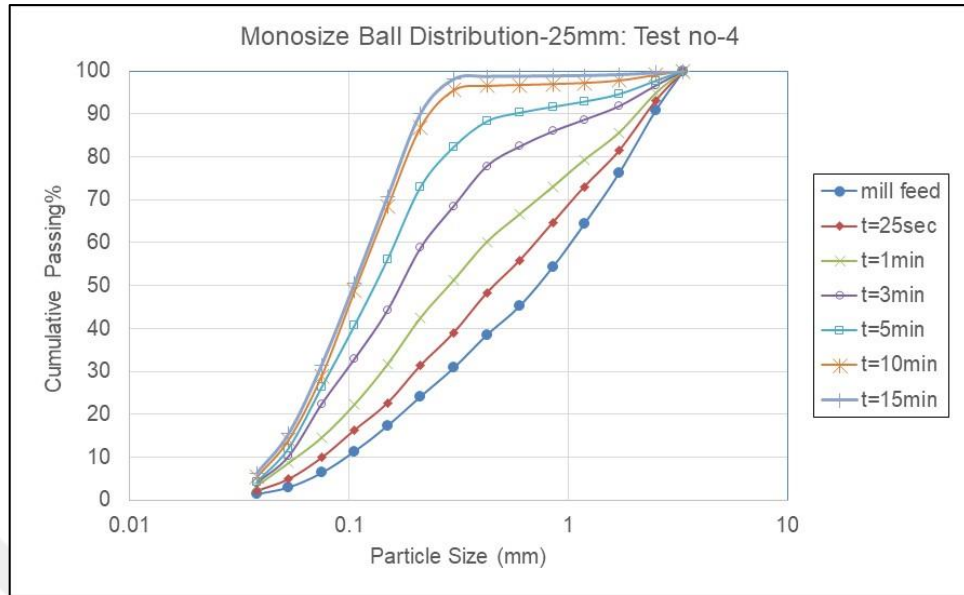


Figure 5.16. Particle size distributions obtained by batch grinding with mono-size ball distribution of 25mm

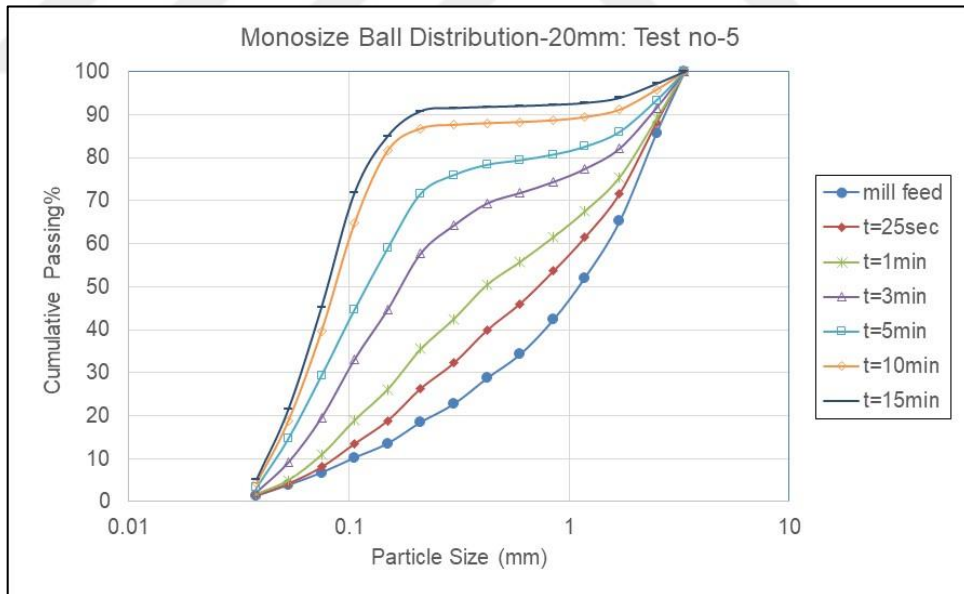


Figure 5.17. Particle size distributions obtained by batch grinding with mono-size ball distribution of 20mm

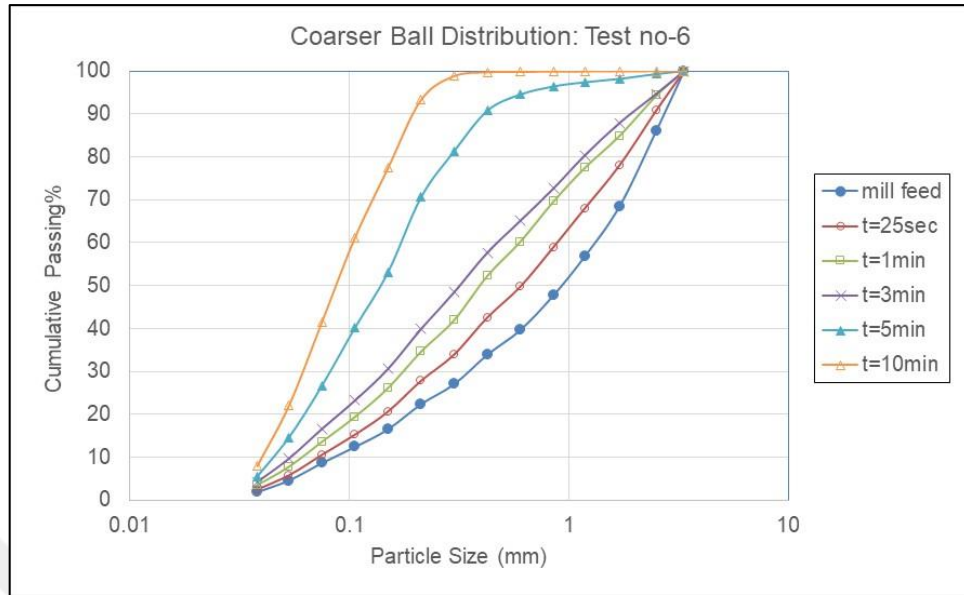


Figure 5.18. Particle size distributions obtained by batch grinding with ball size distribution coarser than Standard Bond charge distribution (D average=36.79mm)

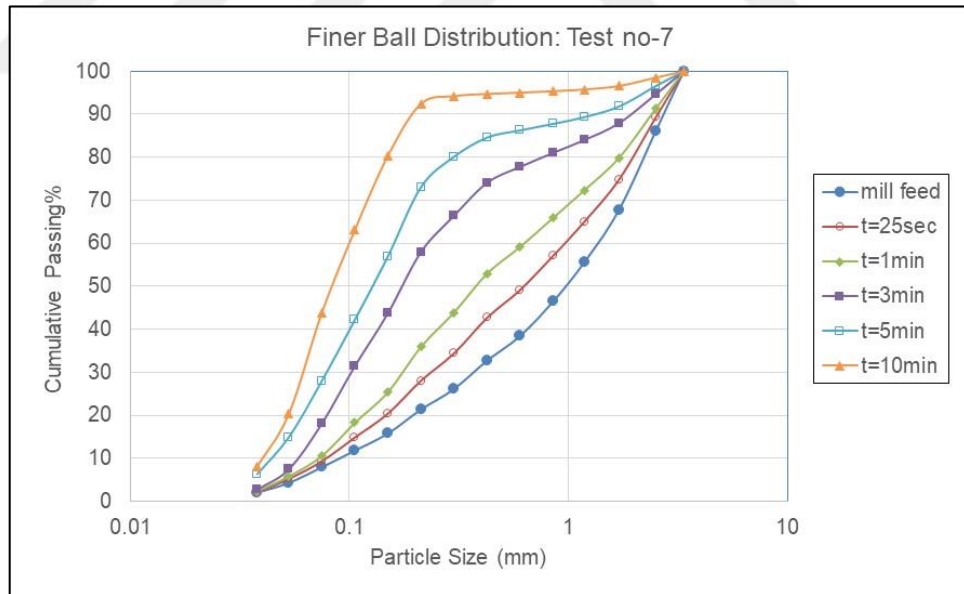


Figure 5.19. Particle size distributions obtained by batch grinding with ball size distribution finer than Standard Bond charge distribution (D average=25.51mm)

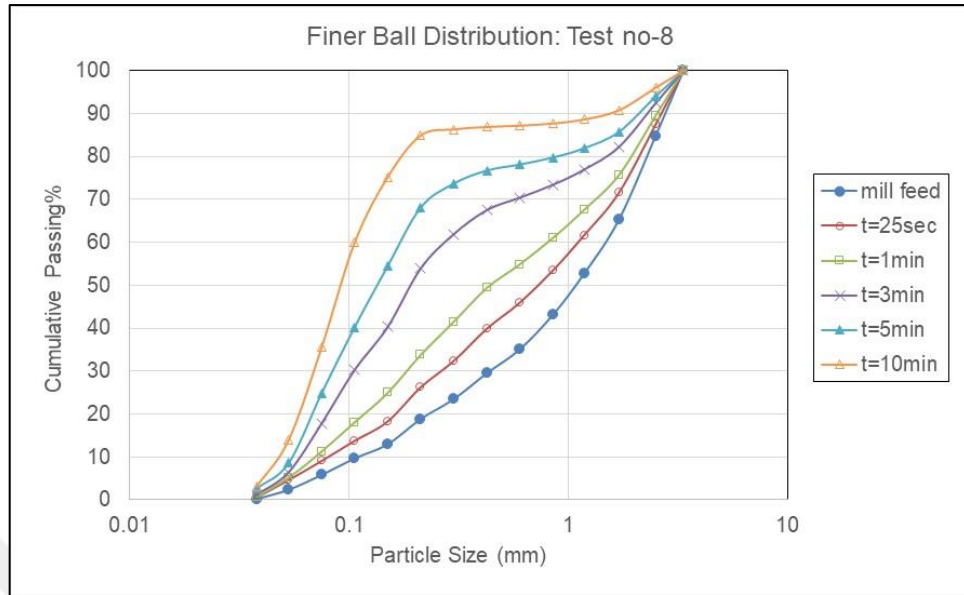


Figure 5.20. Particle size distributions obtained by batch grinding with ball size distribution finer than Standard Bond charge distribution (D average=21.18mm)

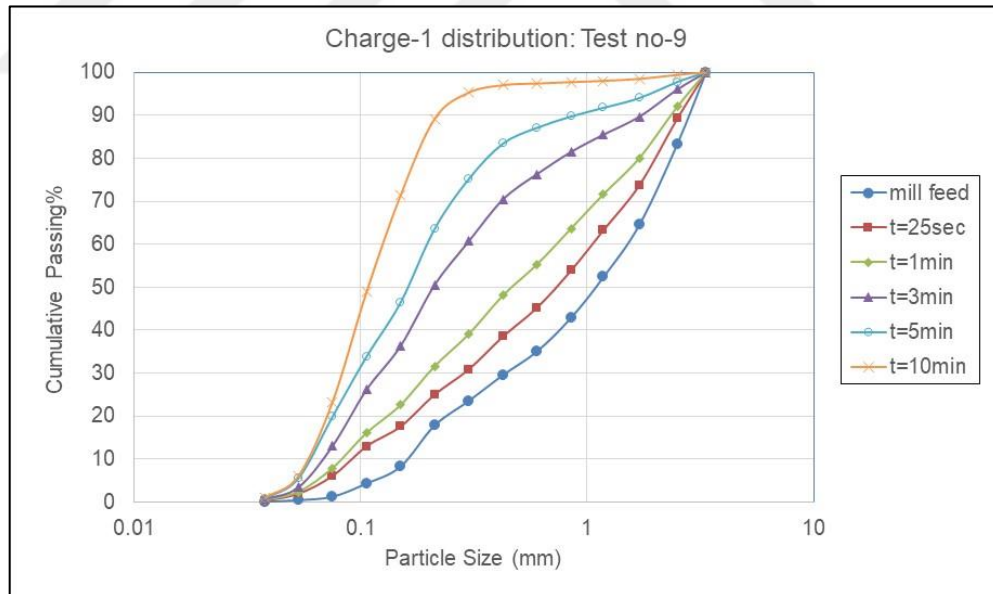


Figure 5.21. Particle size distributions obtained by batch grinding with ball size distribution of charge-1 (D average=30.59mm)

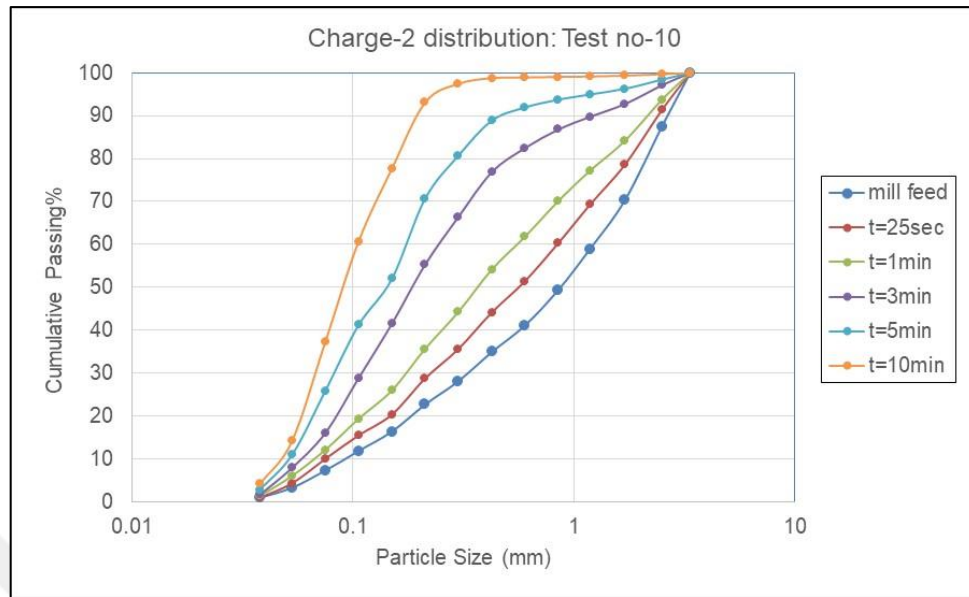


Figure 5.22. Particle size distributions obtained by batch grinding with ball size distribution of charge-2 (D average=30.42mm)

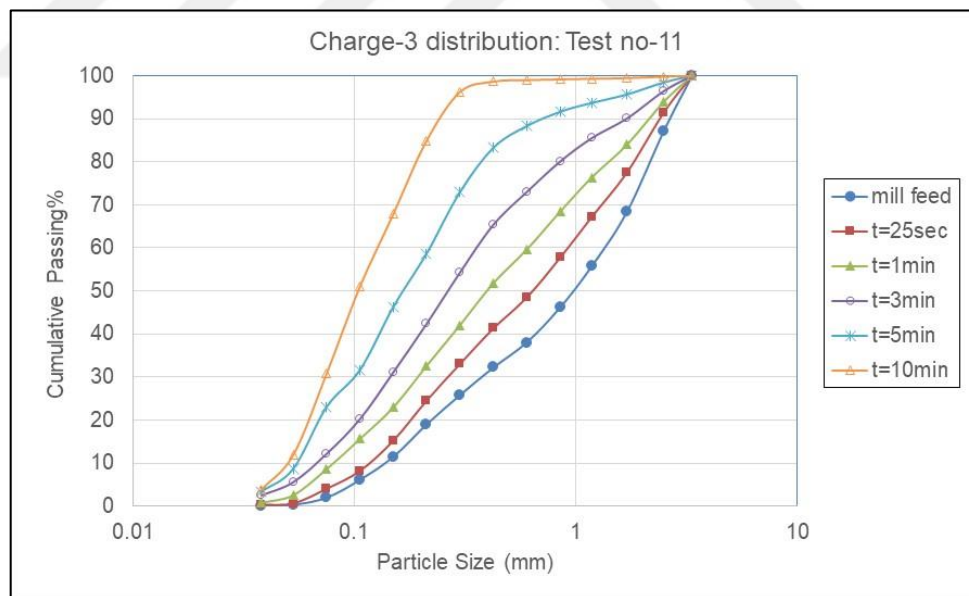


Figure 5.23. Particle size distributions obtained by batch grinding with ball size distribution of charge-3 (D average=30.64mm)

Characteristic particle size distribution analysis that were presented indicated a systematic size reduction in each test condition. Size distributions became finer as the retention in the mill was increased. However, after 10min grinding, coating on the liner

of the mill and balls were observed which was expected to reduce the grinding performance. Thus, the data presented for 15min residence time included the effect of coating on the results. If there had been no coating, finer particle size distributions could have been obtained for 15min grinding condition. During the evaluation of the 15min results, this effect was taken into consideration. Another observation was the production of $-38\mu\text{m}$ material amount could not have been increased significantly with the increase in residence time. This indicated the inefficiency of ball milling in fine grinding. This indicated the necessity of the application of different equipments which will be effective in the production of more fine material in the fine size ranges.

A plateau on the particle size distributions were observed which showed the accumulation of particles coarser than $212\mu\text{m}$. Particles in the coarse size ranges could not have been broken completely by the 20mm balls. Especially particles are accumulated in the size fraction of $-3.35+0.850\text{mm}$. This condition was also observed when grinding with 25mm balls. However, much less particles were accumulated without being broken.

5.6. Comparison of Batch Grinding Test Results

Particle size distributions obtained by batch grinding with Standard Bond ball charge and monosize ball charge compositions are compared for the same batch grinding time intervals and presented in Figure 5.24 to Figure 5.29.

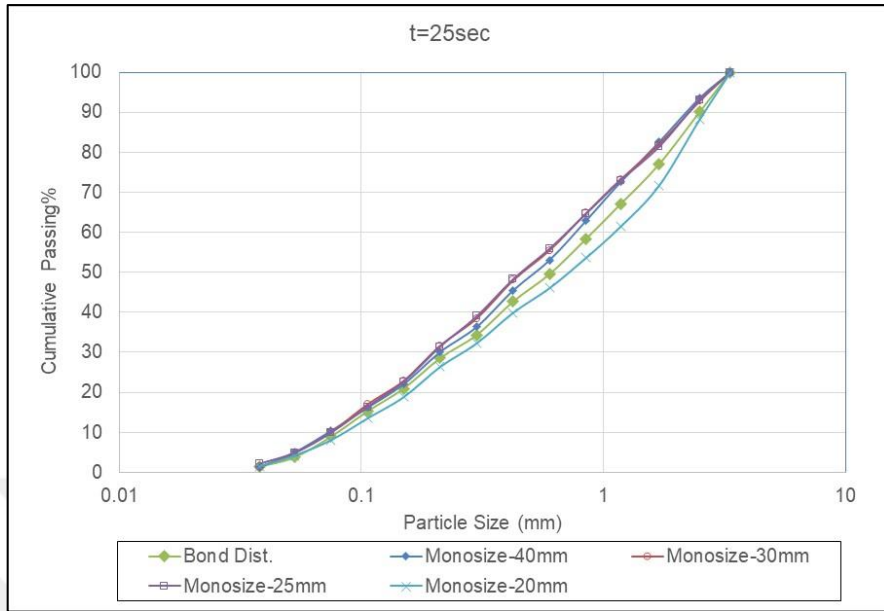


Figure 5.24. Particle size distributions at 25sec obtained by batch grinding with Standard Bond charge and monosize distributions

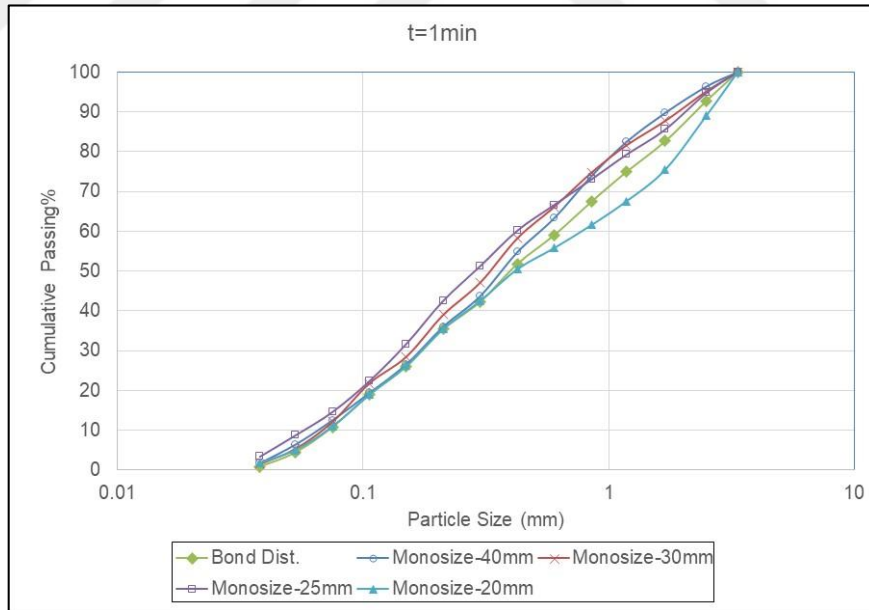


Figure 5.25. Particle size distributions at 1min obtained by batch grinding with Standard Bond charge and monosize distributions

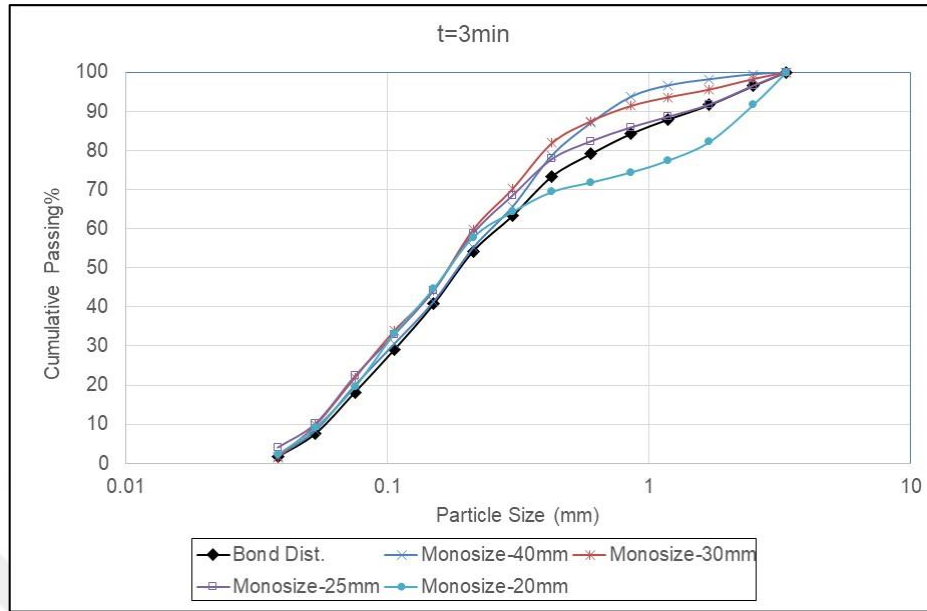


Figure 5.26. Particle size distributions at 3min obtained by batch grinding with Standard Bond charge and monosize distributions

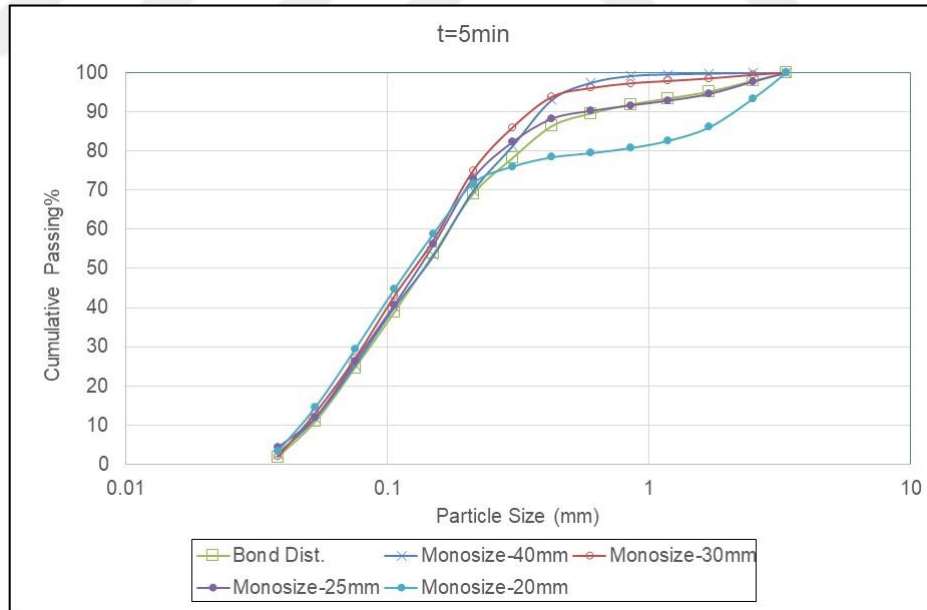


Figure 5.27. Particle size distributions at 5min obtained by batch grinding with Standard Bond charge and monosize distributions

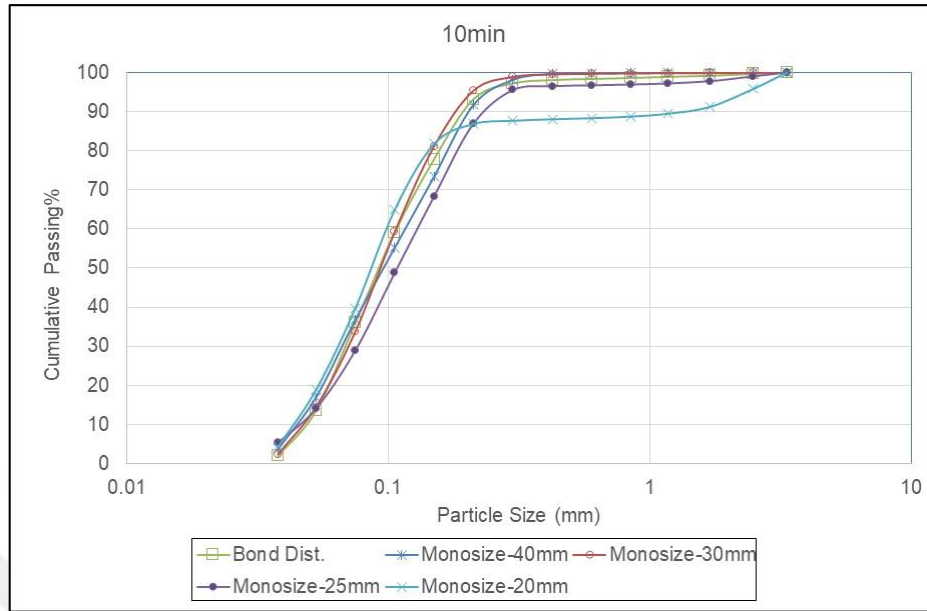


Figure 5.28. Particle size distributions at 10min obtained by batch grinding with Standard Bond charge and monosize distributions

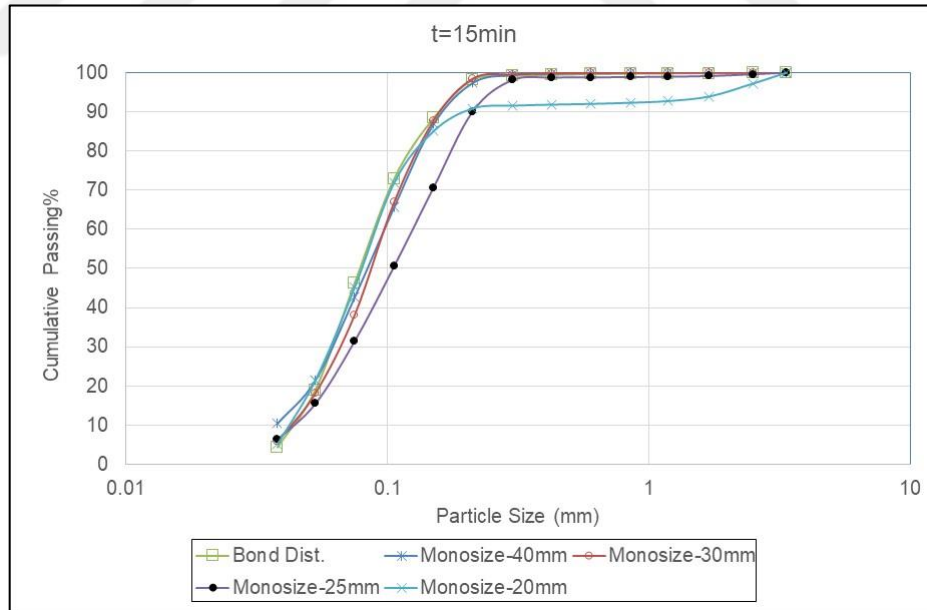


Figure 5.29. Particle size distributions at 15min obtained by batch grinding with Standard Bond charge and monosize distributions

Comparisons indicated that, ball size effects could have been reflected on the mill product size distributions successfully. Grinding performance of 40mm, 30mm and

25mm charge compositions were observed to be higher as compared to Standard Bond distribution at shorter residence time intervals ($t < 10\text{min}$). At higher retention time intervals, grinding performance of 20mm charge composition was observed to increase for the size fractions below approximately $212\mu\text{m}$ as more specific surface area was provided by the ball charge as compared to other distributions which was expected to increase the abrasion in the mill. This effect was started to be observed at 5min grinding time such that, as the ball charge got finer, less fine material was produced in the size ranges coarser than $212\mu\text{m}$. However, grinding performance of finest ball charge (20mm charge) increased below $212\mu\text{m}$.

As the retention time was increased up to 3min, particles coarser than $850\mu\text{m}$ was found to be ground by 40mm with the highest performance. Since specific surface area of the 40mm ball charge distribution was expected to be lower than the other charge distributions, less collisions will occur in the mill in a shorter residence time and lower performance figures are expected to be obtained for coarser particles when charge distribution gets coarser.

Coarse size ranges such that, particles coarser than approximately $600\mu\text{m}$ could have been ground by the coarsest ball charge better as the retention was increased. Material inside the mill become much finer and the effects of finest charge compositions which is 20mm could have been analysed more clearly as the retention time was increased. Grinding performance of the 20mm ball charge was observed to be higher for particles below $212\mu\text{m}$ as compared to the other charge distributions above 3min time interval, since more specific surface area was provided by the charge and no coating problem was observed as well.

It was observed that, particles coarser than $212\mu\text{m}$ can not be ground by the 20mm ball charge distribution. Breakage energy imparted to the particles in the coarse size ranges ($x \geq 212\mu\text{m}$) might not be enough to break particles in addition to the more coating effect which reduced the grinding efficiency in the mill for longer retention time intervals ($t \geq 10\text{min}$). However, much fines could have been produced in the size ranges below $212\mu\text{m}$ by the 20mm balls above 3min time interval as compared to other distributions.

Test results of 15min included the coating effect thus, grinding performance was lower than as expected.

Finer monosize ball charge distributions are suitable for fine feeds such that below 212 μm for retention time intervals longer and equal to 3min. It was observed that, finest monosize ball charge composition (20mm charge) application for longer retention time (10min) produced much fine material below 212 μm .

Particle size distributions obtained by batch grinding with Standard Bond ball charge and selected coarser and finer ball charge compositions are compared for the same batch grinding time intervals and presented in Figure 5.30 to Figure 5.34.

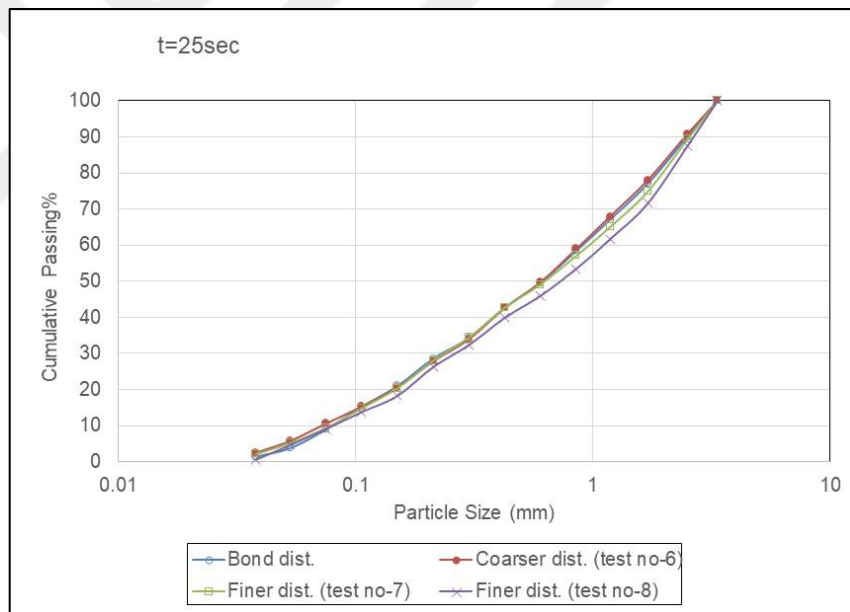


Figure 5.30. Particle size distributions at 25sec obtained by batch grinding with Standard Bond, coarser and finer charge compositions

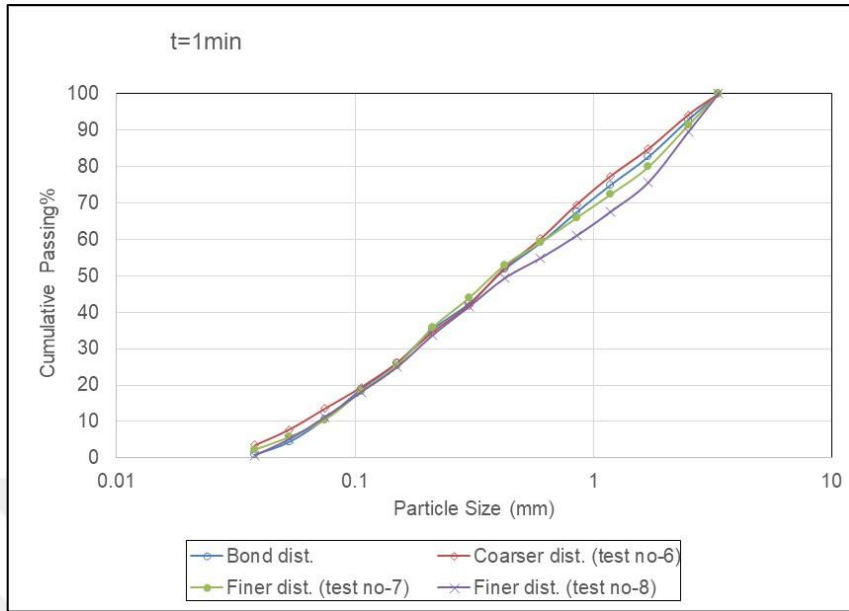


Figure 5.31. Particle size distributions at 1min obtained by batch grinding with Standard Bond, coarser and finer charge compositions

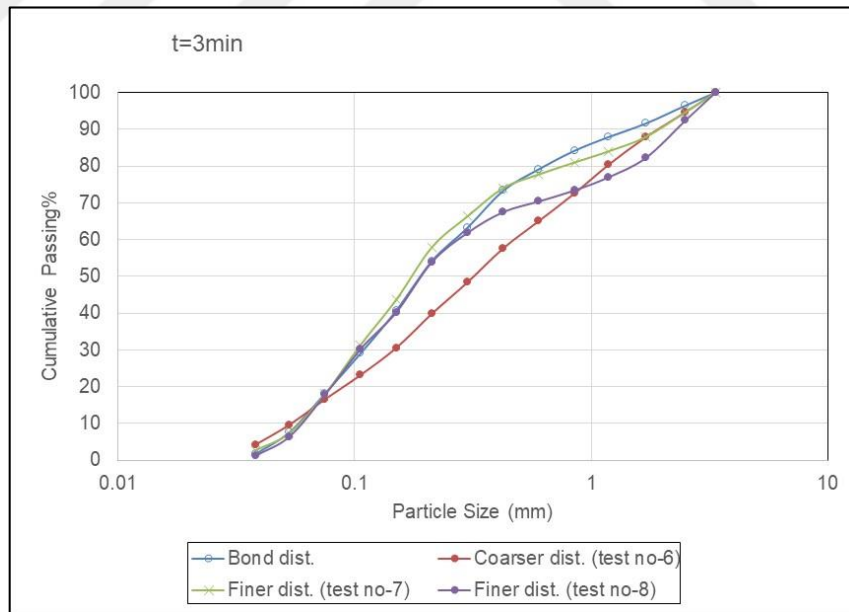


Figure 5.32. Particle size distributions at 3min obtained by batch grinding with Standard Bond, coarser and finer charge compositions

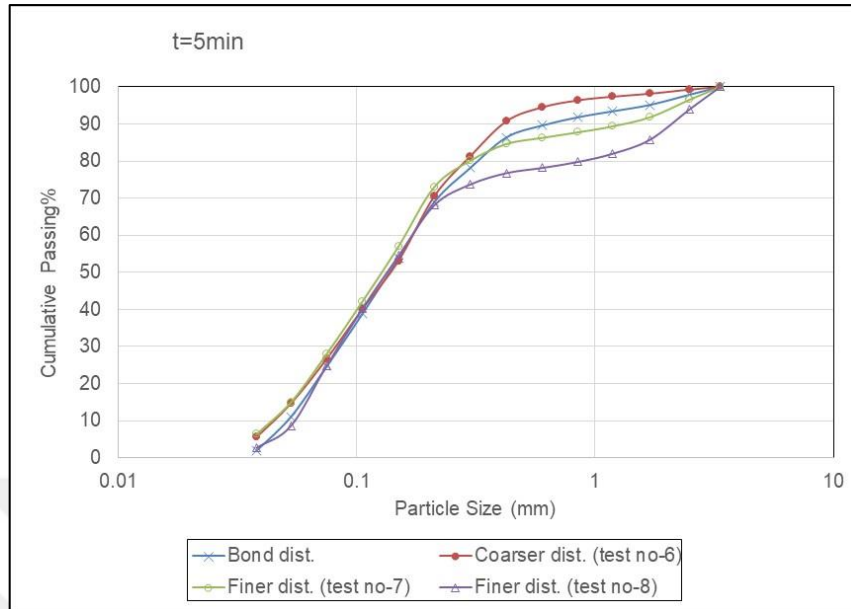


Figure 5.33. Particle size distributions at 5min obtained by batch grinding with Standard Bond, coarser and finer charge compositions

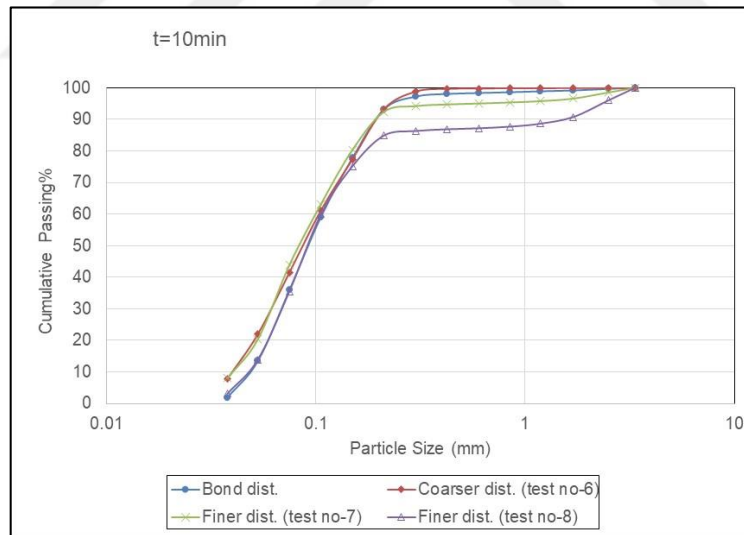


Figure 5.34. Particle size distributions at 10min obtained by batch grinding with Standard Bond, coarser and finer charge compositions

The slope of the ball charge distributions was not changed. However, the fineness of the ball distributions was changed and the effects on mill product fineness was investigated. It was observed that, systematic size reduction progress could have been achieved by the application of the coarser and finer charge distributions as compared to Bond charge

distribution. To see the net effect, mill product particle size distributions obtained at different grinding applications for the same residence time intervals were compared.

Comparisons among coarser and finer charge distribution applications indicated that, for the residence time of 25sec, excluded of the finest charge application (test-8), other charge distributions produced approximately the same of fines. Coarsest particle size distribution was obtained with the finest charge application. As the residence time was increased, coarser charge distribution was observed to be effective in grinding of coarse size ranges ($x > 600\mu\text{m}$). The fineness effect was clearly observed within 1min grinding time.

As the residence time was increased to 3min, mill content size distribution became finer and grinding efficiency of the coarser charge distribution was decreased. Bond distribution and the finer charge distribution (test no-7) showed higher size reduction performance as compared to the other charge distributions. Increasing the residence time further to 5min increased the size reduction performance for the coarser distribution. This indicated that, enough time should be provided so that more collisions should occur in the mill to break coarse particles when coarse ball charge distribution was applied. Charge distribution fineness effect on mill product was clearly observed for particle sizes coarser than $212\mu\text{m}$ such that, coarser charge distribution resulted in finer product. However, as charge distribution got finer, coarser mill product was observed. Production of fine material amount did not change significantly below $212\mu\text{m}$ with the application of different ball distribution fineness.

Increasing the residence time in the mill increased the size reduction performance at coarser ball size distribution applications. This could show the importance of using long mills in which material will spent longer time and also closed circuit grinding with screens and size classifiers. Coarser ball size distribution provided higher levels of breakage energy for impact breakage and could reduce the size of the coarse particles efficiently when enough time was allowed in the mill.

As a consequence, ball size distribution fineness effect could have been reflected on the mill product particle size distributions successfully by the proposed test methodology.

Particle size distributions obtained by batch grinding with Standard Bond ball charge and selected different ball charge compositions are compared for the same batch grinding time intervals and presented in Figure 5.35 to Figure 5.39.

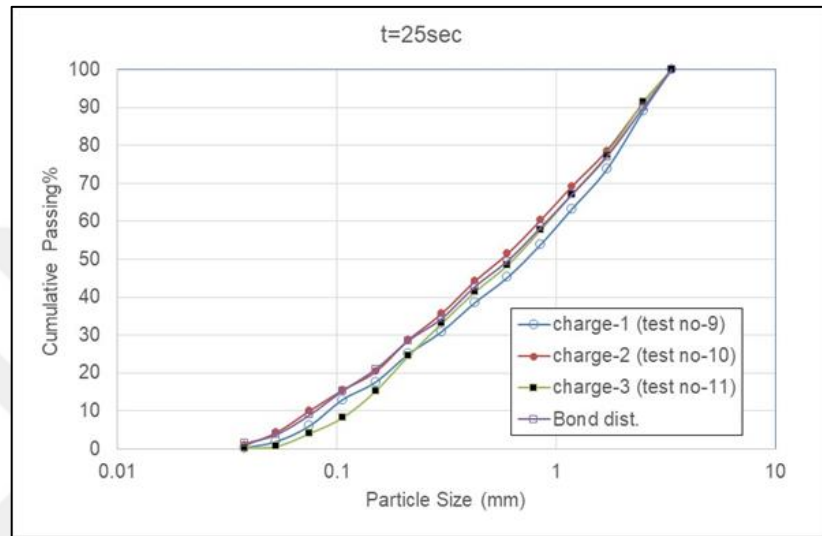


Figure 5.35. Particle size distributions obtained by batch grinding with Standard Bond, charge-1, charge-2 and charge-3 compositions for 25sec

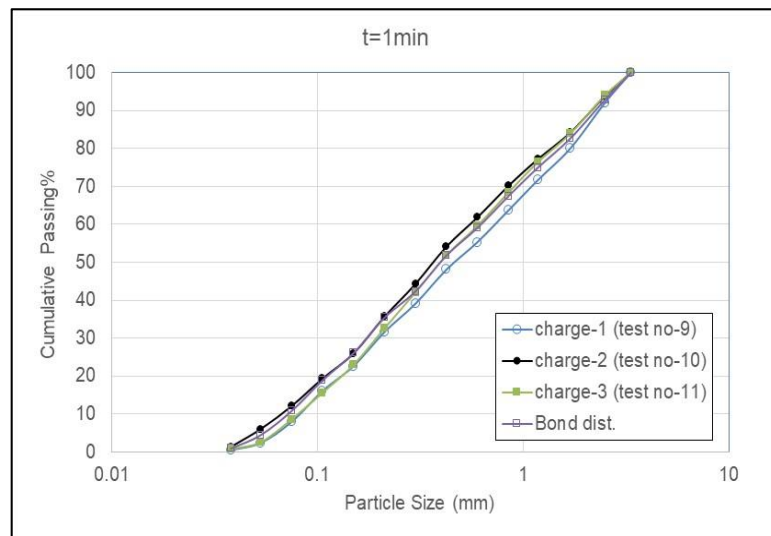


Figure 5.36. Particle size distributions obtained by batch grinding with Standard Bond, charge-1, charge-2 and charge-3 compositions for 1min

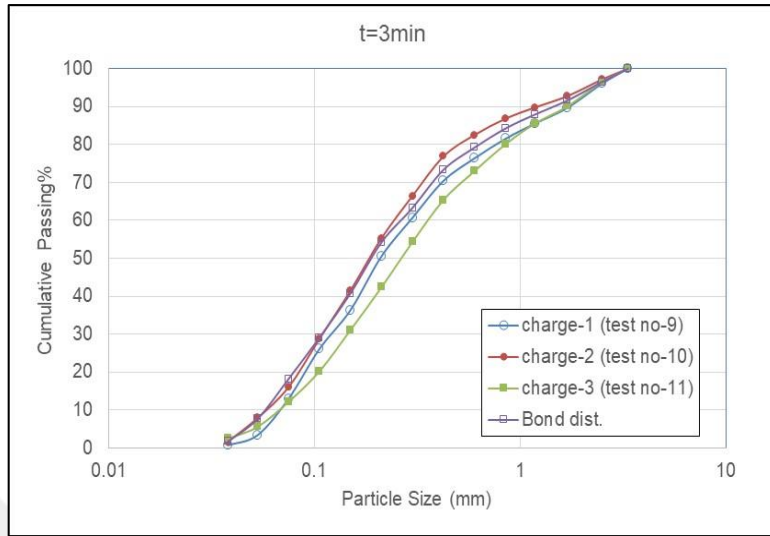


Figure 5.37. Particle size distributions obtained by batch grinding with Standard Bond, charge-1, charge-2 and charge-3 compositions for 3min

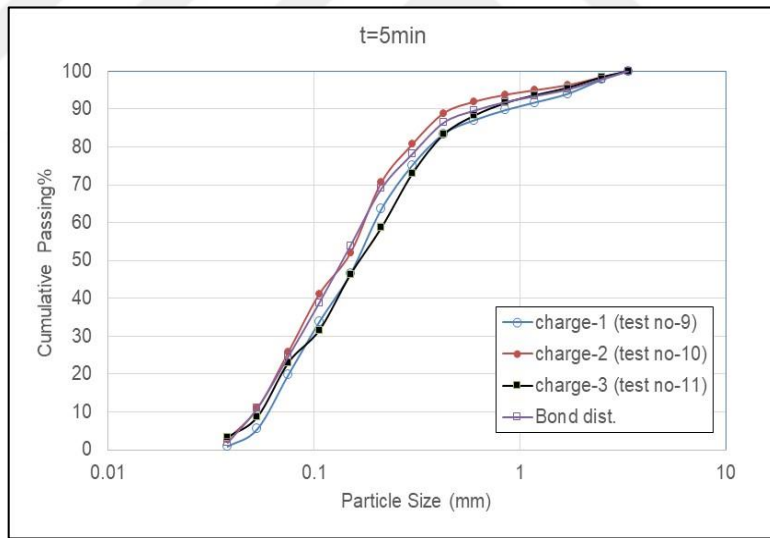


Figure 5.38. Particle size distributions obtained by batch grinding with Standard Bond, charge-1, charge-2 and charge-3 compositions for 5min

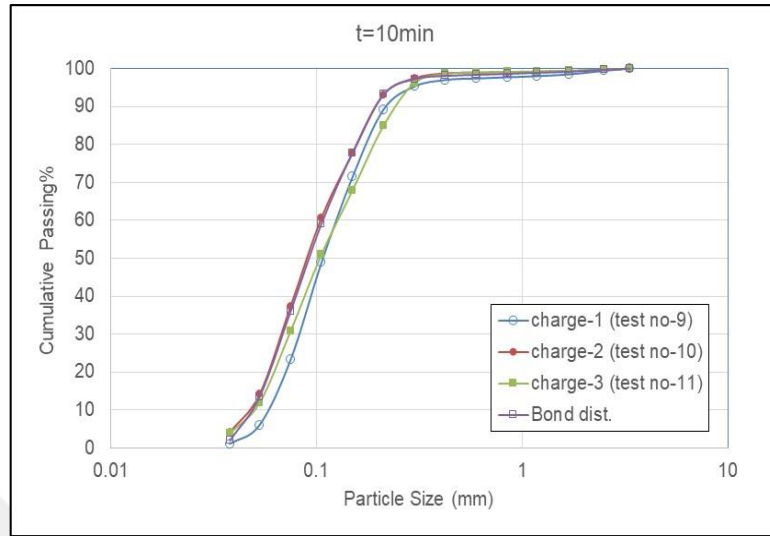


Figure 5.39. Particle size distributions obtained by batch grinding with Standard Bond, charge-1, charge-2 and charge-3 compositions for 10min

Comparisons on the mill product particle size distributions for the same residence time intervals enabled the investigation of the mill charge distribution effect. Average weighed ball size of the distributions were kept constant and the charge distributions were changed. Charge-3 was the finest distribution whereas charge-1 was selected to be the coarsest one. Charge-2 lie between charge-1 and charge-3. Charge-2 application resulted in finer mill product as compared to charge-1 and charge-3 for the shortest residence time. Since charge-3 composition does not include balls finer than 30mm which are required for the breakage of finer size particles under the effect of abrasion and attrition mechanisms, size reduction could not have been improved at fine size ranges such that, typically below 300 μ m as observed for 25sec and 1min grinding cases. Residence time was increased to 1min, charge-2 still remained as the one with the highest grinding performance. Charge-2 composition was found to be the effective one for all residence time intervals which does not include 20mm, 17mm and 15mm balls. Addition of only 25mm balls showed improvement in size reduction performance. As compared to Bond distribution, charge-2 composition also provided approximately the same mill product fineness. It seemed that, application of ball sizes coarser than 20mm would be enough in providing the required level of grinding mechanisms to occur in the mill in obtaining the same degree of size reduction with that of Bond distribution.

As the residence time was increased more fine particles were produced and more impact, abrasion and attrition mechanisms were required for further size reduction. It was known that, smaller balls in the distributions would increase these mechanisms especially abrasion and attrition. However, the claim may not work for all ore types.

The selection of the finest ball in the distribution seems critical according to the test results. The optimum finest ball size may also depend on the ore hardness and also the hardness of the minerals contained in the ore which will totally effect the breakage distribution characteristic thus, production of fine material under different grinding mechanisms.

Consequently, ball distribution effect could have been reflected on the mill product fineness successfully. Results indicated the importance of using different ball sizes which are coarser than 20mm during grinding of chromite ore for higher grinding performance.

5.6.1. Evaluation of mill product fineness as a function of residence time

Relationship between mill product fineness which was represented by the 80% cumulative passing size of the mill discharge particle size distribution obtained from batch test was investigated for selected residence time intervals. A comparison of the obtained relationships is presented in Figure 5.40. Regression analysis was performed and the established relationships for the test conditions are shown on Figure 5.41 to Figure 5.53. Data point corresponding to 15min grinding time was excluded in the regression analysis as high amount of coating was observed during grinding tests. As coating will decrease the grinding efficiency, obtained results for 15min residence time was thought to be not representative.

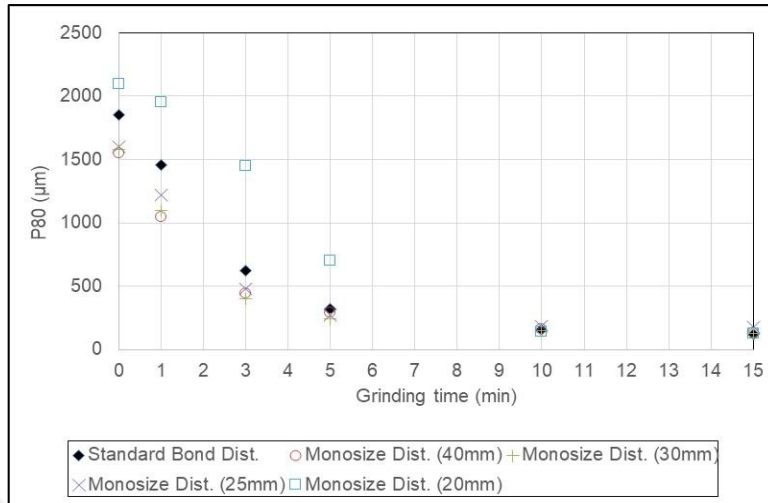


Figure 5.40. Comparisons of relationships between residence time and P80 for the Bond and monosize charge distribution applications

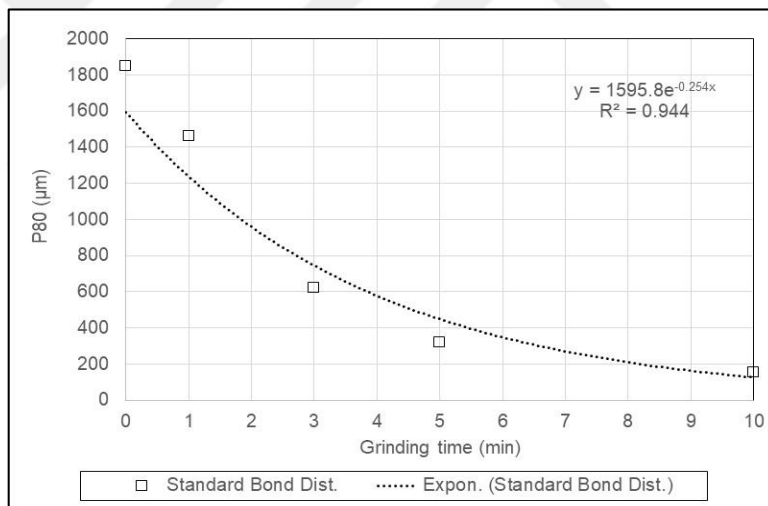


Figure 5.41. Relationship between residence time and P80 for the Bond charge distribution application

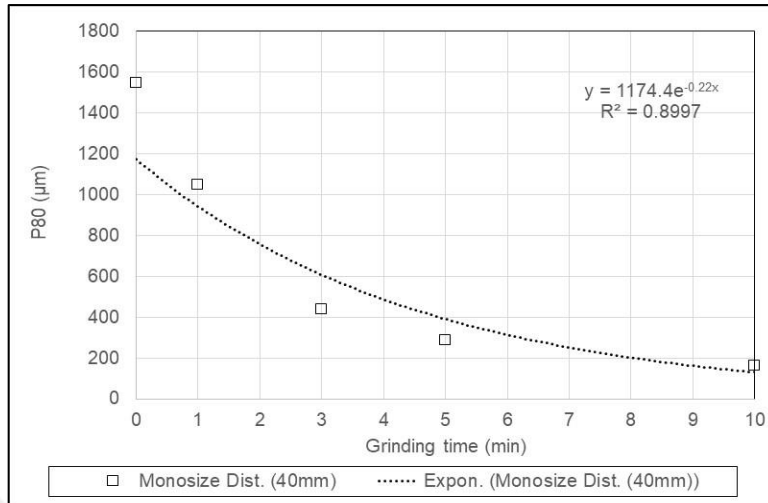


Figure 5.42. Relationship between residence time and P80 for 40mm monosize charge distribution application

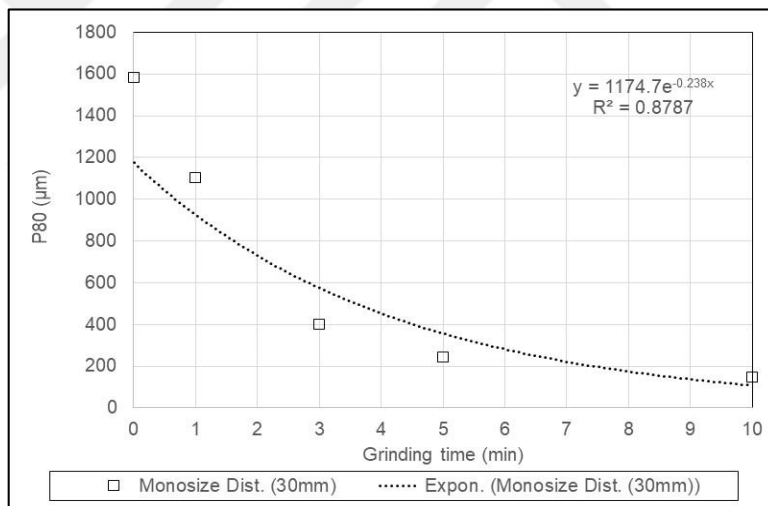


Figure 5.43. Relationship between residence time and P80 for 30mm monosize charge distribution application

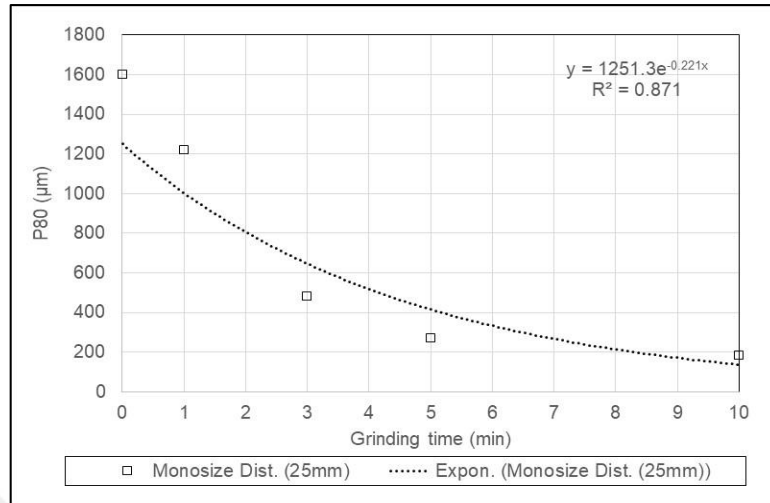


Figure 5.44. Relationship between residence time and P80 for 25mm monosize charge distribution application

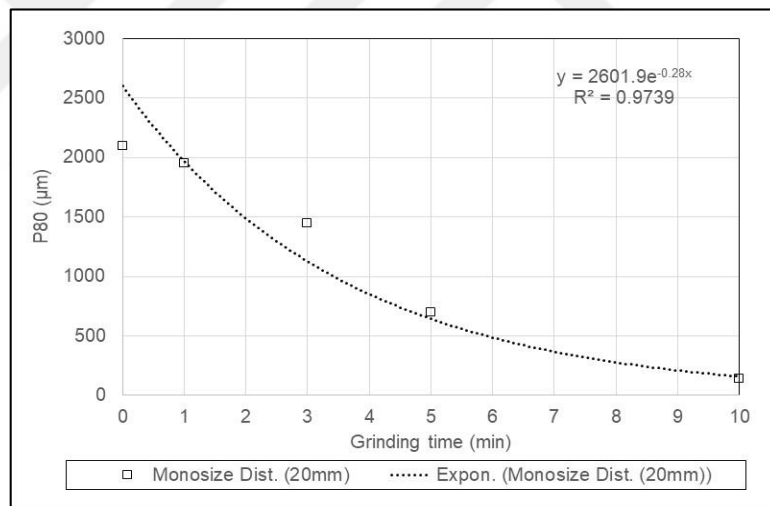


Figure 5.45. Relationship between residence time and P80 for 20mm monosize charge distribution application

It was observed that, size reduction performance was decreased when 20mm monosize ball charge was used (Figure 5.40). Size reduction performance of 40mm and 30mm monosize distributions were determined to be the best based on the mill product P80 size. Ball size effect diminished at 10min residence time interval. Relatively meaningful and reliable correlations could have been drawn between residence time and P80 of the mill product for different ball size applications.

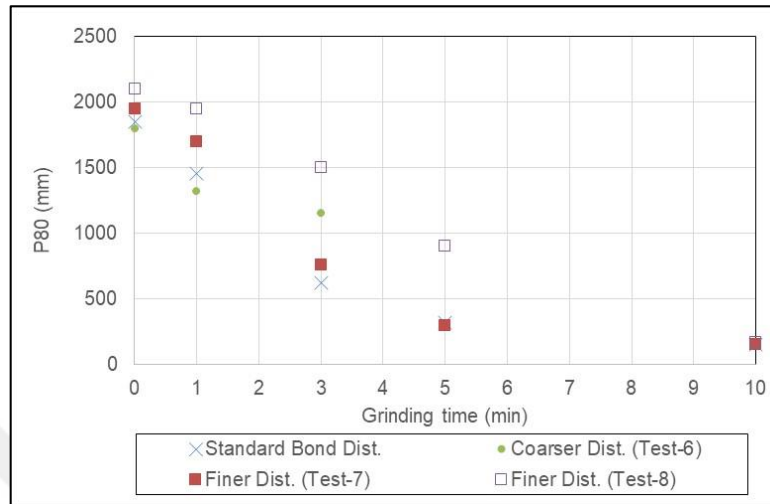


Figure 5.46. Comparison of the relationship between residence time and P80 for Standard Bond, coarser and finer charge distributions

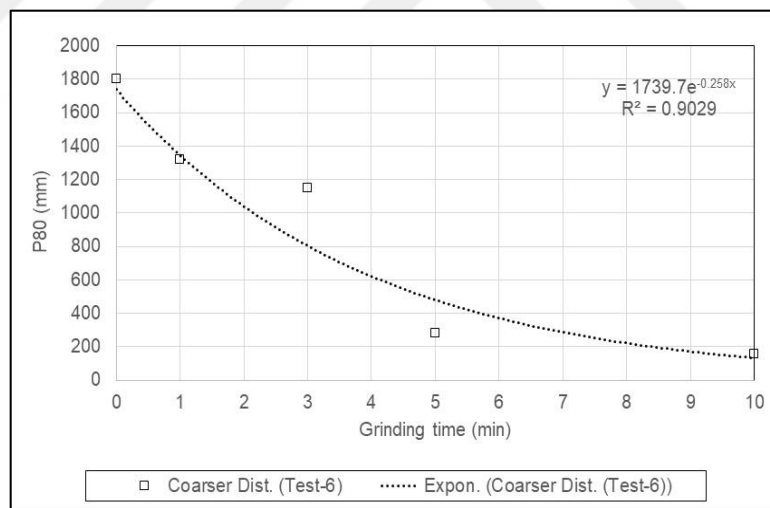


Figure 5.47. Relationship between residence time and P80 for coarser charge distribution (Test-6)

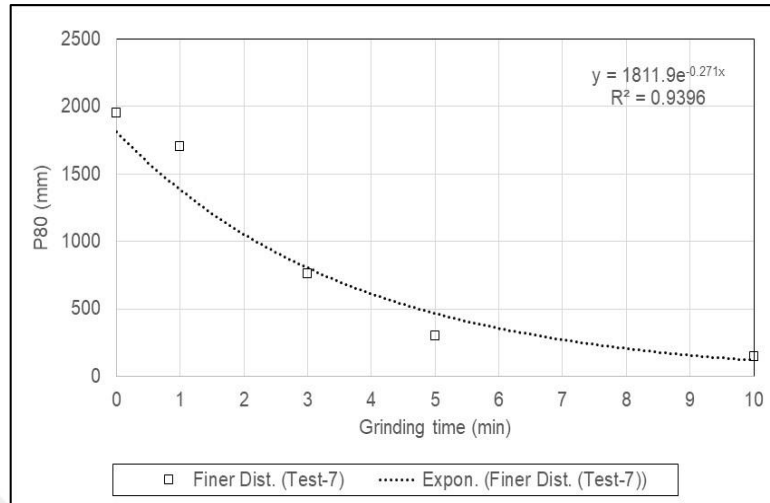


Figure 5.48. Relationship between residence time and P80 for finer charge distribution (Test-7)

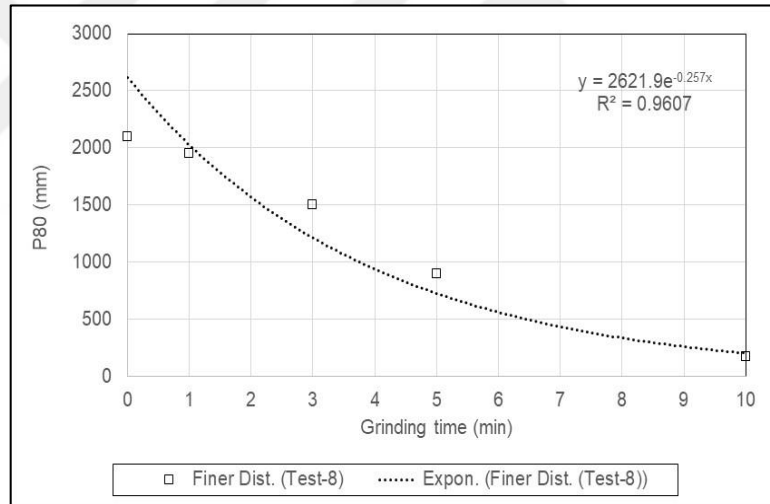


Figure 5.49. Relationship between residence time and P80 for finer charge distribution (Test-8)

Findings indicated that, coarser ball distribution was effective for grinding of coarser mill feeds as in the case of 25sec and 1min time intervals. As the residence time was increased, mill content particle size distribution became finer and the net effect of finer distributions could have been observed successfully at 3min grinding time. However, provided grinding energy with the application of very fine ball distribution (test-8) was thought to be not enough and thus, coarse particles remained in the mill without being broken and probably decreased the breakage probability of fine particles. Material should spend enough time so that the appropriate fineness could have been achieved in

the mill. Ball size distribution fineness effect was diminished at 10min residence time. Relatively meaningful and reliable correlations could have been drawn between residence time and P80 of the mill product for different ball size distribution fineness applications.

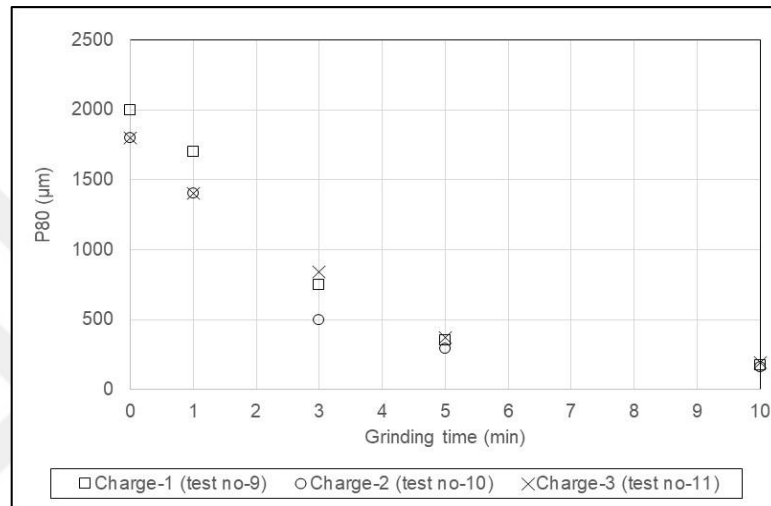


Figure 5.50. Comparison of the relationship between residence time and P80 for different charge distributions

When the weighted average ball size was not changed in the distributions, finer distribution resulted in finer mill product within 1min time. 94% of Charge-3 was composed of 30mm balls by weight and showed the same size reduction degree within 1 min time with that of charge-2 which contains 56%, 30mm balls by weight and also 26%, 25mm balls by weight in the distribution. Application of charge-2 composition resulted to produce much fine particles as the residence time was increased. Grinding performance with charge-2 composition was determined to be the highest. Selecting balls finer than 25mm in the charge distributions did not increase the size reduction performance for the grinding case. Ball size distribution effect started to diminish at 5min residence time interval and the same fineness degree was obtained at 10min time. On the other hand, relatively meaningful and reliable correlations could have been drawn between residence time and mill product fineness (P80).

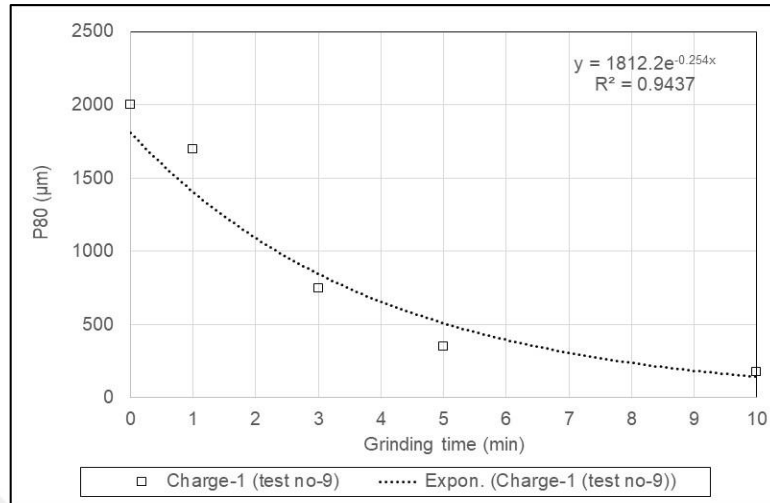


Figure 5.51. Relationship between residence time and P80 for charge-1 distribution (Test-9)

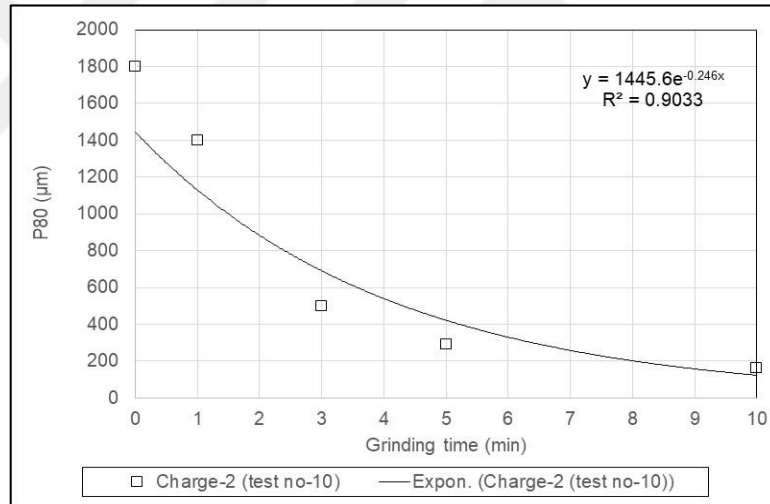


Figure 5.52. Relationship between residence time and P80 for charge-2 distribution (Test-10)

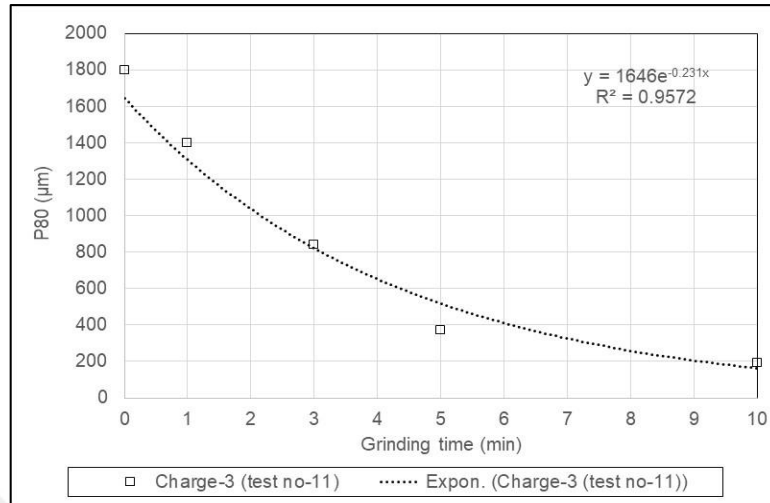


Figure 5.53. Relationship between residence time and P80 for charge-3 distribution (Test-11)

5.7. Specific Energy Consumption Evaluation

Bond proposed that, the energy required to crush or grind a material is the total energy required to produce the 80% passing size of the product from an infinite size minus the energy used to produce 80% passing size of the feed from an infinite size. Specific energy consumptions for each grinding test in units of kWh/t was estimated according to Bond's energy theory which is given as below:

$$\text{Work (W)} = 10 \times W_i \times (1/\sqrt{P80} - 1/\sqrt{F80}) \quad (5.6)$$

Where;

W : Work input in kilowatt hours per ton

W_i : Bond ball mill work index (kWh/ton)

F80 : Particle size which 80% of the mill feed passes (µm)

P80 : Particle size which 80% of the mill product passes (µm)

The Bond equation was used to calculate the grinding energy required. It should be mentioned that, the power (kW) required calculated from Bond's equation is the power

that should be delivered to the mill and does not include motor or drive losses. It is a simple tool for use in as stated in Rowland (2006):

- Determining the power required for crushing and grinding by crushers and grinding mills,
- Calculating the size reduction efficiency of crushers and grinding mills,
- Comparing crushing and grinding circuits with the same feed to the same product sizes and the same work index based upon laboratory crushability and grindability tests.

5.7.1. Relationship between specific energy consumption and P80

Overall empirical relationship between specific energy consumptions and mill product fineness which was represented by the 80% cumulative passing size (P80) was established and presented for all the test conditions in Figure 5.54. There is a logarithmic correlation between grinding energy requirement and mill product fineness (P80). R^2 value is 0.98 and thus, it is relatively a good correlation which gives mill product fineness size and the required specific energy for chromite ore grinding.

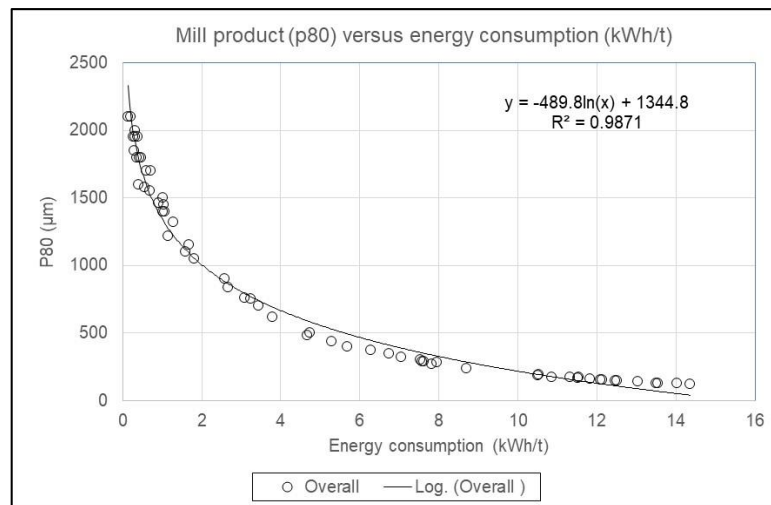


Figure 5.54. Overall relationship between specific energy consumption and P80

5.7.2. Relationship between residence time and specific energy consumption

Additionally, empirical relationships between batch grinding time intervals (residence or retention time) and energy requirements were investigated. Related regression analysis results are presented in Figure 5.55 to Figure 5.68.

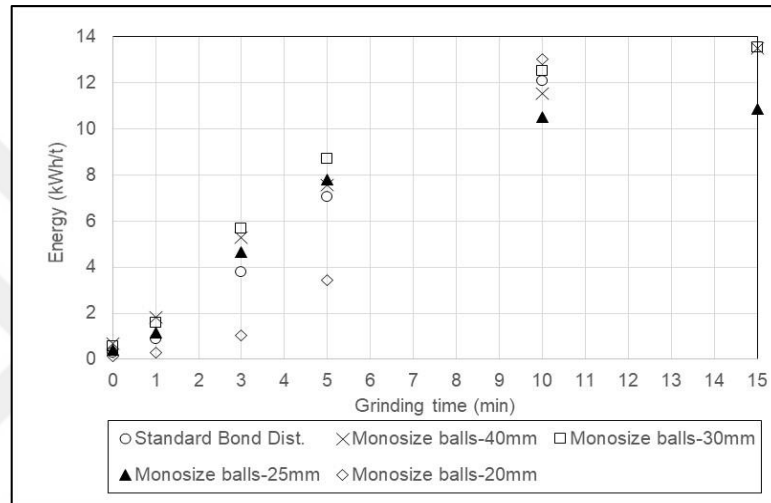


Figure 5.55. Relationship between residence time and energy consumption for Bond and monosize charge distribution applications

Lowest energy requirement was obtained for 20mm monosize ball distribution application within 5 min time. However, highest grinding energy consumption was observed for 20mm balls for 10min grinding time. Grinding efficiency was decreased for 20mm ball size distribution case. For longer residence time cases ($t > 10\text{min}$), grinding efficiency of 25mm balls was determined to be higher.

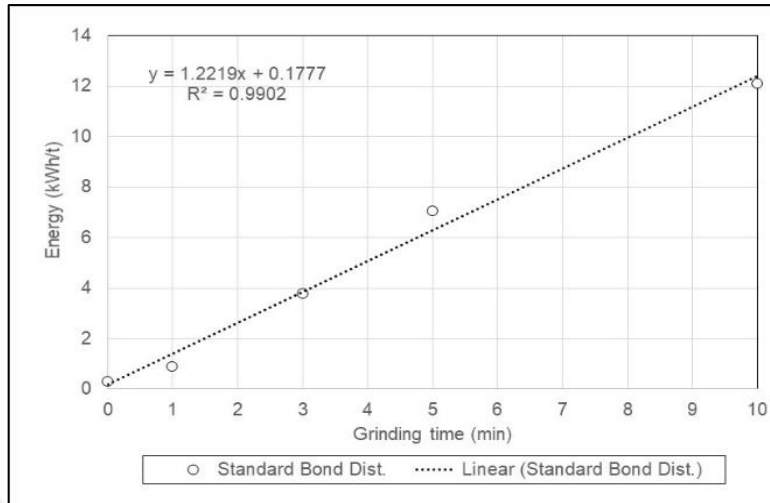


Figure 5.56. Relationship between residence time and energy consumption for Bond charge distribution application

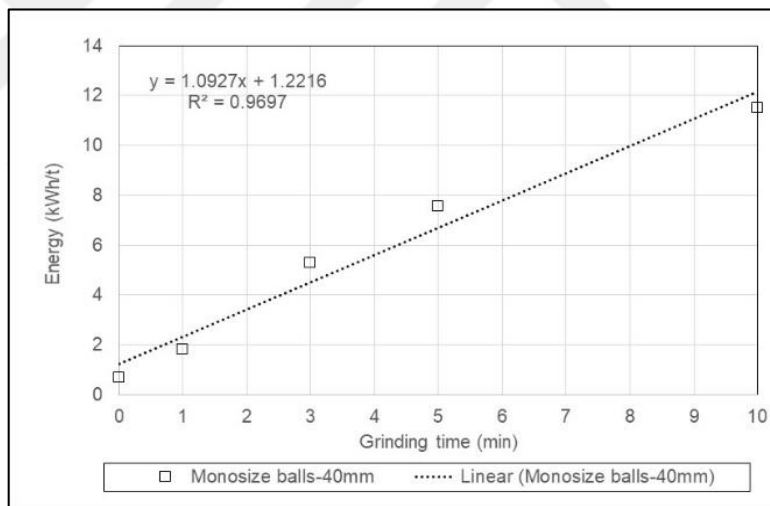


Figure 5.57. Relationship between residence time and energy consumption for 40mm monosize charge distribution application

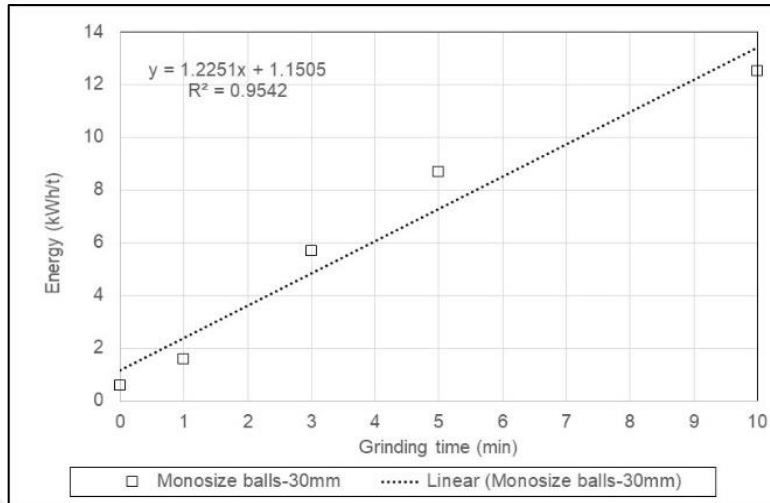


Figure 5.58. Relationship between residence time and energy consumption for 30mm monosize charge distribution application

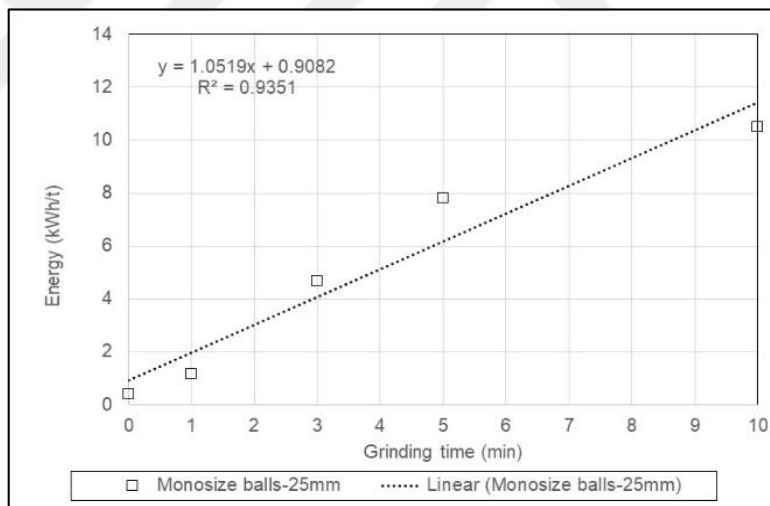


Figure 5.59. Relationship between residence time and energy consumption for 25mm monosize charge distribution application

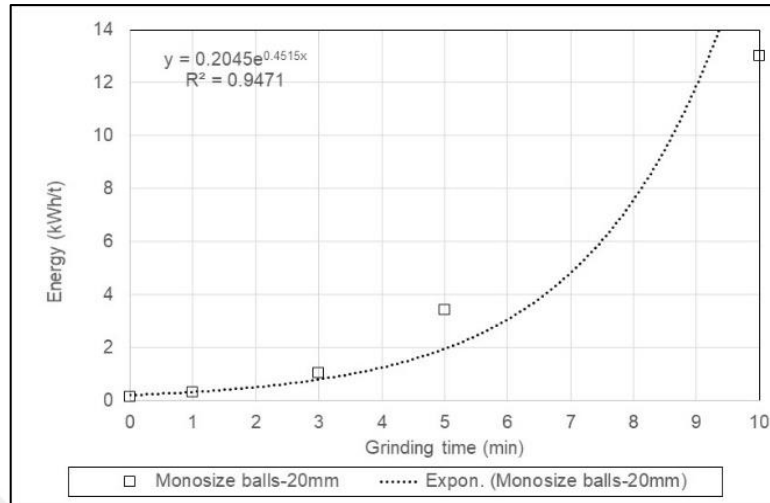


Figure 5.60. Relationship between residence time and energy consumption for 20mm monosize charge distribution application

Relatively good correlations could have been derived between residence time and energy consumption for different ball size applications. Grinding conditions of 20mm monosize ball distribution was found to be different than the other monosize distributions as shown in Figure 5.60.

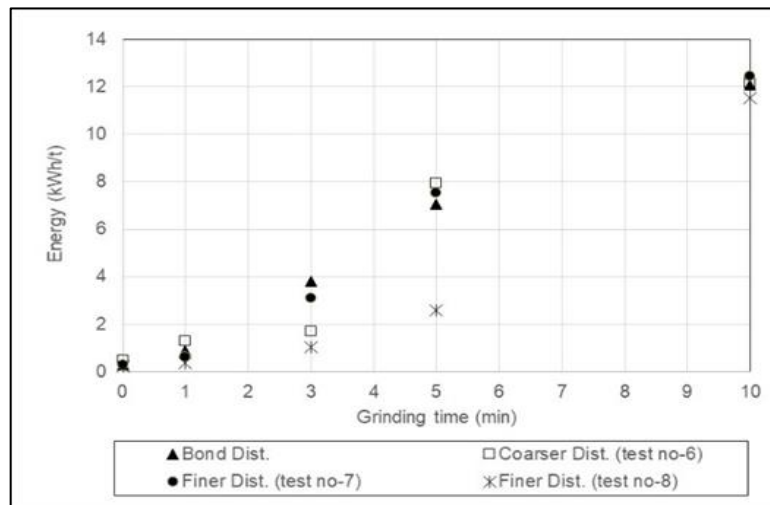


Figure 5.61. Comparison of the relationship between residence time and energy consumption for Bond, coarser, and finer charge distribution applications

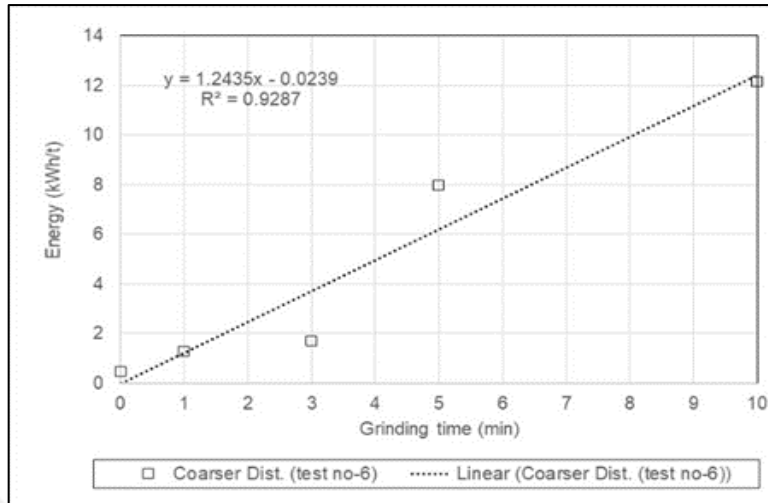


Figure 5.62. Relationship between residence time and energy consumption for coarser charge distribution application (test-6)

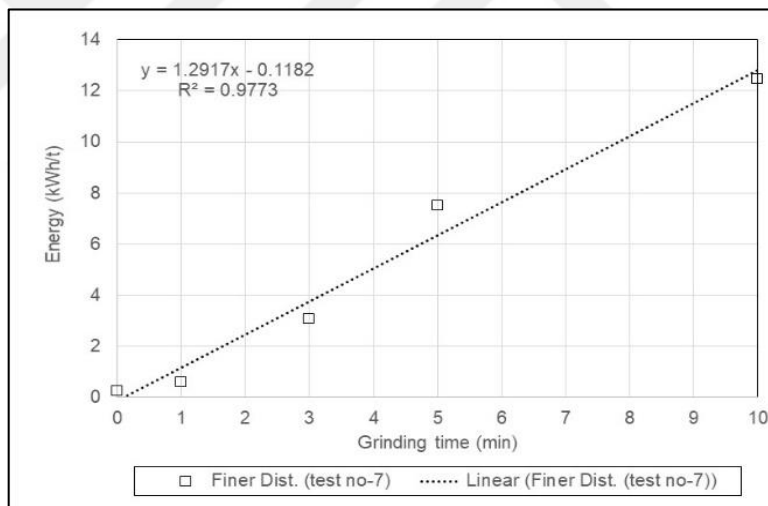


Figure 5.63. Relationship between residence time and energy consumption for finer charge distribution application (test-7)

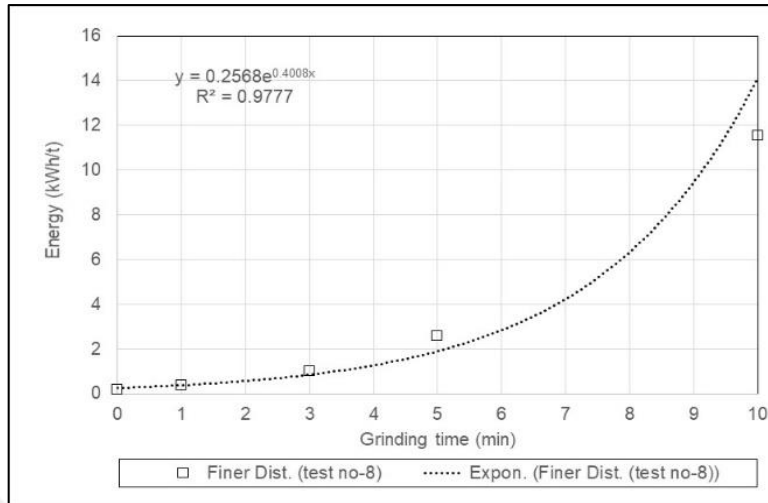


Figure 5.64. Relationship between residence time and energy consumption for finer charge distribution application (test-8)

Finest distribution (test-8) was determined to provide energy efficient grinding conditions. Coarsest distribution required more grinding energy for the same residence time as compared to the other distributions excluded of 3min condition. Relatively meaningful correlations could have been drawn between residence time and energy consumption for the test conditions.

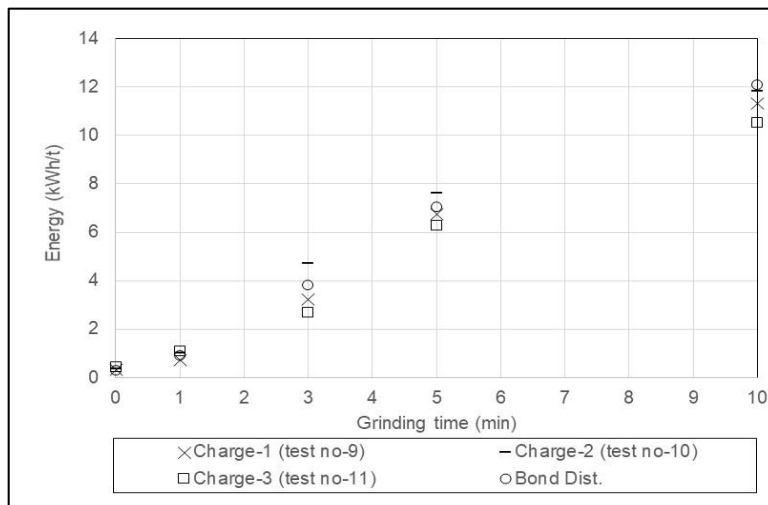


Figure 5.65. Comparison of the relationship between residence time and energy consumption for Bond, charge-1 (test-9), charge-2 (test-10) and charge-3 (test-11) distribution applications

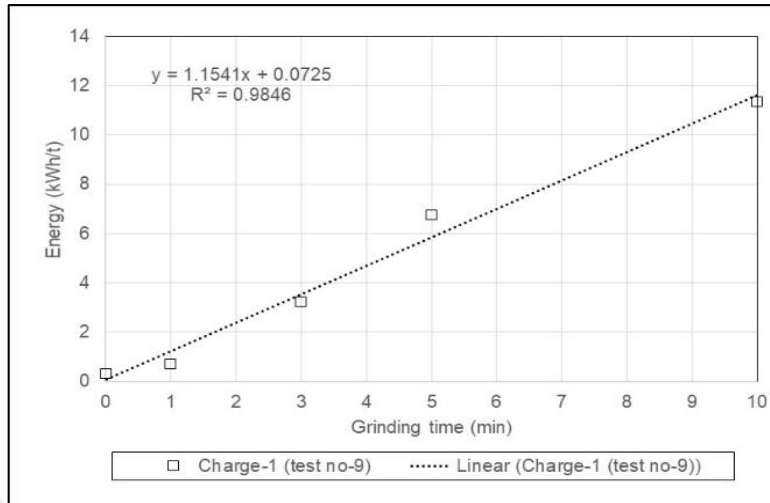


Figure 5.66. Relationship between residence time and energy consumption for charge-1 (test-9) distribution application

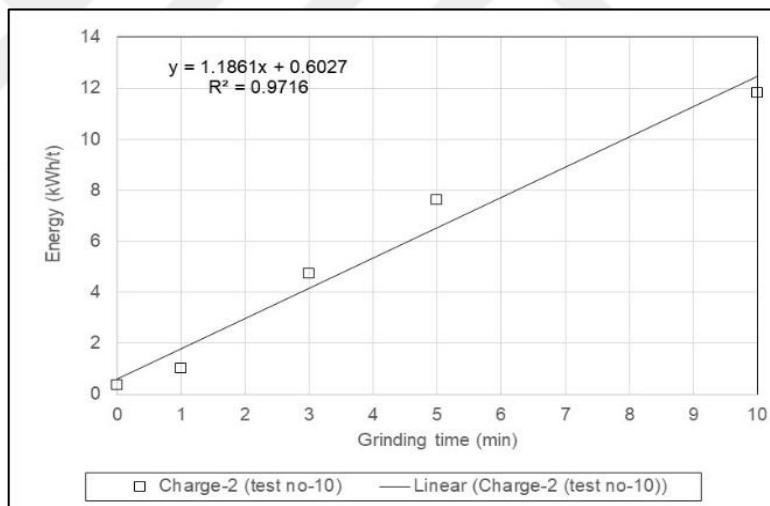


Figure 5.67. Relationship between residence time and energy consumption for charge-2 (test-10) distribution application

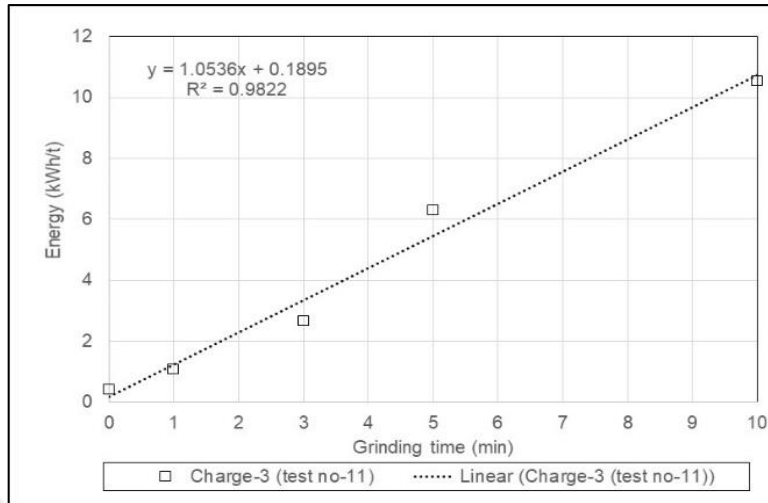


Figure 5.68. Relationship between residence time and energy consumption for charge-3 (test-11) distribution application

Charge-3 composition was determined to be energy efficient for all the residence time intervals. Relatively good correlations could have been drawn between residence time and energy consumption for the test conditions.

6. SPECIFIC BREAKAGE RATE FUNCTION ESTIMATION

Modelling and simulation methodologies require reliable industrial scale data to establish grinding models to perform simulations. Simulation work will show, what will happen to the mill product under different operational conditions. Besides the simulation work, effect of different operational parameters of a mill such as ball size and its distribution, ball load, mill feed fineness or operational solids% in wet grinding conditions etc. on mill product fineness and thus on size reduction performance can be tested by trials in full-scale (industrial scale). However, such trials are time consuming and costly. In this context, laboratory scale or pilot scale tests become favorable which can be performed under easily controlled conditions and can provide insightful information on industrial scale operations. Theoretical approaches can be tested easily and implemented to make predictions on any size reduction machine by using the information obtained from laboratory scale tests. Scale-up relationships can be established to predict full-scale operations or already known scale-up relationships can be tested and verified so that to be able to use in simulations.

size reduction modelling approach proposed in Austin (1984) by has been implemented in the literature by many researchers to investigate the effect of operational parameters of a ball such as ball load, ball size etc. on specific breakage rate functions. The disadvantage of widely applied Austin's (1984) approach is the number of model parameters. The models developed include many parameters and more than one solution could be obtained during the estimation of model parameters. Additionally, the method estimates the breakage rates of monosize fractions. In this context, perfect mixing grinding model was selected for the estimation of the specific breakage rates of particles. Proposed methodology considered a full particle size distribution (-3.35mm) as the mill feed. As only single size fraction was not used as the mill feed in the batch tests, an average specific breakage rate was estimated for the milling conditions. Specific

breakage rates of each particle was estimated at different grinding media size applications. The tests were batch type so that to be able to analyze the variations in breakage rate functions as a function of residence time in the mill.

Specific breakage rate functions were back-calculated by using perfect mixing mathematical model proposed by Whiten (1976) for the mill products for each grinding time. The components of the mill model are, mill feed particle size distribution, mill product particle size distribution, specific breakage rate (hr^{-1}), specific discharge rate (hr^{-1}), specific breakage function (a_{ij}). Mill feed and product particle size distributions were measured experimentally. A theoretical breakage function defined by Broadbent and Callcott (1956) was used in solving the model. The breakage function values are given in Table 6.1.

Table 6.1. Broadbent and Callcott breakage (appearance) function used in the JKSimMet software (JKSimMet Software V4.32, 1998)

Particle size (mm)	Appearance
38	0.000
26.87	0.193
19	0.157
13.44	0.126
9.5	0.101
6.72	0.082
4.75	0.066
3.36	0.053
2.38	0.043
1.68	0.035
1.19	0.028
0.840	0.022
0.594	0.018
0.420	0.015
0.297	0.012
0.210	0.010
0.148	0.008
0.105	0.006
0.074	0.004
0.052	0.003
0.037	0.002
0.026	0.0015
0.019	0.001
0.013	0.0005

When these three parameters are defined, the ratio of breakage rate to discharge rate function which is denoted by “r/d” component in the grinding model could be back-calculated. The r/d is known to be the ball mill model parameter and can be estimated by non-linear least squares techniques. JKSimmet mineral processing software was used in the back-calculation stage of the breakage rates by non-linear least squares techniques using spline mathematical functions as given in Whiten (1972). Model fitting module of the JKSimMet software calculates “r/d*” which gives the ratio of breakage rate to normalized discharge rate “d*” values. “r/d*” values can be obtained when discharge rate function “di” is scaled in terms of mill volume and volumetric feed rate “Q” (m³/h) to the term d*. By this way, variations in residence time in each test can be corrected and Equation (6.1) was used in the calculations.

$$d^* = \frac{d_i}{\frac{4Q}{LD^2}} \quad (6.1)$$

Where, “D” and “L” are the diameter and length of the Bond ball mill (Napier Munn et.al., 2005). Perfect mixing mathematical model is coded in the JKSimMet software and can be used directly when the required mill feed, discharge and breakage function data are provided. The mill discharge rate function is defined as the ratio of mill product size distribution to the size distribution of the material inside the mill which is equal to 1 (di=1). Thus, specific breakage rate functions “r” can be estimated directly from the perfect mixing mathematical equation once the “r/d*” values are determined. Relationships between particle size and “r/d*” values can be established for different test conditions. However, the estimated breakage rates “r” should be normalized according to the batch grinding time interval “t” in minutes to obtain the unit of breakage rate in min⁻¹.

In this study, variations in specific breakage rates or specific breakage rate functions estimated from perfect mixing model were analysed for different retention time intervals and selected ball charge distribution applications. Ball charge filling ratios were set to a constant value which was selected as the Standard Bond charge filling (CF) ratio which is calculated as 0.21 in all grinding test conditions.

It should be mentioned that, in industrial scale operations, if specific breakage rates in the mill could be increased, the production capacity (t/h) of the mills could be increased as well. That's why, analysis of the specific breakage rates under different operational conditions have a vital importance.

6.1. Variation of Specific Breakage Rate Functions with Particle Size at Different Ball Charge Compositions

Batch grinding test results were fitted to the perfect mixing mathematical model with the aid of model fitting module of the JKSimMet software to estimate empirical “ r/d^* ” values for each test condition. Discharge rate function was set to a value of 1 ($d_i=1$) and estimated “ r/d^* ” values used to calculate breakage rate function denoted by “ r ”. Breakage rate functions were then normalized according to the residence time in the mill denoted by “ t ” to obtain specific breakage rates in units of min^{-1} . Standard deviation (SD) variations for the perfect mixing model fitting calculations obtained from JKSimMet software are tabulated in Table 6.2. When SD value approaches to a value one, there is a good match between experimental and calculated data for that stream when the model is fitted. Statistical data presented in Table 6.2 confirmed the success of the model fitting thus, the estimation of the breakage rates. Sufficiently good agreement was observed between experimental and back-calculated (model fitted) particle size distributions for each test condition. Best fit estimates for the data sets were observed for the 0.25sec, 1 and 3min grinding time intervals. It should be mentioned that, breakage rates obtained for 15min grinding time included the coating effect. Resulting breakage rates are shown on the graphs. It should be mentioned that, related results for all the test conditions do not show the actual grinding performance in the mill. Thus, related rates are not included in the grinding performance discussions. Back-calculated specific breakage rate functions for the Standard Bond and monosize ball distribution applications are given in Figure 6.1 to Figure 6.9. for the test conditions.

Table 6.2. Standard deviation (SD) variations obtained in the back-calculation of breakage rates from perfect mixing model using JKSimMet Software V4.32

Batch Tests	Standard Deviation (SD)					
	t=25sec	t=1min	t=3min	t=5min	t=10min	t=15min
Test-1	0.30	0.78	1.86	2.49	4.35	5.16
Test-2	0.34	0.48	1.61	2.3	3.56	3.41
Test-3	0.45	0.84	1.95	2.75	4.36	4.43
Test-4	0.42	0.73	1.72	2.43	3.06	3.05
Test-5	0.76	0.99	2.22	3.01	4.73	5.20
Test-6	0.25	0.47	0.69	2.50	3.55	-
Test-7	0.42	0.91	2.68	2.32	4.07	3.92
Test-8	0.41	0.79	1.96	2.76	4.37	-
Test-9	0.97	1.21	2.14	2.85	4.66	-
Test-10	0.42	0.71	1.80	2.65	4.65	-
Test-11	0.45	0.84	1.03	2.23	3.70	-

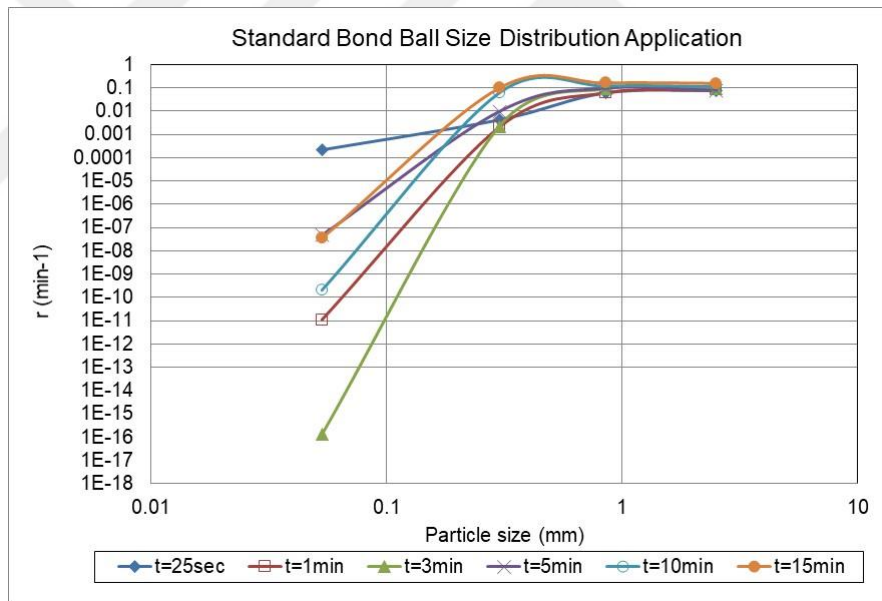


Figure 6.1. Specific breakage rates obtained by grinding with Standard Bond charge distribution

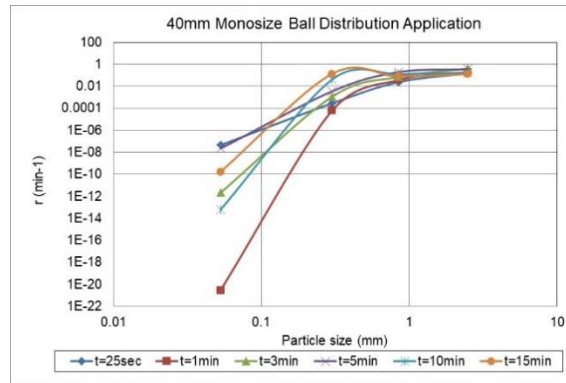


Figure 6.2. Specific breakage rates obtained by grinding with 40mm monosize ball charge distribution

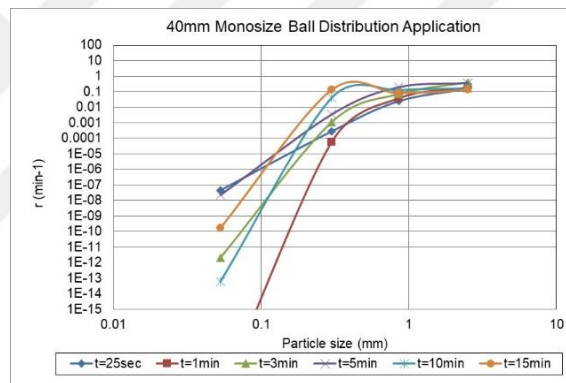


Figure 6.3. Specific breakage rates obtained by grinding with 40mm monosize ball charge distribution (Enlarged y-scale)

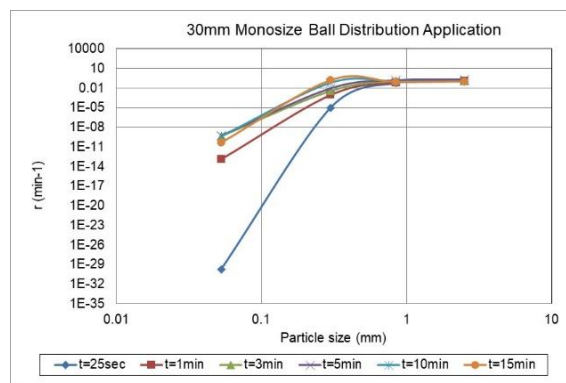


Figure 6.4. Specific breakage rates obtained by grinding with 30mm monosize ball charge distribution

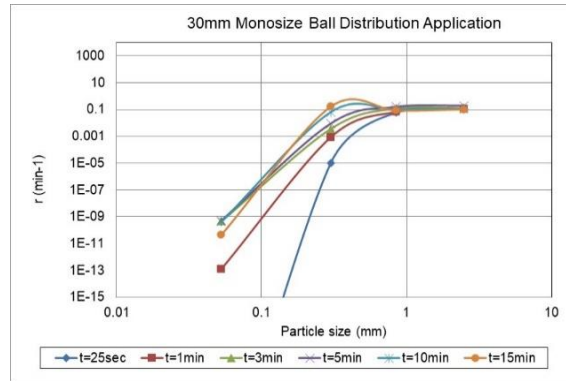


Figure 6.5. Specific breakage rates obtained by grinding with 30mm monosize ball charge distribution (Enlarged y-scale)

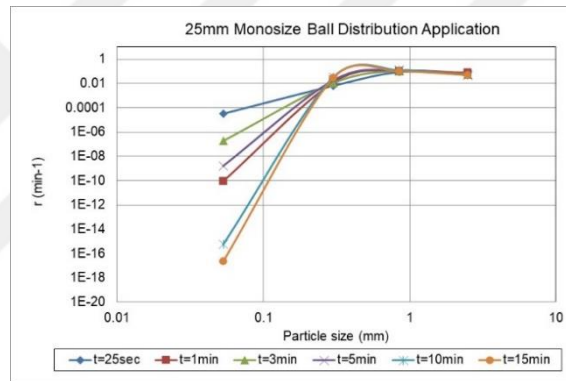


Figure 6.6. Specific breakage rates obtained by grinding with 25mm monosize ball charge distribution

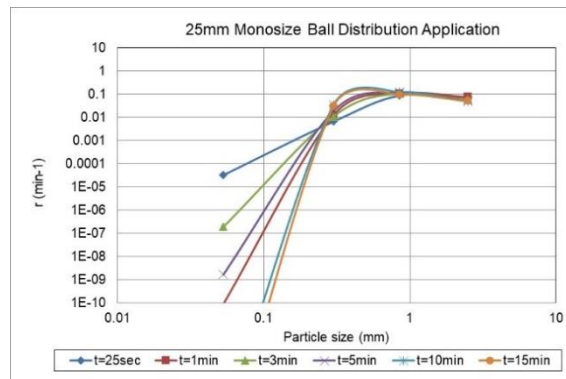


Figure 6.7. Specific breakage rates obtained by grinding with 25mm monosize ball charge distribution (Enlarged y-scale)

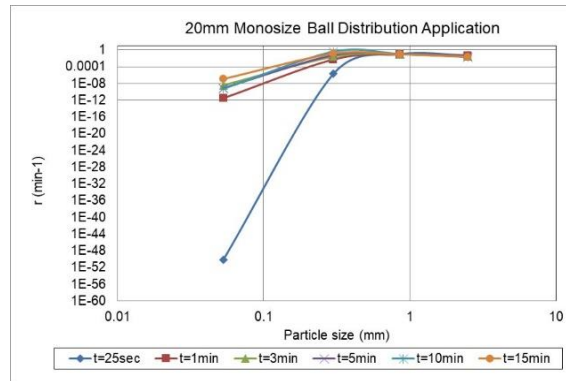


Figure 6.8. Specific breakage rates obtained by grinding with 20mm monosize ball charge distribution

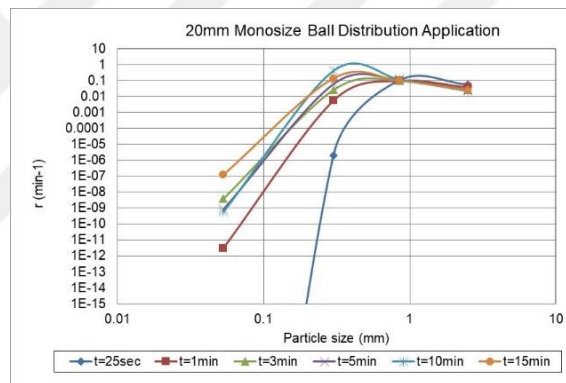


Figure 6.9. Specific breakage rates obtained by grinding with 20mm monosize ball charge distribution (Enlarged y-scale)

Characteristic average specific breakage rate functions as given in Figure 6.1 to Figure 6.9. were determined to change with time in the mill. As mill content (hold-up) distribution was changed with time, specific breakage rate functions were accordingly changed. Particles coarser than 300 μ m were observed to break approximately at the same rate. Maximum particle size that can be broken by the maximum ball size in the mill was observed to change with time. X_m sizes were found to vary as 1.25mm, 0.884mm and 0.442 mm. Below X_m size attrition breakage predominates and above X_m size, impact breakage predominates as stated in Napier Munn et.al. (2005). In this context, at attrition region of the breakage rate curve, breakage rate curves were found to change as the residence time was increased A systematic increase or decrease could not have been observed with time. Highest breakage rates were observed in the first 25sec

for particles finer than X_m size. Attrition effect resulted in lower rates at residence time intervals lower than 25sec.

Specific breakage rates were observed to not change for particles coarser than $850\mu\text{m}$ in 40mm monosize ball distribution application. However, the rate curves were changed below this size for different residence time intervals in the mill. It could be concluded that, highest breakage rates were determined for 5min residence time.

In the case of 30mm monosize application, similarly, specific breakage rates were observed to not change for particles coarser than $850\mu\text{m}$. Breakage rate functions varied with residence time below this size. Highest and approximately the same breakage rates were observed for 3, 5 and 10min time intervals. Breakage rates did not vary considerably. Lowest breakage rate was observed for the grinding times shorter than 3min. As could be seen, as the residence time was increased, breakage rates were increased as well. A systematic change could have been obtained with the grinding conditions attained by 30mm monosize ball application.

In the case of grinding with 25mm monosize ball distribution, at the shortest and highest time intervals specific breakage rates were observed to not change for particles coarser than $850\mu\text{m}$. Specific breakage rates were also not changed for particles coarser than $300\mu\text{m}$ for grinding time intervals of 1, 3 and 5min. Below $300\mu\text{m}$, breakage rates were varied. Highest breakage rates were observed for 25sec time interval. Results indicated that, high breakage rates could be attained in very short grinding times as in the case of 25mm ball application.

Grinding with 20mm monosize balls in the mill indicated the similar typical variation in breakage rates with that of 30mm grinding case. Breakage rates were increased with residence time for particles finer than $850\mu\text{m}$. However, the rates did not change above this size. Effect of impact mechanism resulted in the same rate values. Highest rate was observed for 10min grinding with 20mm monosize balls below $850\mu\text{m}$.

Findings indicated that, grinding conditions such that, number of collisions of balls and particles, collision probabilities etc. are all expected to change depending on the applied ball size and number of balls included in the distributions. Hence, breakage rates were changed with residence time.

Back-calculated specific breakage rates for different charge distributions are presented in Figure 6.10 to Figure 6.12.

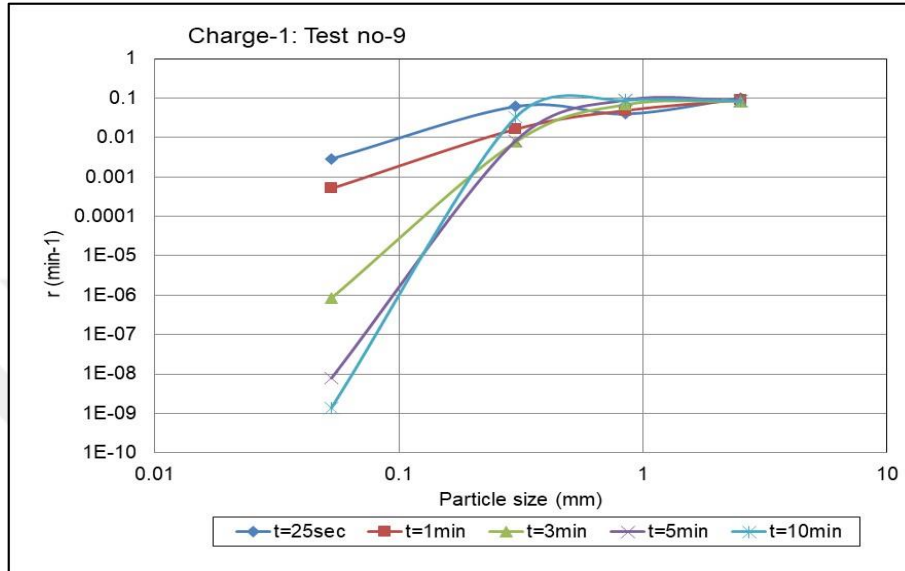


Figure 6.10. Specific breakage rates obtained by grinding with charge-1 distribution (test-9)

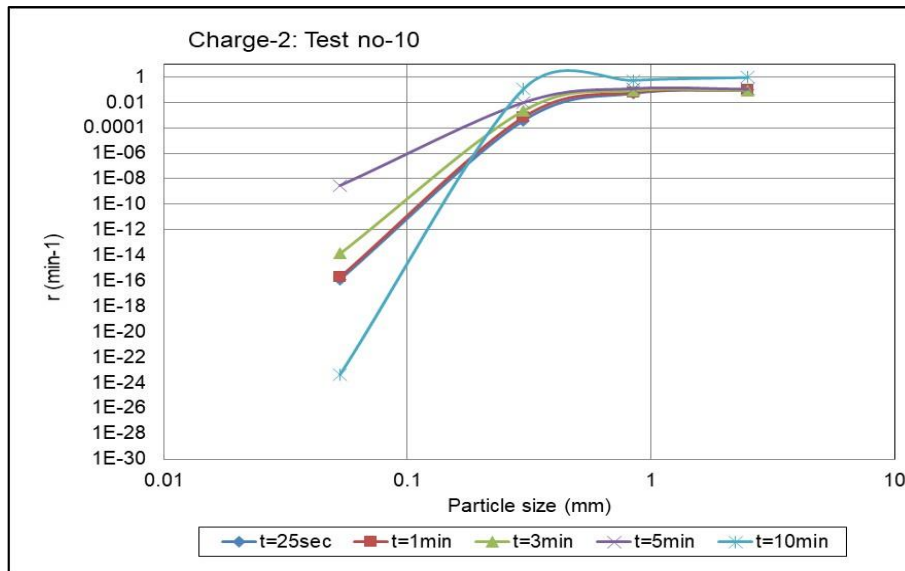


Figure 6.11. Specific breakage rates obtained by grinding with charge-2 distribution (test-10)

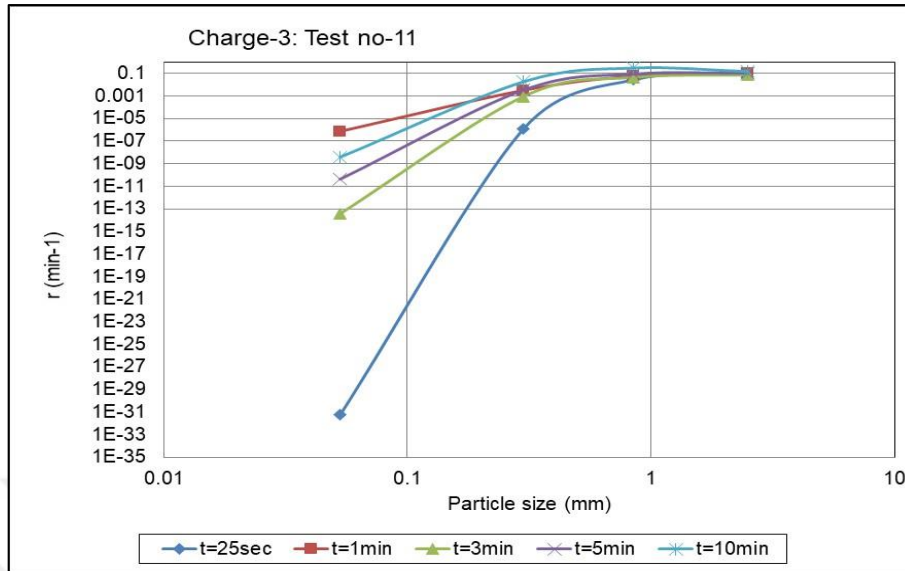


Figure 6.12. Specific breakage rates obtained by grinding with charge-3 distribution (test-11)

Specific breakage rates were observed to not change for particles coarser than 850 μ m in charge-1 ball distribution application. Breakage rates of particles finer than 850 μ m varied with residence time. Highest rates were observed for 25sec grinding condition.

Specific breakage rates were observed to not change for particles coarser than 850 μ m in charge-2 composition application within 5min time. However, rates were increased for the particles coarser than 300 μ m for 10min grinding time. 20mm, 17mm and 15mm balls were discarded from the charge composition in charge-2 application case and a systematic increase in the rates were observed within 5min for particles finer than 850 μ m. Highest size reduction performance was observed for 5min grinding condition. As a consequence, a systematic increase in the breakage rates could have been achieved with finer ball size distribution application (charge-2) which do not include balls below 25mm within 5min.

In charge-3 application case, increase in breakage rates within 1min could have been achieved. The charge was composed of only 40mm and 30mm balls. 94% of the charge-3 composition was 30mm balls.

6.1.1. Evaluation of monosize ball distribution effect on specific breakage rate functions

Comparisons among the back-calculated specific breakage rate functions for Bond and monosize ball charge distributions are presented in Figure 6.13 to Figure 6.17.

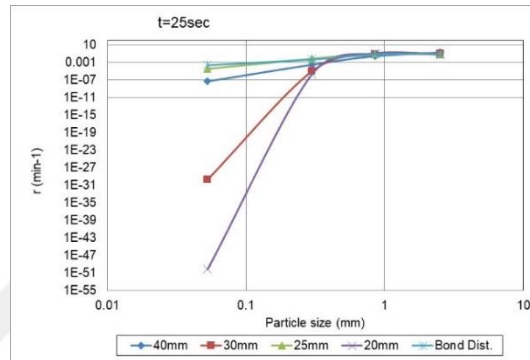


Figure 6.13. Specific breakage rates obtained by grinding with Bond and monosize distributions for 25 sec

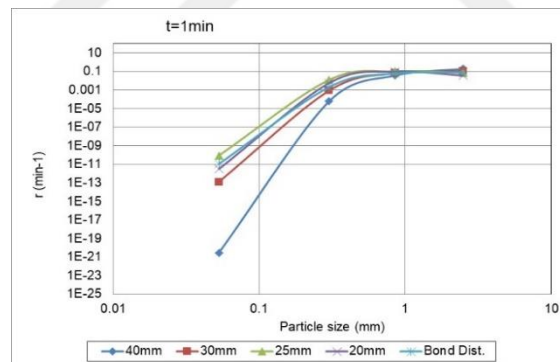


Figure 6.14. Specific breakage rates obtained by grinding with Bond and monosize distributions for 1min

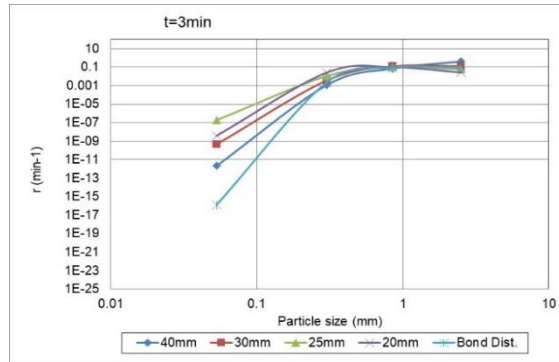


Figure 6.15. Specific breakage rates obtained by grinding with Bond and monosize distributions for 3min

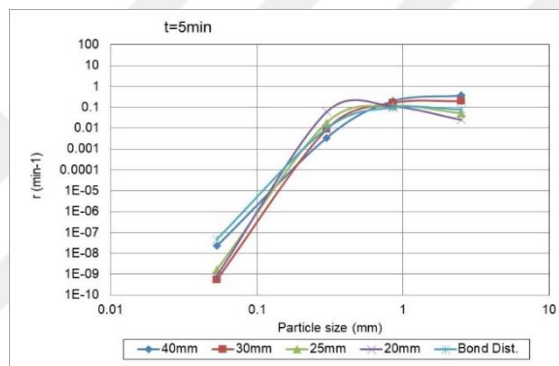


Figure 6.16. Specific breakage rates obtained by grinding with Bond and monosize distributions for 5min

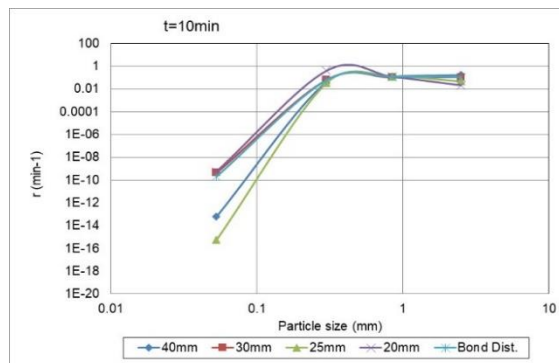


Figure 6.17. Specific breakage rates obtained by grinding with Bond and monosize distributions for 10min

Highest breakage rates were obtained with standard bond charge within 25sec as compared to monosize applications. Highest breakage rates were observed with 25mm balls for 1min and 3min grinding cases when monosize application results are considered only. As the residence time was increased and mill content size distribution got finer as in the case of 10min time interval, 20mm monosize ball distribution indicated the highest performance for particles finer than 850 μ m. Longer residence time in the mill with finer monosize ball charge application (20mm) indicated to increase the specific breakage rates.

6.1.1.1. Empirical relationships between X_m and maximum ball size (b_{max})

Ball size effects on “r/d” functions are reflected by using the relationship between X_m and maximum ball size denoted by b_{max} in simulation of ball mill grinding. “r/d” functions were estimated in the simulation work since it is difficult to determine discharge rate function, “d” in wet grinding conditions as given in Napier Munn et.al. (2005). In this context, it is important to know the relationship between X_m and b_{max} values at different grinding conditions. The relationship between X_m and maximum ball size (b_{max}) was investigated. Established relationships and regression equations are given in Figure 6.18 to Figure 6.23 for each residence time interval.

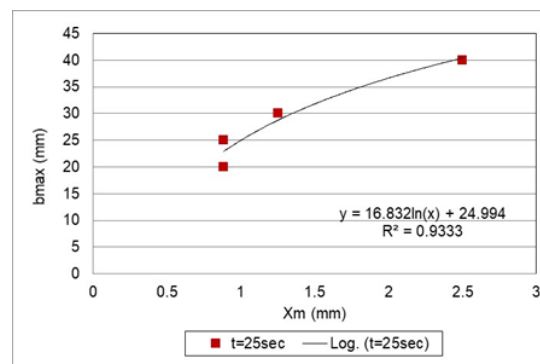


Figure 6.18. Relationship between X_m and b_{max} for 25sec

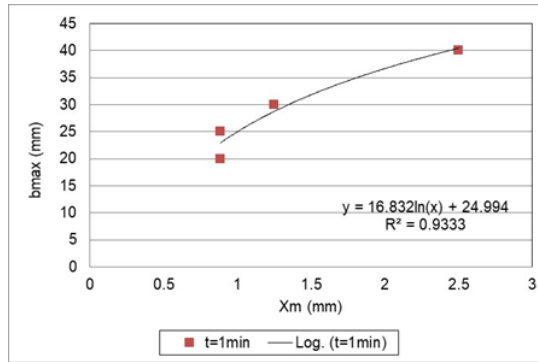


Figure 6.19. Relationship between X_m and b_{max} for 1min

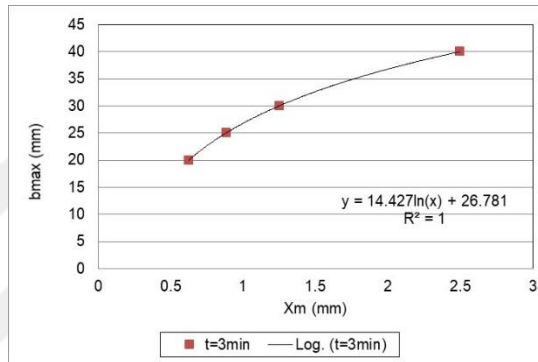


Figure 6.20. Relationship between X_m and b_{max} for 3min

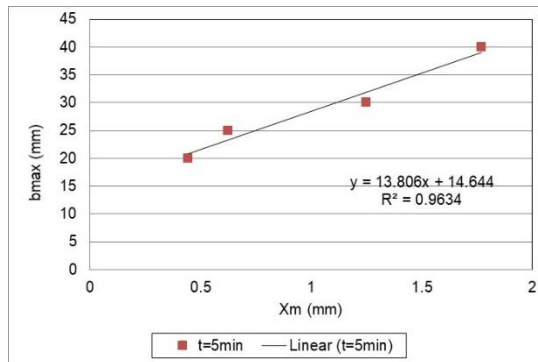


Figure 6.21. Relationship between X_m and b_{max} for 5min

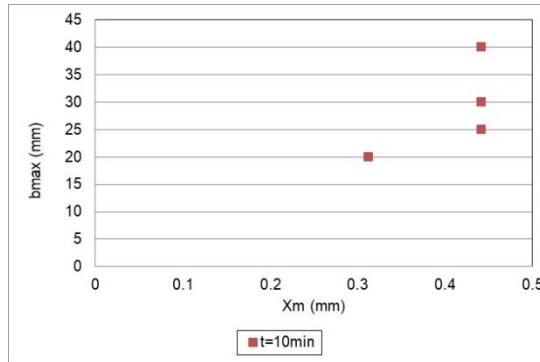


Figure 6.22. Relationship between Xm and bmax for 10 min

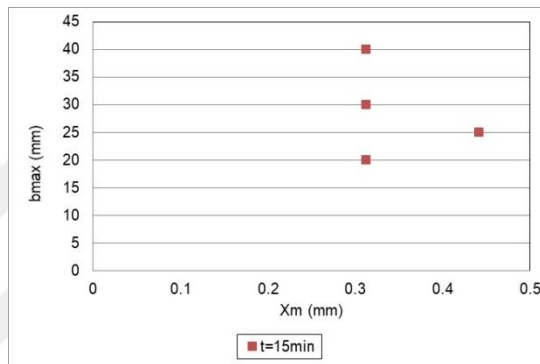


Figure 6.23. Relationship between Xm and bmax for 15 min

Meaningful correlations could have been derived for the test conditions. However, data points start to show more scatter and could not have been fitted to the linear regression equation for residence time of 10min since the same Xm was observed for 40mm and 30mm balls. By increasing the residence time in the mill, sufficient grinding time was allowed to the particles with Xm size and they could have been broken by both 40mm, 30mm and 25mm ball sizes in the mill. Thus, it was concluded that, longer residence time diminished the effect ball size on Xm size for bmax value greater and equal to 25mm ($b_{max} \geq 25\text{mm}$). Any meaningful relationship between Xm and bmax could not be observed for 15min grinding time interval as the same Xm value was obtained for different ball size applications which indicated that the same grinding conditions prevail in the mill.

6.1.1.2. Empirical relationships between X_m and maximum breakage rate (r_{max})

The relationship between maximum ball size (b_{max}) and maximum breakage rate (r_{max}) was investigated. Established relationships and regression equations are given in Figure 6.24 to Figure 6.29 for each residence time interval.

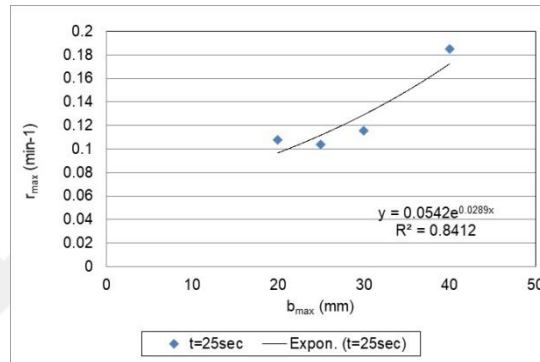


Figure 6.24. Relationship between b_{max} (mm) and r_{max} (min^{-1}) for 25 sec

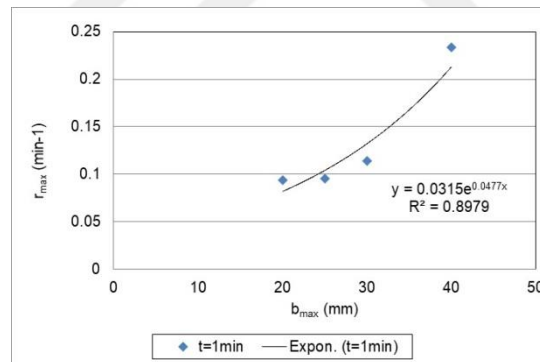


Figure 6.25. Relationship between b_{max} (mm) and r_{max} (min^{-1}) for 1min

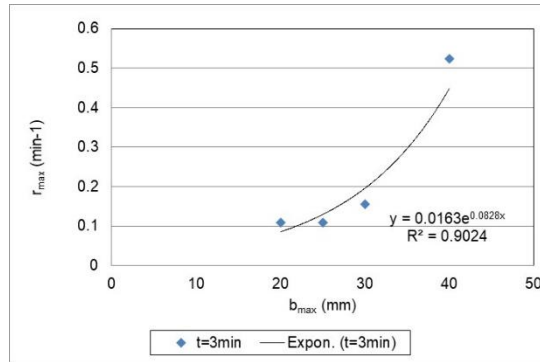


Figure 6.26. Relationship between b_{max} (mm) and r_{max} (min^{-1}) for 3min

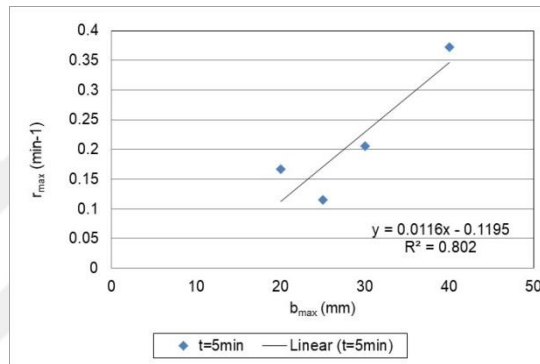


Figure 6.27. Relationship between b_{max} (mm) and r_{max} (min^{-1}) for 5min

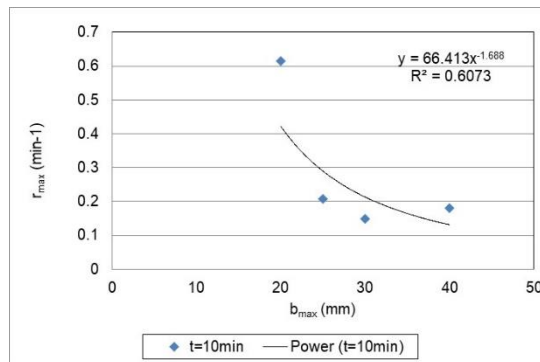


Figure 6.28. Relationship between b_{max} (mm) and r_{max} (min^{-1}) for 10 min

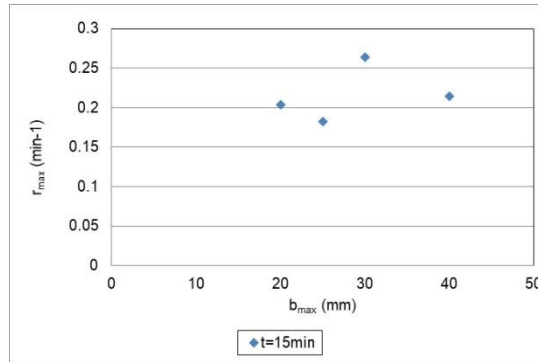


Figure 6.29. Relationship between b_{max} (mm) and r_{max} (min^{-1}) for 15 min

Relatively good correlations could have been drawn between b_{max} (mm) and r_{max} values for the test conditions. However, data was scattered for milling time 15min and any meaningful correlation was not observed.

6.1.2. Evaluation of ball distribution fineness effect on specific breakage rate functions

Comparisons among the back-calculated specific breakage rate functions for the same residence time intervals as compared to Bond charge distribution are presented in Figure 6.30 to Figure 6.34.

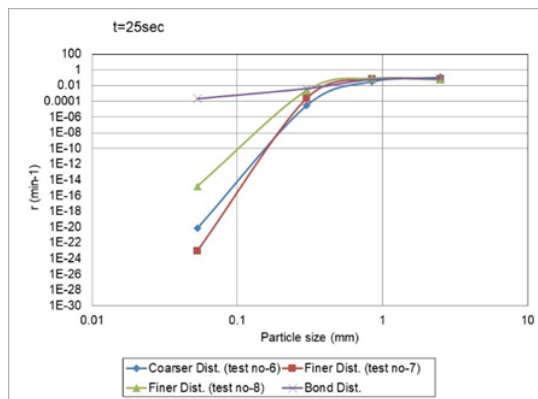


Figure 6.30. Specific breakage rates for 25 sec obtained by grinding with ball distributions of different fineness values

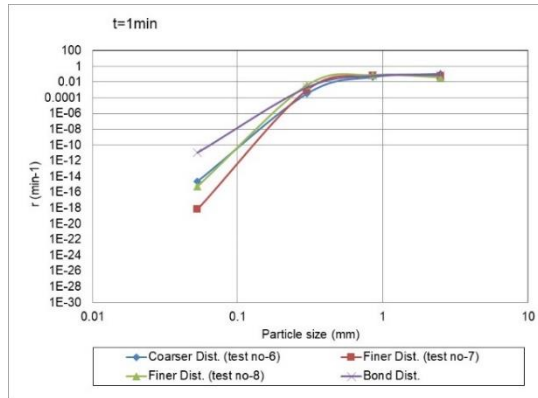


Figure 6.31. Specific breakage rates for 1min obtained by grinding with ball distributions of different fineness values

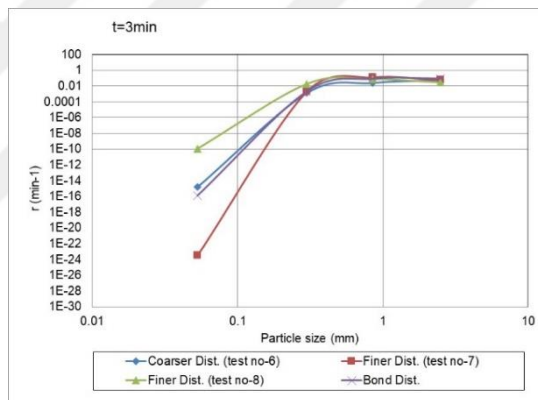


Figure 6.32. Specific breakage rates for 3min obtained by grinding with ball distributions of different fineness values

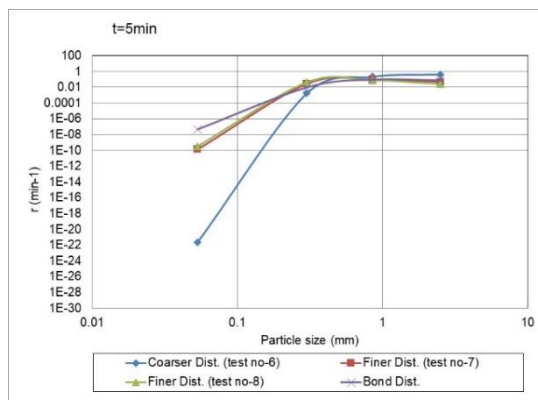


Figure 6.33. Specific breakage rates for 5min obtained by grinding with ball distributions of different fineness values

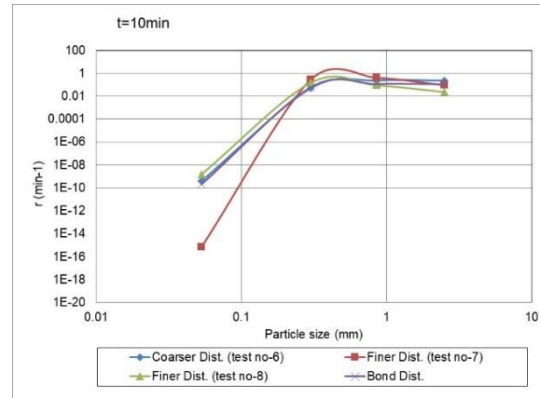


Figure 6.34. Specific breakage rates for 10min obtained by grinding with ball distributions of different fineness values

Specific breakage rates were observed to not change for particles coarser than $850\mu\text{m}$ for 25sec residence time. Highest size reduction performance was observed by grinding with Bond charge composition. Applied finest charge composition (test no-8) resulted in relatively higher breakage rates as compared to the charge compositions in test-6 and test-7. Finer ball charge application increased the specific breakage rates. Bond charge showed higher grinding performance for 1min grinding time. Selected finest distribution resulted in higher rates as compared to the fine charge composition in test-7. As the charge composition got finer, higher rates were observed. In case of 3min grinding time, selected finest charge composition (test no-8) gave highest breakage rates. When the residence time was increased to 5min, finer charge compositions still showed higher grinding performance as compared to coarser ball charge composition. As mill inside particle size distribution got finer, size reduction performance of the coarser ball distribution was observed to be reduced. Finer ball size distribution was found to be effective for grinding of finer mill feed size distributions. It was shown that, coarse ball charge distribution could increase the breakage rates of coarse size fractions as in the case of 5min grinding time interval. Ball size effect was observed to diminish at 10min grinding time. Since the mill content size distribution became finer, ball size effects could not have been observed at longer residence time intervals.

It could be concluded that, ball size distribution fineness effect could have been reflected on the specific breakage functions successfully.

6.1.2.1. Empirical relationships between X_m and maximum ball size (b_{max}) for different ball charge fineness conditions

The relationship between X_m and maximum ball size (b_{max}) for the test conditions are presented with their regression equations for each residence time interval. Relatively meaningful correlations were obtained between X_m and b_{max} for the test conditions. However, it should be mentioned that, correlations were based on three data points and should be improved by obtaining more data points on the graphs.

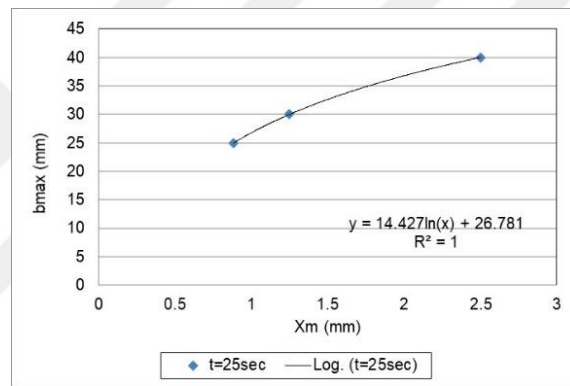


Figure 6.35. Relationship between X_m and b_{max} for 25sec

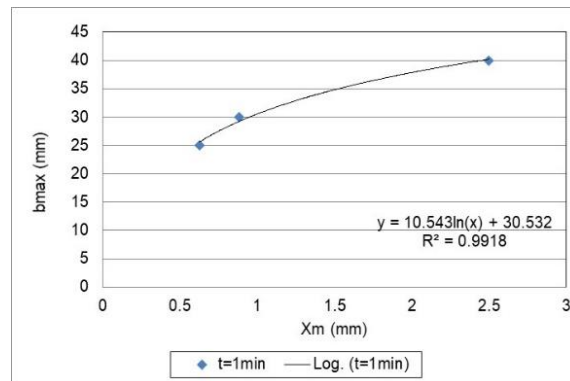


Figure 6.36. Relationship between X_m and b_{max} for 1min

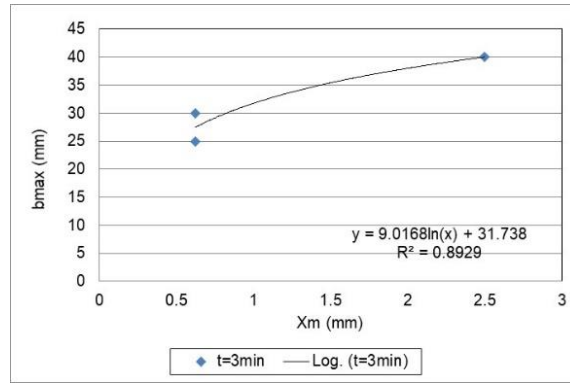


Figure 6.37. Relationship between X_m and b_{max} for 3min

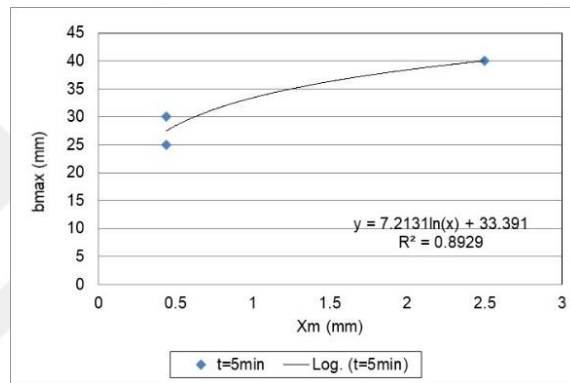


Figure 6.38. Relationship between X_m and b_{max} for 5min

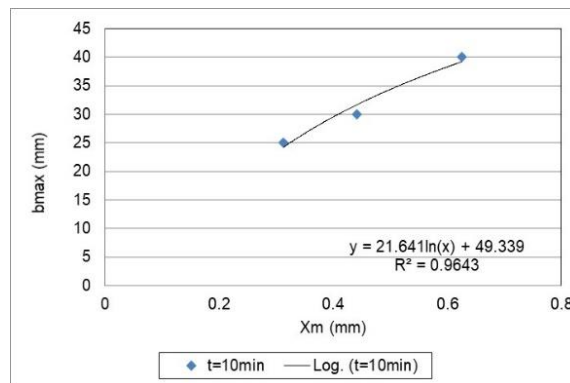


Figure 6.39. Relationship between X_m and b_{max} for 10 min

6.1.2.2. Empirical relationship between X_m and maximum breakage rate (r_{max}) for different ball charge fineness conditions

The relationships between X_m and maximum breakage rate (r_{max}) are presented in Figure 6.40 to Figure 6.44 with the regression equations.

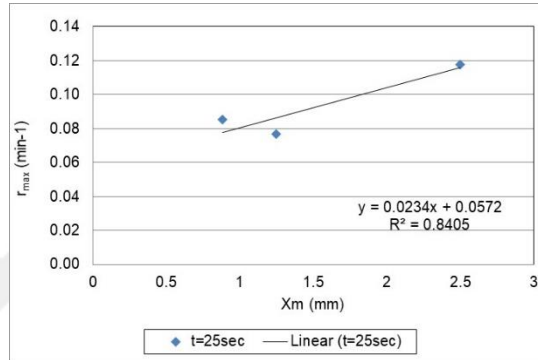


Figure 6.40. Relationship between X_m (mm) and r_{max} (min^{-1}) for 25sec

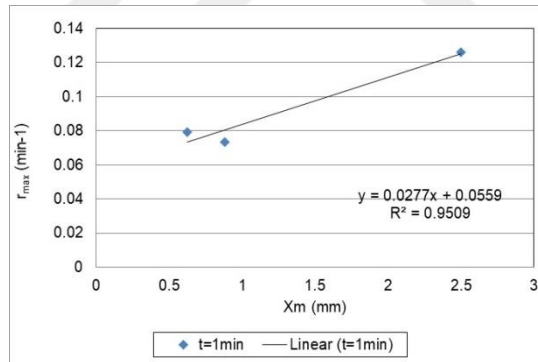


Figure 6.41. Relationship between X_m (mm) and r_{max} (min^{-1}) for 1min

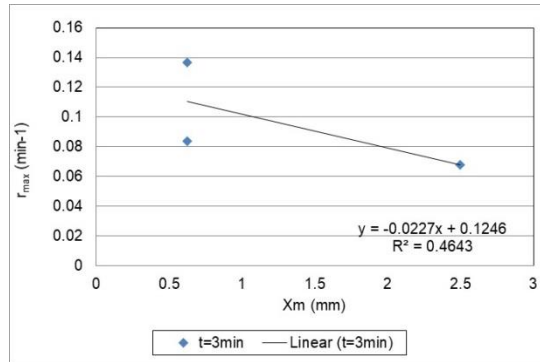


Figure 6.42. Relationship between X_m (mm) and r_{max} (min^{-1}) for 3min

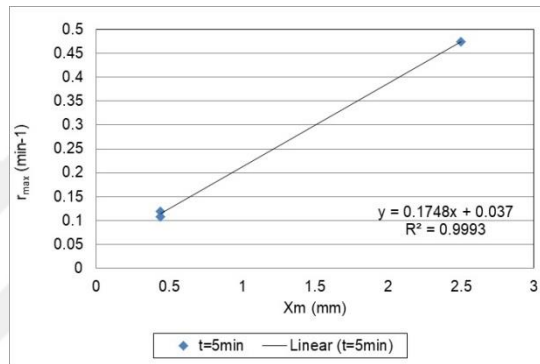


Figure 6.43. Relationship between X_m (mm) and r_{max} (min^{-1}) for 5min

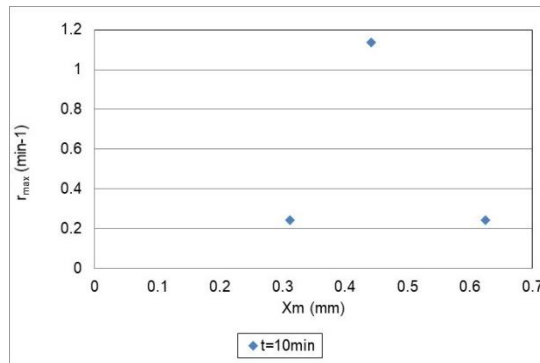


Figure 6.44. Relationship between X_m (mm) and r_{max} (min^{-1}) for 10 min

X_m size is expected to get finer at finer ball charge distribution application and specific breakage rates are expected to increase below X_m size as recorded in the literature (Napier Munn et.al., 2005).

Findings indicated that, as the ball size got coarser, X_m size got coarser and specific breakage rate was increased as well in accordance with the literature. Thus, ball size effects could have been reflected on the breakage rates. The relationship was best observed at 5min residence time interval. It should be mentioned that, in order to be able to generalize the relationship, at least one more test with an appropriate ball charge distribution should be performed.

6.1.2.3. Empirical relationship between maximum ball size (b_{max}) and maximum breakage rate (r_{max}) for different ball charge fineness conditions

Empirical relationships between maximum ball size (b_{max}) and maximum breakage rate are given in Figure 6.45 to Figure 6.49 with the regression equations. Any meaningful trend could not have been observed for residence time intervals of 3min and 10min. Presented trends should be improved with more data sets.

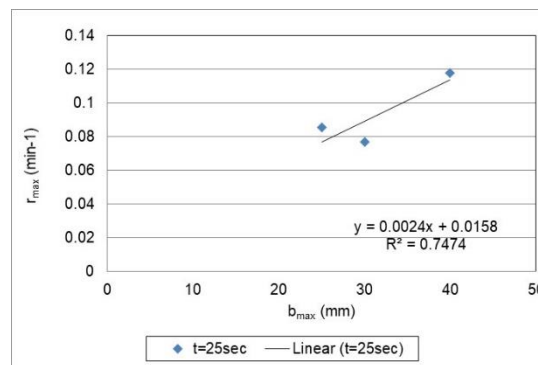


Figure 6.45. Relationship between X_m (mm) and r_{max} (min^{-1}) for 25sec

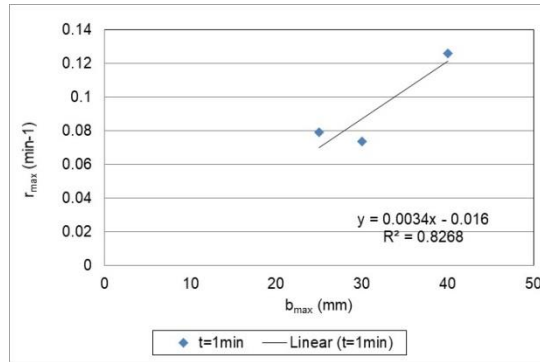


Figure 6.46. Relationship between X_m (mm) and r_{max} (min^{-1}) for 1min

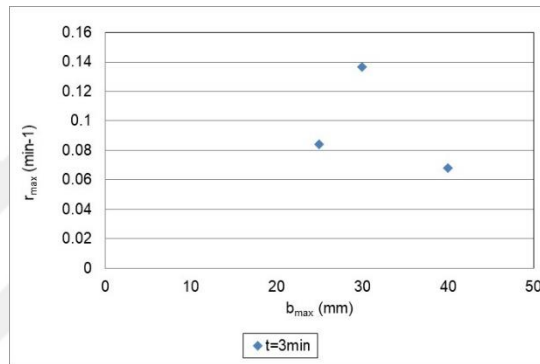


Figure 6.47. Relationship between X_m (mm) and r_{max} (min^{-1}) for 3min

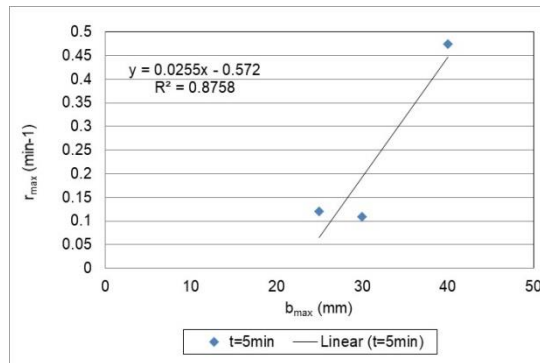


Figure 6.48. Relationship between X_m (mm) and r_{max} (min^{-1}) for 5min

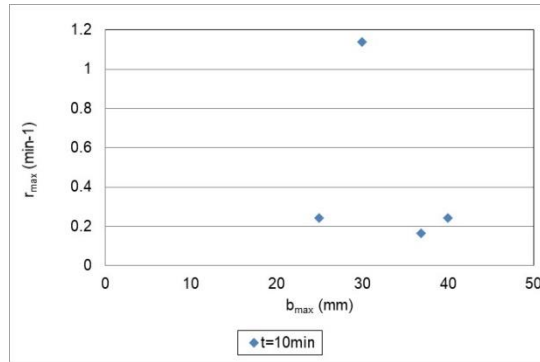


Figure 6.49. Relationship between X_m (mm) and r_{max} (min^{-1}) for 10 min

6.1.3. Evaluation of ball size distribution effect on specific breakage rate functions

Comparisons among the back-calculated specific breakage rate functions are presented in Figure 6.50 to Figure 6.54.

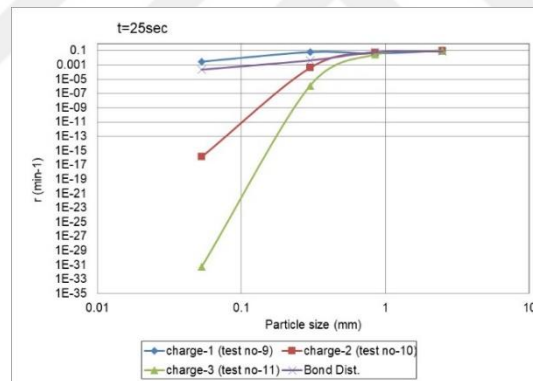


Figure 6.50. Specific breakage rates for 25sec obtained by grinding with different ball distributions

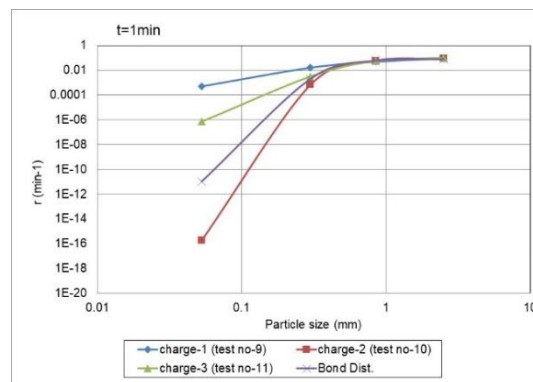


Figure 6.51. Specific breakage rates for 1min obtained by grinding with different ball distributions

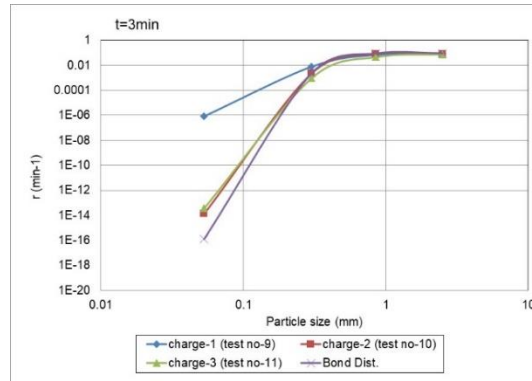


Figure 6.52. Specific breakage rates for 3min obtained by grinding with different ball distributions

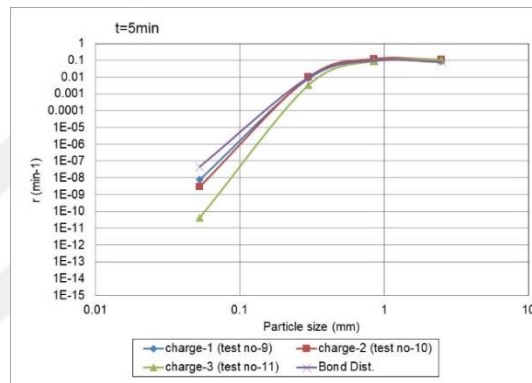


Figure 6.53. Specific breakage rates for 5min obtained by grinding with different ball distributions

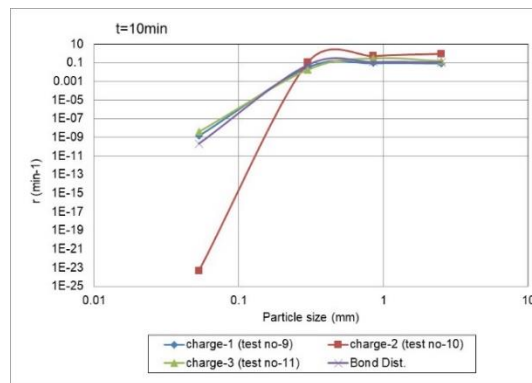


Figure 6.54. Specific breakage rates for 10min obtained by grinding with different ball distributions

Specific breakage rates were observed to not change for particles coarser than 850 μm for the residence time intervals. Coarser ball charge application (charge-1) increased the specific breakage rates for particles finer than 300 μm . Coarser ball charge application (charge-1) resulted in higher breakage rates for 25sec, 1min, 3min and 5min time intervals. Finest charge composition resulted in lower breakage rates as the residence time was increased. Charge-2 composition was observed to increase the rates for

particles coarser than $300\mu\text{m}$. However, specific breakage rates were decreased for particles finer than $300\mu\text{m}$ as compared to the other distributions. Grinding performance of finer ball charge (charge-3) was observed to increase as compared to charge-2 composition in 10min time interval which could be linked to the mill content fineness such that, as the residence time was increased, mill content became finer. Finer charge distribution was observed to increase the breakage rates. Ball charge effect start to diminish at 10min grinding time interval excluded of the charge-2 application case.

As maximum ball was not charged in charge-1, charge-2 and charge-3 compositions, any empirical relationship between X_m and maximum ball size (b_{max}) for the test conditions could not have been drawn. Similarly, relationship between maximum ball size (b_{max}) and maximum breakage rate (r_{max}) for different ball charge conditions could not have been drawn. It was observed that maximum ball size in the distribution which is 40mm resulted in different breakage rates as shown in Figure 6.55. when different charge compositions are used. Maximum breakage rates were found to change for the same X_m size when different charge distributions are used excluded of the trend obtained for 3min grinding time as shown in Figure 6.56. Time interval of 3min was concluded to be optimum time to observe the ball size effect on X_m when the weighted average ball size in the ball charge distributions did not changed.

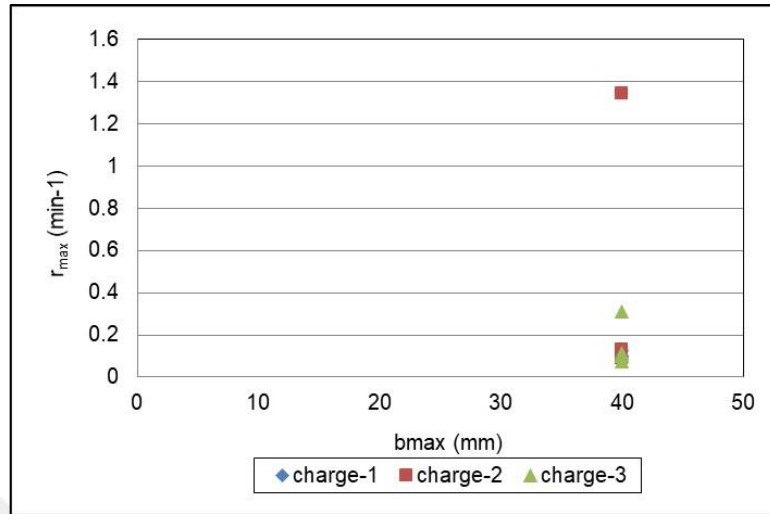


Figure 6.55. Relationship between bmax (mm) and rmax (min⁻¹) for different charge compositions

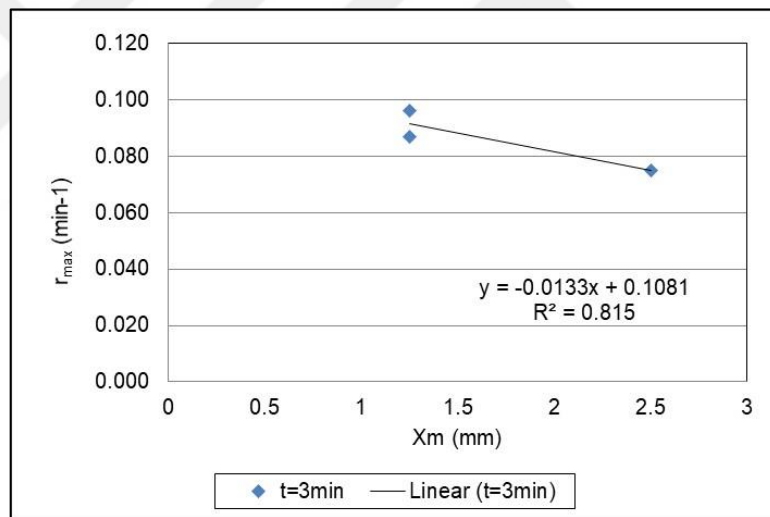


Figure 6.56. Relationship between X_m size and rmax (min⁻¹) for 3min

7. GENERAL DISCUSSIONS

Ball mills are widely applied size reduction equipments in the processing of chromite ore. The ore should be ground and then concentrated so that, it could find market in the minerals industry. It is important not to produce too much fine material during grinding of chromite ores as valuable minerals may be lost as slimes during concentration processes. Grinding in ball mills is very energy intensive and should be performed at optimum conditions without overgrinding. In this context, it is crucial to know the grind size which can be represented usually by the 80% passing size of the mill product (P80). On the other hand, dry grinding has become very popular in recent years in countries where there is a water scarcity and when downstream concentration process will be handled in dry mode such as magnetic separation. In this context tests were held in dry grinding conditions to present an insight about size reduction performance in ball mills for probable dry grinding applications in the industry. It should be mentioned that, since this study is a laboratory scale work, the results will not represent exactly what will happen in industrial scale applications. However, research outputs provided insightful information on dry ball milling performance and typical specific energy consumptions of the comminution process under different operational conditions (ball charge applications). Additionally, detailed analysis on the investigation of the ball size effects on mill product fineness and specific breakage rates provided an extensive data base. Mathematical relationships were derived which could be beneficial for mill modelling and simulation.

In this context, research results are beneficial in terms of:

- estimation of grind size and typical specific energy consumptions,
- estimation of fine material amounts at fine size fractions,
- determining optimum grinding conditions by analyzing the size reduction performance at different ball size distribution applications,

- establishing size reduction models to estimate mill products under different operational conditions such as work index of the ore, feed size distribution, ball size, ball load etc.

In this context, batch type grinding tests were performed by using a laboratory scale Standard Bond mill to analyse ball size and its distribution effects. Test results are used to develop grinding models at different grinding media distributions on the basis of the perfect mixing modelling approach.

In this study, instead of estimating the specific breakage rates of monosize particles as in the work of Austin et.al (1984) an average specific breakage rate function was estimated from the perfect mixing model for the batch grinding conditions and the variations in specific breakage rate functions were analysed for different residence time intervals in the mill. In this respect, test results are thought to be more representative of the industrial scale mills as a full size distribution (-3.35mm) was fed to the mill as similar to the industrial scale applications. Additionally, the modelling approach which was previously used by Hosseinzadehgharehgheshlagh (2014) was determined to be more simple and convenient as compared to Austin's approach (1984). Calculated breakage rate functions provided more realistic and predictive results on dry grinding performance of the chromite ore in ball mills.

8. CONCLUSIONS AND RECOMMENDATIONS

Research results have provided significant information to the literature on size reduction modelling and estimation of performance of ball mills under different ball charge applications in dry conditions. Main conclusions were;

- Repeatable particle size distributions were obtained by the proposed test methodology,
- Batch grinding test results provided estimation of grind size for different residence time intervals and specific energy consumptions,
- Batch grinding test results provided estimation of grind size for different ball size and distribution applications and the related specific energy consumptions,
- Batch grinding test results could have been successfully fitted to the perfect mixing mathematical model to estimate specific breakage rates in the mill,
- Ball size and distribution effects could have been reflected on the mill product particle size distributions,
- Optimum grinding time intervals were concluded to be 3 and 5min to observe the effect of ball size and its distribution,
- Ball size effects could have been reflected on the specific breakage rates estimated from perfect mixing mathematical model which is not a complex model as compared to Austin's approach,
- Ball size distribution and fineness effects could have been reflected on the specific breakage rates successfully with the proposed methodology,
- Specific breakage rates have been successfully estimated based on the perfect mixing modelling approach which reflect ball size and distribution effects.

Recommendations are;

- Size reduction performance of different grinding media shapes such as silpebs (cylindrical grinding media) can be tested and required energy consumptions can be estimated for comparisons with the ball distributions,
- Mill feed size distribution is another important parameter in size reduction performance and thus, its effect should be investigated,

- Wet grinding of chromite ore can be studied under different operational conditions (i.e. ball load, ball size, ball size distribution, solids%, feed size distribution etc.) and compared with the dry grinding performance as most of the concentration processes are held in wet conditions.



REFERENCES

- Acar, C. and Anagül, A. (2018) Beneficiation of low grade chromite ores and process tailings via two-stage enrichment method. *16th International Mineral Processing Symposium Proceedings*. October, 23-25, Antalya, Turkey.
- Anonymous, *Muğla İşletme Projesi Raporu (Ruhsat No:200810162), Teknik Rapor*, Çevre ve Şehircilik Bakanlığı, 2017, 20.
- Austin, L.G., Klimpel, R.R., and Luckie, P.T., 1984. *Process Engineering of Size Reduction: Ball Milling*, A.I.M.E., S.M.E., New York, USA.
- Austin, L.G. and Bagga, P. (1981) An analysis of fine dry grinding in ball mills, *Powder Technology*, 28: 83-90.
- Austin, L.G., Brame, K., 1983, *A comparison of the Bond method for sizing wet tumbling mills with a size mass balance simulation model*, *Powder Technology*, 34: 261-274.
- Austin, L.G., Luckie, P.L., 1971, Methods for determination of breakage distribution parameters, *Powder Technology*, 5: 215-222.
- Benzer, A.H., 2000, *Mathematical modelling of clinker grinding process*, Ph.D. Thesis, Hacettepe University, Ankara, Turkey,138.
- Benzer, A.H., Ergün, Ş.L., Öner, M., Lynch, A.J., 2001, *Simulation of open circuit clinker grinding*. *Minerals Engineering* 14 (7),701-710.
- Bond F.C. 1952. The third theory of comminution. *Trans SME/AIME*, 193, 484-494.
- Bond, F.C. 1960. Crushing and grinding calculations. *British Chemical Eng.* 6(378-391), 543-548.
- Brandes, E.A., Greenaway, H.T., Stone, H.E.N., 1956. Ductility in chromium. *Nature*. 178 (587):587.
- Broadbent, S.R., Callcott, T.G., 1956, *A matrix of processes involving particle assemblies*, *Phil. Trans.R.Soc.London., Ser., A*, 249: 99-123.

- Burt, R.O., 1987, *Gravity concentration methods, Mineral Processing Design*, Ed: Yazar B and Doğan Z.M., NATO ASI Series E: Applied Sciences - No. 122, 106-137.
- Çakmak, I., 2006. *Elazığ-Guleman Yöresi Kromit Cevheri Yataklarının Analizi ve Analiz Sonuçlarına Göre Kullanım Alanlarının Araştırılması*”, Fırat Üniversitesi Fen-Edebiyat Fakültesi, Kimya Bölümü, Elazığ.
- D.P.T.,2001.*Madencilik Özel İhtisas Komisyonu Raporu Metal Madenler Alt Komisyonu Krom Çalışma Grubu Raporu*, Ankara DPT:2626ÖİK:637.
- Dahlin, D.C., Rule, A.R., 1993. *Magnetic Susceptibility of Minerals in High Magnetic Fields*. United States Department of the Interior Bureau of Mines.
- Deniz V., 2004. *Relationships between Bond's grindability (G_{bg}) and breakage parameters of grinding kinetic on limestone*. Powder Technology, Vol.139, 208-213.
- Deniz, V., Gelir, A., Demir, A., 2003. The effect of fraction of mill critical speed on kinetic breakage parameters of clinker and limestone in a laboratory ball mill, 18th *International Mining Congress and Exhibition of Turkey*, IMCET, 443-450.
- Deniz, V., Onur, T., 2002. Investigation of the breakage kinetics of pumice samples as dependent on powder filling in a ball mill, *Int J. Miner. Process*, Volume 67, 71-78.
- Denver Equipment Company, *Modern Mineral Processing Flowsheets*, Denver Equipment Co.,1962.
- Devlet Planlama Teşkilatı (DPT), 2001. *Metal Madenler Alt Komisyonu Krom Çalışma Grubu Raporu*. Sekizinci 5 Yıllık Kalkınma Planı. Ankara, DPT: 2626-ÖİK:637, 1-8, 11-14.
- Epstein, B., 1947. Logarithmico-normal distribution in breakage of solids. *Ind. Eng. Chem.*, Volume 40, 2289-2291.
- Fawcett, E., 1988. Spin-density-wave anti ferromagnetism in chromium. *Reviews of modern Physics*. 60:209.

- Genç, Ö., 2008a, Analysis of single particle breakage characteristics of cement clinker and cement additives by drop-weight technique, *The Journal of the Chamber of Mining Engineers of Turkey*, Vol. 47, No.1, March, 13-26.
- Genç, Ö., 2008b, *An investigation on the effect of design and operational parameters on grinding performance of multi-compartment ball mills used in the cement industry*, PhD Thesis, Hacettepe University, Mining Engineering Department, Turkey (In English)
- Gu, F., Wills, B., 1988. Chromite mineralogy and processing. *Minerals Engineering*, 1(3): 235.
- JKSimMet Software V4.32, 1998, JK Tech, SMI, The University of Queensland, Brisbane, Australia.
- Önal, G., Özpeker, I., Doğan, Z., Atak, S., Gürkan, V., 1986. *Kromit Oluşumu, Zenginleştirilmesi ve Kullanım Alanları*, İTÜ Maden Fakültesi Ofset Atölyesi-İstanbul
- Günay, K., Çolakoğlu, A.R., 2015. Spinel compositions of mantle-hosted chromite from the Eastern Anatolian ophiolite body, Turkey: Implications for deep and shallow magmatic processes, *Ore geology reviews*, 73, 29-41.
- Güney A., Yüce A.E., Kangal, M.O., Burat F., Kokılcı O., Gurkan V., 2009. Beneficiation and process flowsheet development of chromite ores, *XIII. Balkan Mineral Processing Congress*, Edts: S.Krausz, L. Ciobanu, N.Cristea, V.Ciocan, G.Cristea, ISBN: 978-973-677-159-0, Vol:1, 401-408, June, 14-17, Bucharest, Romania.
- Güney, A. 1994. Flotation of fine chromite tailings using novel techniques. In: Demirel, H., Ersayın, S. (Eds.), *Progress in Mineral Processing Technology*. Balkema, Rotterdam, The Netherlands, 473-477.
- Güney, A., 1992. Concentration of chromite gravity tailings by free jet type and column flotation system. *In Proceedings of the First International Conference on Modern Process Mineralogy and Mineral Processing*, Beijing, China.

Güney, A., Önal G., Doğan M.Z., Çelik, M.S., 1993. Mechanism of anionic collector adsorption in chromite flotation. *In Proceedings of XVIII International Mineral Processing Congress*, Vol. 4. Sydney, Australia, 937-940.

Hacıoğlu, S., 2010. *Kayseri Pınarbaşı Kromitlerinin Kuru Zenginleştirilmesi*, Yüksek Lisans Tezi, İstanbul Teknik Üniversitesi, Fen Bilimleri Enstitüsü, Maden Mühendisliği, İstanbul.

Hashim, S., 2003. *Mathematical modelling the two-compartment mill and classification*, PhD Thesis, Julius Kruttschnitt Mineral Research Centre, The University of Queensland, Australia, September.

Herbst, J.A., Fuerstenau, D.W., 1968. The zero order production of fine size in comminution and its implications in simulation. *Trans. Am.Inst. Min.Engrs.* 241., 538-548.

Herbst, J.A., Grandy, G. A., Fuerstenau, D.W., 1972, Population batch models for design of continuous grinding mills, *Proceedings of Tenth Inter. Miner. Process. Congress*. London, 23-45.

Hosseinzadehgharegheshlagh, H., 2014. *Bilyalı Değirmenlerde Ölçek Büyütme Üzerine Bir İnceleme*. Doktora Tezi, Hacettepe Üniversitesi, Fen Bilimleri Enstitüsü, Maden Mühendisliği, Beytepe, Ankara.

<http://www.mta.gov.tr>, alındığı tarih 21.04.2010

Kavetsky, A. And Whiten, W.J., 1982a. *Scale-up relations for industrial ball mills*, *Proc. Australas. Inst. Min. Metall.* 282, 47-55.

Kavetsky, A. And Whiten, W.J., 1982b. Studies on the scale-up of ball mills, *Mill operations conference*, September, Australas, Inst.Min.Metall., 113-121.

Kavetsky, A., McKee, D.J., 1984. Analysis and design of industrial grinding and classification circuits by use of computer simulation. In application of computers and mathematics in the mineral industries: *18th Int. Symp.* London, (London: IMM 1984), 57-67.

- Kelsall, D.F., Reid, K.J., Stewart, P.S.B., 1969. A study of grinding processes by mathematical modelling, *Presented at IFAC Symposium*, Sydney, Australia, Paper, 2509, 205-218.
- Knorrning, V.O., Condliffe, E., Tong, Y.L., 1986. *Some mineralogical and geochemical aspects of chromium-bearing skarn minerals from northern Karelia, Finland*. Bull.Geol.Soc. Finland. 58, Part1, 277-292.
- Lynch, A.J., Öner, M., Benzer, A.H., 2000. *Simulation of a closed cement grinding circuit*, ZKG, No 10, 560-568.
- Lynch, A.J., 2015. *Comminution Handbook, Chapter 1: Comminution—An Overview*, The Australasian Institute of mining and Metallurgy, Spectrum Series 21, Australia, 1-10.
- Man Y.T., 2001. Model-Based Procedure For Scale-up of Wet, Overflow Ball Mills Part-2: Validation and Discussion, *Minerals Engineering*, Volume 14, No.10, 1259-1265.
- McKee, D.J., Napier Munn, T.J., 1990. The status of comminution simulation in Australia, *Mineral Engineering*, Volume 3, 7-21.
- Mular, L.A., Halbe, N.D., Barrat, J.D., *Mineral Processing Plant Design, Practice and Control Proceedings*, Volume 1, Society for Mining, Metallurgy, and Exploration, Inc. (SME)., 2002., pp712.
- Munn, N., Morrell, S., Morrison, R.D., Kojovic T., 2005. *Mineral Comminution Circuits Their Operation and Optimization*, JKMRRC, Brisbane, 413.
- Narayanan, S.S., 1986. *Development of a laboratory single particle breakage technique and its application to ball mill modelling and scale-up*. PhD Thesis, University of Queensland, Australia.
- Narayanan, S.S., 1987. Modelling the performance of industrial ball mills using single particle breakage data., *Int J. Miner. Process.* Volume 20, 211-228.

- Narayanan, S.S., Lean P.J., Baker, D.C., 1987. Relationship between breakage parameters and process variables in ball milling- An industrial case study. *Int. J. Miner. Process.*, Volume 20, 241-251.
- Önal, G., Özpeker, I., Doğan, Z., Altıntığ, A. ve Renda, D., 1995. *Türkiye Krom Envanteri*, İMMİB, Mart, İstanbul.
- Önal, G. ve diğ., 1986. *Kromit Oluşum, Zenginleştirilmesi ve Kullanım Alanları*, Etibank
- Özdağ, H., Üçbaş, Y., Koca, S., 1993. *Enrichment of chromite ore by means of Multi-Gravity Separator*. Geosound, 167-176.
- Özdağ, H., Üçbaş, Y., Koca, S., 1994. Recovery of chromite from slime and table tailings by multigravity separator. *Proceedings of International Conference on Innovations in Mineral Processing*, Sudbury, Ontario, Canada, 267-278.
- Özkan, 1982. *Guleman ofiyolitinin jeolojisi ve petrolojisi*. Doktora Tezi. İstanbul Üniversitesi.
- Özkan, A., Düzyol, S., Uçbeyiay, H., Ağaçayak, T., 2006. *Krom cevherinin kuru ve yaş öğütme kinetiği ve pülp yoğunluğunun etkisi*, Pamukkale Üniversitesi, Mühendislik Bilimleri Dergisi, Cilt:12, Sayı:1, 73-78.
- Papp, J. F., 1994. *Chromium life cycle study*: U. S. Bureau of Mines Information Circular 9411, 94.
- Rowland, A. Chester, 2006. Advances in Comminution, Part: *Bond's method for selection of ball mills*. Editor, Kawatra, S. Komar. 385-397.
- Stief, D.E., Lawruk, W.A., Wilson, L.J., 1987. Tower mill and its application to fine grinding, *Min. Metall Proc*, 4(1): 45-50.
- TS 7700, 1989, Determination method of grinding work index, First Edition.
- USGS, 2018. *Mineral commodity summaries*, Chromium.
- Üçbaş, V., Özdağ, H., 1994. Relationships between shake frequency and amplitude in the concentration of chromite fines by multi-gravity separator. In: Demirel, H., Ersayın, S. (Eds.), *Progress in Mineral Processing Technology*, Balkema, Rotterdam, The Netherlands, 71-76.

- Weedon, D.M., 2001. *A perfect matrix model for ball mills*, *Minerals Engineering Pergamon Pres.* Volume 14, No. 10., 1225-1236.
- Whiten, W. J., 1972. The use of periodic spline functions for regression and smoothing, *The Australian Computer Journal*, 4: 31-34.
- Whiten, W. J., 1974. *A matrix theory of comminution machines*. *Chemical Engineering Science.*, 29, 588-599.
- Whiten, W.J., 1976. *Ball mill simulation using small calculators*, *Proc. Australas. Inst. Min, Metall.* 258: 47-53.
- Whiten, W.J., Kavetsky, A., 1983. Studies on scale-up of ball mills., Mill design and grinding performance of large ball mills I, *SME/AIME Mini Symp.* No.83-MPD-09, Salt Lake City, Utah, October, 85-94.
- Wills, B.A., Finch, A.J., 2016. *Mineral Processing Technology*, Eighth Edition.
- Yüce, A. Ekrem. 2017. *Grinding size estimation and beneficiation studies based on simple properties of ore components*. *Physicochemical Problems of Mineral Processing.* 53(1), 2017, 541-552.
- Zhang, Y.M., 1992. *Simulation of Comminution and Classification in Cement Manufacture*, PhD Thesis, JKMRRC, University of Queensland.

APPENDIX

Mineralogical Analysis Results with Image Analysis System

In polished section, trace amount of ore minerals are detected; in a decreasing order they are as follows: chromite, magnetite, pyrite, chalcopyrite and native copper. Chromites are in euhedral habit with a size range between 15-600 μ m. Almost all of the grains appear to undergo cataclasis in that some chromite fragments through the lamellae start to alter into magnetite.



CURRICULUM VITAE

Personnel Information

Name-Surname	: Zehra GÖKALP
Nationality	: Republic of Turkey
Birth Date and Place	: 15.03.1991 - DİYARBAKIR
Phone	: 0090 536 329 91 12
e-mail	: zehragokalp2010@hotmail.com

Education

Degree	Affinity	Graduate Year
Primary School	Diyarbakır Cumhuriyet İlköğretim Okulu	2005
High School	Diyarbakır Melik Ahmet Lisesi	2009
Bachelor	Muğla Sıtkı Koçman Üniversitesi Maden Mühendisliği	2015
Master of Science	Muğla Sıtkı Koçman Üniversitesi Maden Mühendisliği	2018

Experience

Year	Place-Company	Position
01.08.2013- 01.09.2013	Kastamonu/Küre Eti Bakır A.Ş Küre/Kastamonu Yeraltı Madenciliği	Intern
23.06.2014- 07.08.2014	Adana/Aladağ Akmetal Madencilik A.Ş. Yetimli Köyü Kumbükü Mevkii Aladağ/Adana Cevher Zenginleştirme	Intern
2017-2018	Muğla/Karacaören Eti Krom A.Ş KromElİnş.Mad.Tic.A.Ş.Karacaören Mah.Sarikaya Mevkii Menteşe/Muğla Yeraltı Madenciliği	Engineer

Language

English, Pre-Intermediate level

French, Beginner level

Social Activities

Social responsibility projects

Volunteering of youth center training programs

Awards

Graduation of Mining Engineering Department in the first row

Membership in organizations and organizations

Chamber of Mining Engineers, Young Miners of Muğla Sıtkı Koçman University
Representative

Board Member of Muğla Sıtkı Koçman University Innovation Society

Muğla Sıtkı Koçman University Bridge Member

Member of the Theater Society
